Dual Temperature Evaporator Refrigerator Design and Optimization

S. Kelman and C. W. Bullard

ACRC TR-148 January 1999

For additional information:

Air Conditioning and Refrigeration Center
University of Illinois
Mechanical & Industrial Engineering Dept.
1206 West Green Street
Urbana, IL 61801

(217) 333-3115

Prepared as part of ACRC Project 66
Refrigerator Systems Analysis
C. W. Bullard, Principal Investigator

The Air Conditioning and Refrigeration Center was founded in 1988 with a grant from the estate of Richard W. Kritzer, the founder of Peerless of America Inc. A State of Illinois Technology Challenge Grant helped build the laboratory facilities. The ACRC receives continuing support from the Richard W. Kritzer Endowment and the National Science Foundation. The following organizations have also become sponsors of the Center.

Amana Refrigeration, Inc.
Brazeway, Inc.
Carrier Corporation
Caterpillar, Inc.
Chrysler Corporation
Copeland Corporation
Delphi Harrison Thermal Systems
Eaton Corporation
Frigidaire Company
General Electric Company
Hill PHOENIX
Hussmann Corporation
Hydro Aluminum Adrian, Inc.
Indiana Tube Corporation
Lennox International, Inc.
Modine Manufacturing Co.
Peerless of America, Inc.
The Trane Company
Thermo King Corporation
Visteon Automotive Systems
Whirlpool Corporation
York International, Inc.

For additional information:

Air Conditioning & Refrigeration Center
Mechanical & Industrial Engineering Dept.
University of Illinois
1206 West Green Street
Urbana IL 61801

217 333 3115

Abstract

The primary focus of this thesis is on performance advantages of a dual-temperature evaporator refrigerator system over a conventional design. Through extensive use of computer-aided modeling, it is demonstrated that energy savings of at least 8-10% can be achieved if this design is coupled with variable speed compressor technology. In addition to the validation study, various optimization techniques that can be used to reduce energy consumption of sequential cooling systems are also introduced. These methods are subsequently applied to a particular experimental prototype design.

The thesis also explores ways of reducing overall charge requirements for a refrigerator system by means of introducing parallel circuits in the heat exchangers. Other topics include evaporator de-superheating phenomenon, a series of studies on flow instabilities in capillary tubes, and a dual-speed compressor performance analysis.

Table of Contents

Appendix

List of Figures

List of Tables

Chapter 1

Introduction

1.1 Dual-temperature evaporator system definition

This chapter gives a brief introduction to the concepts behind the design of a sequential cycle (also known as "dual-temperature") single-evaporator refrigerator system. In this type of refrigerator design the same evaporator is sequentially used first to cool the freezer compartment and then the fresh food compartment. The air flow over the evaporator coil is directed into one compartment at a time and is switched back and forth.

The basic benefit of a dual-temperature evaporator system is that the evaporating temperature can be fully optimized for maximum performance and efficiency while running in each mode. The optimization techniques for such systems are relatively complex as compared to those for conventional refrigerator layouts. Nevertheless, a few distinct performance advantages can be worth the extra design efforts and the cost of dual-temperature evaporator systems is only slightly higher than that of conventional refrigerators with similar performance characteristics.

1.2 Design advantages

The major advantage of a dual-temperature evaporator system is that while the refrigerator is running in the fresh food mode, the lower temperature lift in the evaporator can increase the steady state COP by nearly a factor of two. Figure 1.1 shows that the compressor EER for a typical freezer operating condition (the bold point on the left) is about half of that for the fresh food mode (the bold point on the right).

Theoretically, since the fresh food compartment represents about 1/3 of the total evaporator load and the operating efficiency in this mode can be nearly doubled, the overall system COP might be reduced by as much as 15-20%.

Furthermore, if the system is optimized for each compartment separately, the COP in the freezer mode can be also enhanced by using a different capillary tube or varying the compressor speed.

An additional performance improvement might result from using the relatively warm fresh food compartment air to defrost the evaporator during the off-cycle. This could lengthen the defrost cycle, or possibly eliminate the auxiliary power requirements entirely, reducing the system complexity, its initial cost, and overall energy usage.

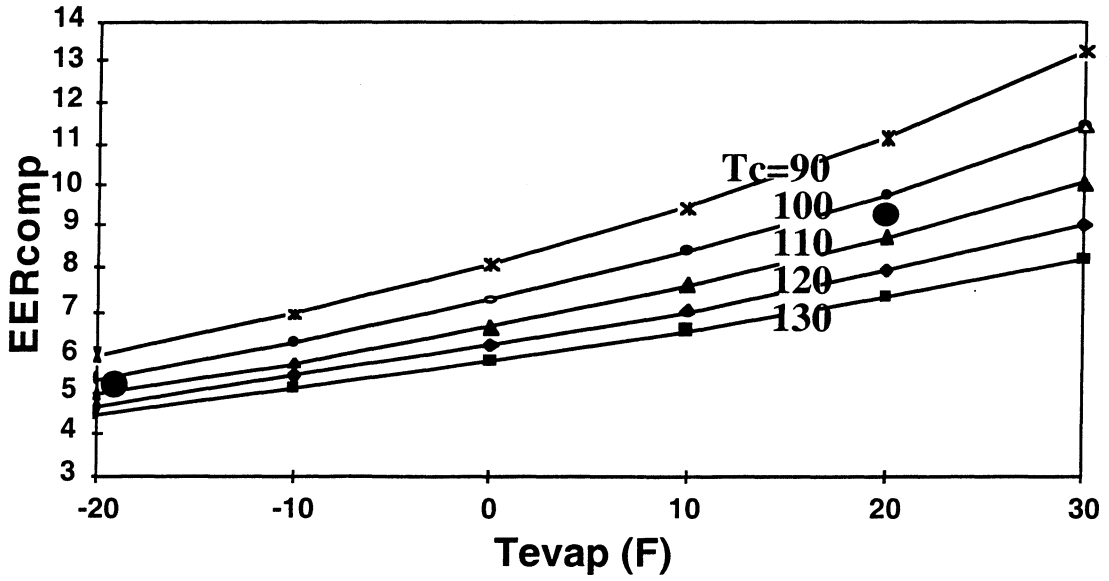

Figure 1.1 Compressor EER in freezer and fresh food operation modes

Unlike the proposed design, most alternative concepts such as a dual evaporator system (Lee et al., 1997), an alternating evaporator duty system (Lavanis et al., 1998) or a tandem cycle system (Kim et al., 1995) incorporate two separate evaporators, which alone can become a significant initial cost consideration. On the other hand, the dual-temperature evaporator system uses a single evaporator coil. As compared to a conventional design, it only requires two additional air valves (inlet and outlet) to switch the air flow between the compartments and a solenoid valve if separate captubes are used for each of the two operating modes. These are all relatively small devices that cost considerably less than an additional evaporator coil.

Also, it might be possible to use the same captube while operating in either mode, as demonstrated in Chapter 5. This can help to keep the total cost down, although it limits the designers' ability to fully optimize the system operation separately for each mode.

1.3 Design obstacles

While dual evaporator systems offer quite a few attractive benefits, as described above, some additional steps are required to take advantage of all the performance enhancements offered by this new design.

Most importantly, the same evaporator is used to deliver cold air to each compartment, which means that one of the compartments (namely the fresh food, as demonstrated below) may require a larger heat transfer area to operate effectively. This can restrict the design space for the system optimization.

In order to improve the system performance in the fresh food mode, a dual-speed (or a multi-speed) compressor might be implemented. A control system is required to make sure that the compressor is running at the correct speed for each mode.

Two additional points must be made regarding the use of a dual-speed compressor. On the positive side, when the compressor is running at a lower speed than in a conventional system (which is the case in the fresh mode) some additional energy savings could result. However, as pointed out in Appendix C, the isentropic efficiency of the compressor similar to the one installed in our prototype system was independent of the operating speed. On the negative side, multi-speed compressors can be less reliable since lubrication at a lower speed setting might not be very effective.

Finally, the runtime fraction of the system operating in the fresh food mode can be very small, resulting in performance loss due to inability of the system to quickly reach steady state and therefore introducing higher cycling losses.

A detailed tradeoff analysis is presented in Chapter 2.

Chapter 2

Tradeoff analysis

2.1 Design method

The ACRC refrigerator simulation model was used to model a dual-temperature evaporator system (for a complete description of the model see Woodall and Bullard 1996, 1997). The tradeoff analysis was done separately for the fresh food and the freezer compartments. In each case the air flow over the evaporator to the "inactive" compartment was set to be zero, forcing the split air fraction to be either 1.0 (for the freezer) or 0.0 (for the fresh food).

Five design variables under consideration were the total areas of the condenser and evaporator coils, compressor speed, and condenser and evaporator fan speeds. Most of analysis was done for the system running at the standard Department of Energy test conditions.

The annual energy consumption and the system COP were calculated to quantify the performance advantages of a redesigned system. Each proposed design was also examined for the required total refrigerant charge.

The fresh food mode runtime fraction and the operating temperature lift in the evaporator were used as sensitivity indicators for the optimization.

2.2 Proposed component changes

2.2.1 Compressor speed

The compressor turndown ratios (calculated as the maximum operating speed over the minimum speed) that are currently available in mass production units at a reasonable cost are limited to a factor of 2.0. Using turndown ratios higher than 2.0 could result in greater energy savings, but might cause lubrication problems which could lead to poor reliability. However, some prototype units that are currently being tested by various manufacturers might have turndown ratios as high as 5.0, enabling overall energy savings of up to 20%.

The ACRC model predicted that slowing the compressor down by just a factor of 2.0 while running in the fresh food mode might still result in a respectable performance gain for this part of the cycle, as compared to the system running at the speed optimized for the conventional design. It was found that during the fresh food compartment cooling part of the cycle the steady state COP of the system should increase by as much as 22%.

Naturally, these savings are not as dramatic as those that could be achieved with higher turndown ratios. For example, a turndown ratio of 3.0 could result in a 32% COP increase for the fresh food mode.

Higher COP would be achieved primarily because the air-to-refrigerant temperature difference decreases as refrigerant flow rate (and therefore evaporator capacity) is reduced. This occurs when the incoming temperature difference in the evaporator ($\Delta T_{evap} = T_{air\ evap\ in} - T_{evap\ in}$) is decreased, as shown in Figure 2.1.

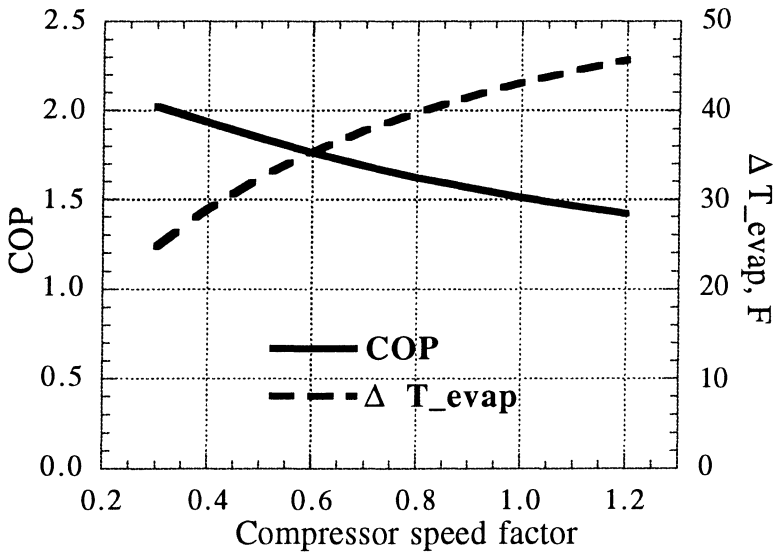

Figure 2.1 Compressor speed change effects (1)

When the compressor speed is reduced by a factor of 2.0 during fresh food operation, the runtime fraction in this mode will increase more than 40%. This could help ensure that the system has enough time to reach steady state and that cycling losses are reduced. Meanwhile, the compressor has to deal with only about 30% smaller mass flow rate as the suction gas density is increased.

However, just over 10% more total refrigerant charge is required to run the system properly. It might be possible to design an accumulator or a receiver that could release this amount of refrigerant while operating in the fresh food mode and store it during the freezer operation to prevent compressor flooding. Access to this receiver could be controlled by the same solenoid valve that is used to switch the flow between the two captubes.

The fresh food runtime fraction and the total amount of refrigerant charge in the system are shown in Figure 2.2 as a function of turndown ratio.

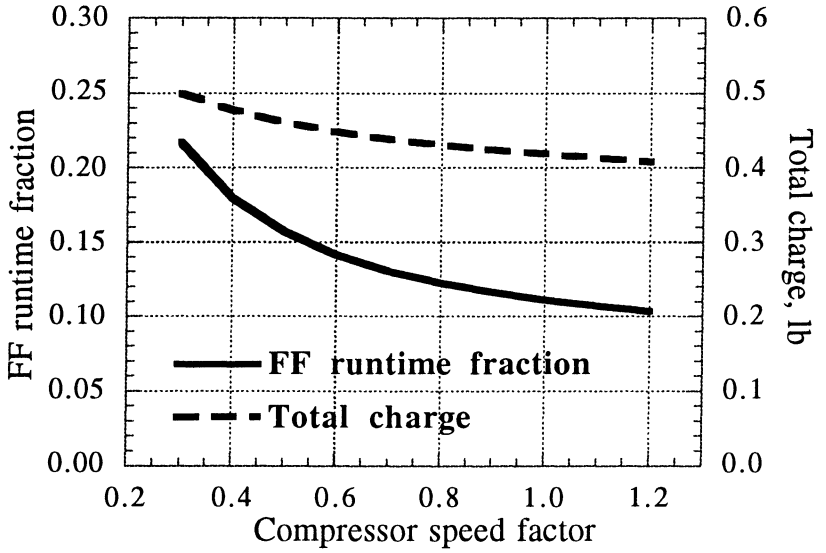

Figure 2.2 Compressor speed change effects (2)

During the freezer mode operation, no significant advantage of either speeding the compressor up or slowing it down was predicted, perhaps because the operating temperatures were very close to the original design conditions of a conventional refrigerator.

2.2.2 Fan speeds

The calculations in this section are based on the assumption that the air side heat transfer coefficient is proportional to the fan speed taken to the power of 0.6. This correlation is used for both condenser and evaporator. Experimental results obtained by Cavallaro and Bullard (1995) indicate that this exponent can actually vary from about 0.5 to over 0.7 depending of the particular fan and coil combination. However, the changes in the fan energy consumption with operating speed were considered negligibly small and were not taken into account.

Figure 2.3 demonstrates the gain in the steady state COP when the evaporator fan speed is increased. This performance boost results from decreasing the air side heat transfer resistance and improving the match between refrigerant and air side capacities. The reference fan speed measured for the original Amana system was about 45 cfm.

Figure 2.3 shows the expected performance improvement in the steady state COP. However, the correspondingly shorter runtime fractions could lead to higher transient losses.

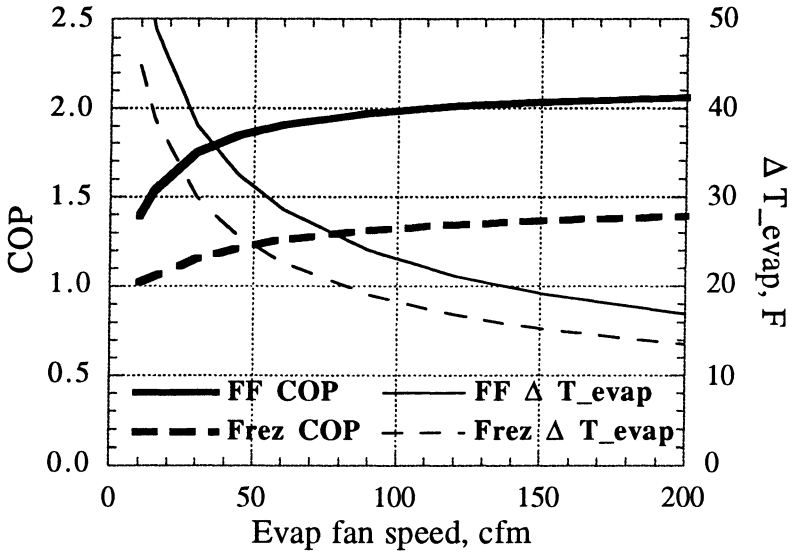

Figure 2.3 Evaporator fan speed change effects (1)

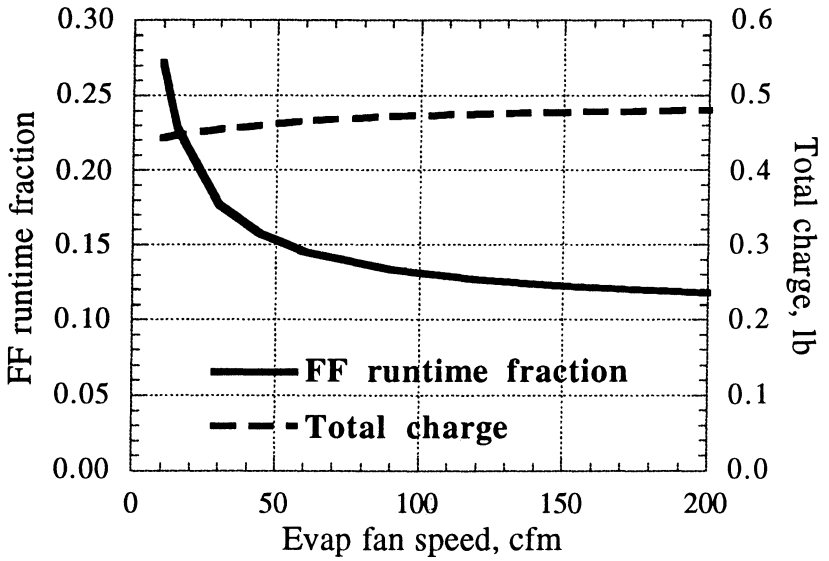

Figure 2.4 Evaporator fan speed change effects (2)

Increasing the condenser fan speed affects the system COP in the same way as increasing the evaporator fan speed. The results shown in Figure 2.5 are very similar to those in Figure 2.3. The condenser fan installed in the original system produced approximately 116 cfm.

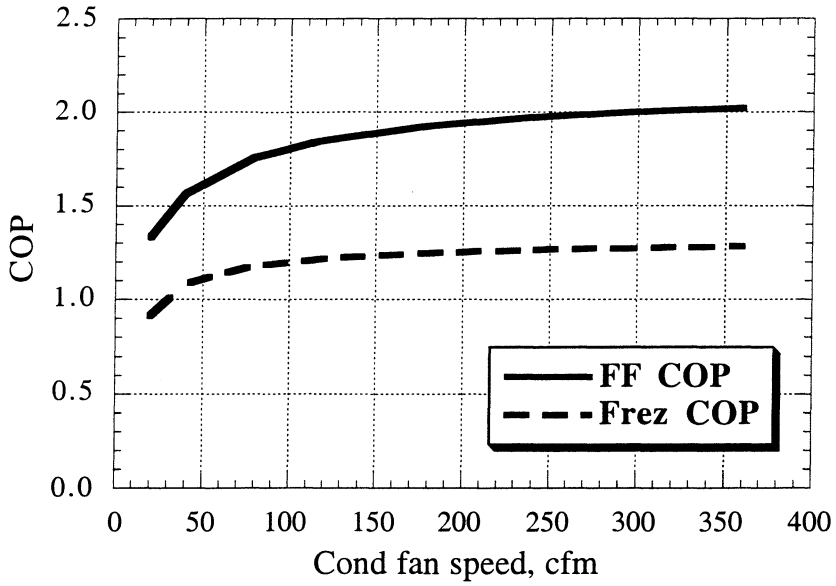

Figure 2.5 Condenser fan speed change effects (1)

Doubling either fan speed leads to roughly a 7% increase in the fresh food mode COP. However, the fresh food runtime fraction does not drop nearly as much when the condenser fan speed is increased, as in the case of the evaporator fan (see Figures 2.4 and 2.6). This implies that fewer cycling losses might be introduced by speeding up the condenser fan than the evaporator fan.

It should be noted that faster fans produce extra noise, with the noise power roughly proportional to the cube of the speed. These fans also require extra energy to operate and could have shorter lifetimes. All of these considerations set a limit the maximum fan speed.

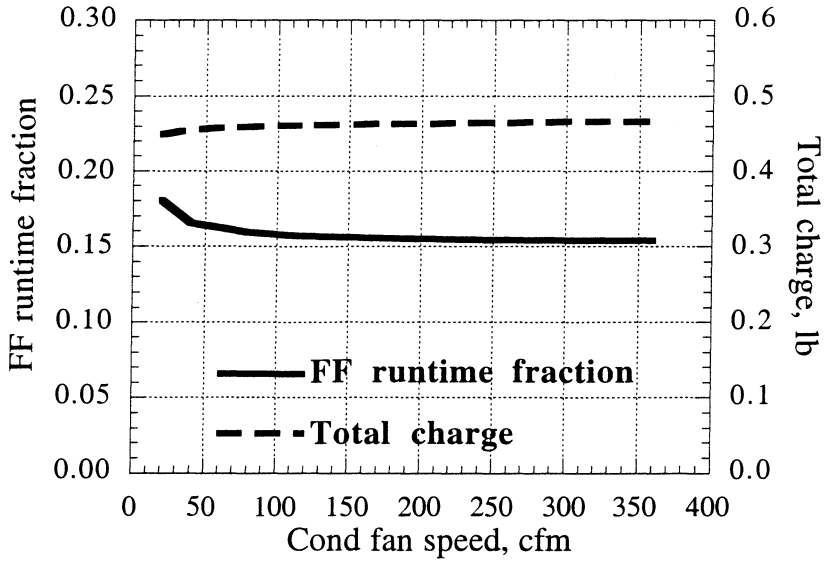

Figure 2.6 Condenser fan speed change effects (2)

2.2.3 Evaporator and condenser size

Increasing the size of a heat exchanger has the same kind of effect on the system performance as speeding up the fans. However, larger heat exchangers cost more to produce than faster fans and might require extra space, thus reducing the usable volume inside the compartments. Alternatively, since the dual-temperature evaporator system allows for self-defrost during the off-cycle, the evaporator fin density might be increased without being afraid of ice formation blocking the air flow.

As in the previous section, higher air side heat transfer coefficients in the evaporator lead to higher steady state COPs, as demonstrated in Figure 2.7. The base case evaporator area was 25.2 ft^2.

The tradeoff between steady state COP and transient losses has the same nature as described above for the evaporator speed. The fresh food runtime fractions for the system are shown as a function of the evaporator area in Figure 2.8.

Finally, the trends predicted for the COP and runtime fraction as the condenser area is being varied are presented in Figures 2.9 and 2.10, which look very similar to the results obtained for the condenser fan speed variation in the previous section. The original system included a condenser with 13.7 ft^2 of total surface area.

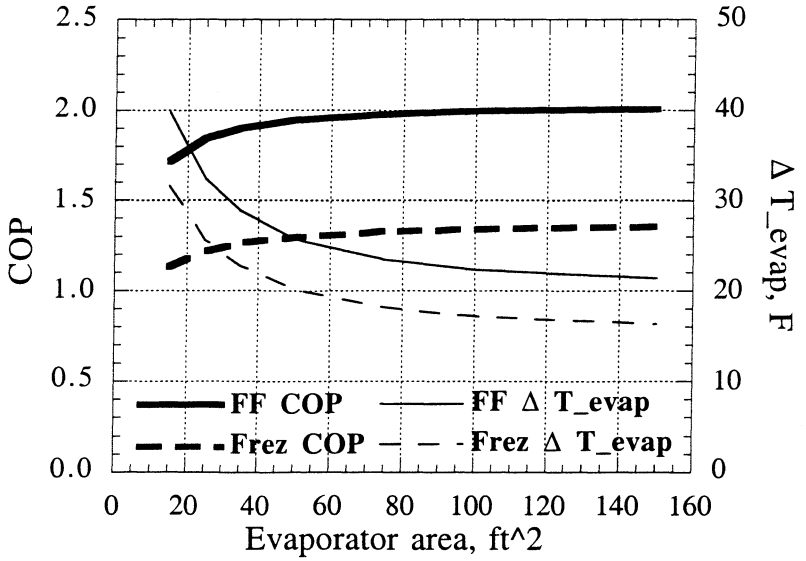

Figure 2.7 Evaporator size effects (1)

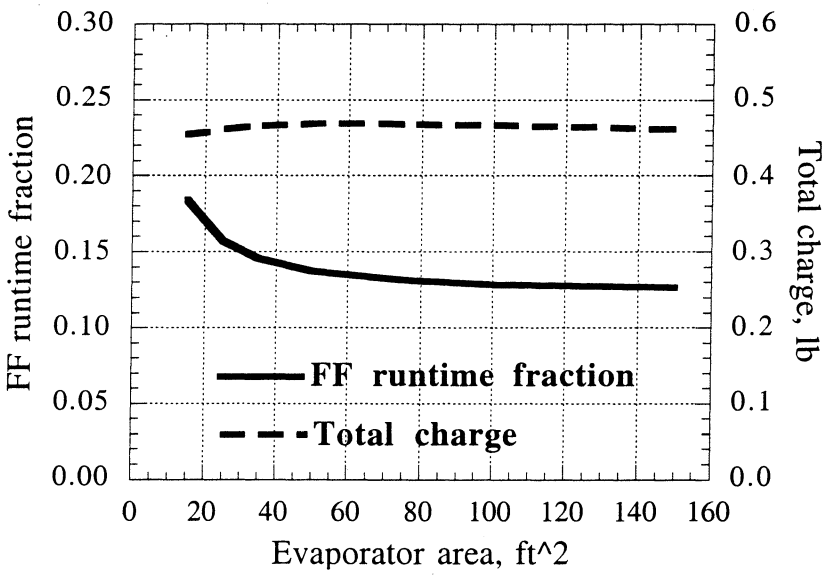

Figure 2.8 Evaporator size effects (2)

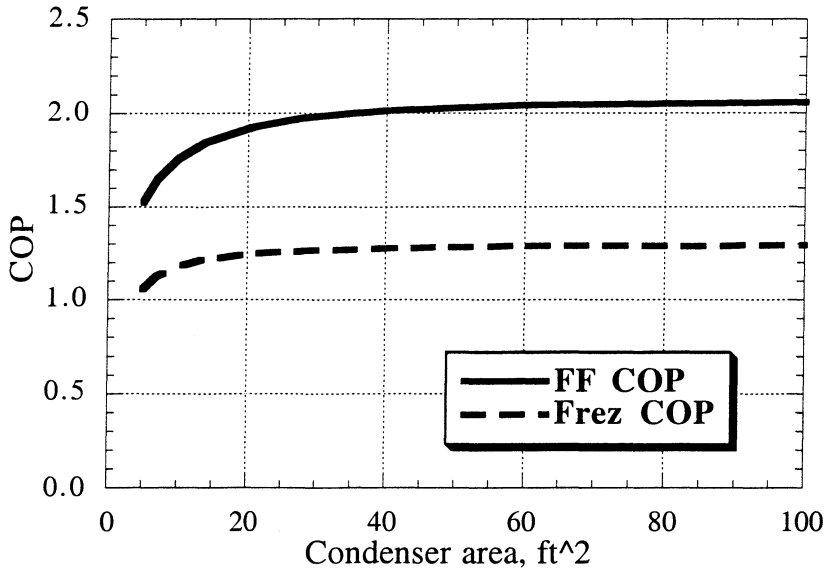

Figure 2.9 Condenser size effects (1)

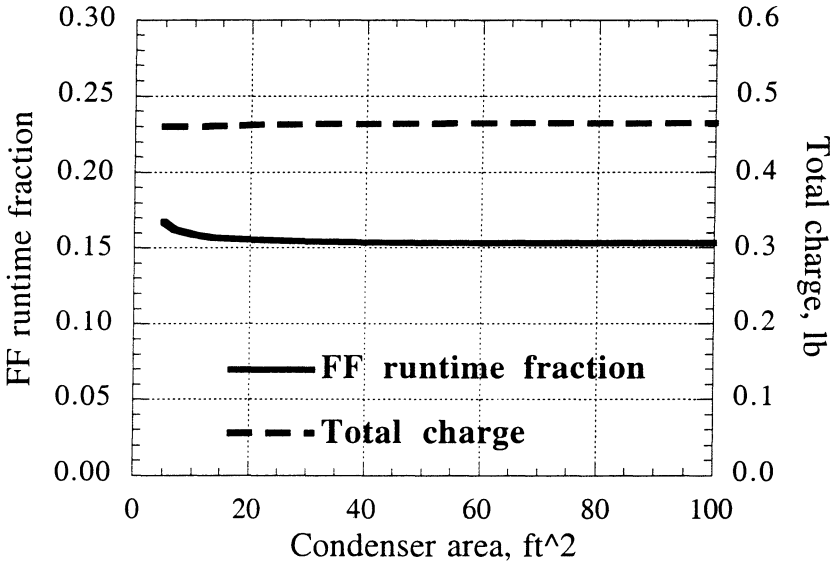

Figure 2.10 Condenser size effects (2)

2.3 Options overview

It is clear that the most effective method to increase the COP of a dual-temperature evaporator system is to reduce the speed of the compressor while running in the fresh food mode. Table 2.1 shows that even if both condenser and evaporator are replaced with units that are twice as large, and both fan speeds are increased by a factor of two, the combined effect of all these changes on the fresh food COP would be approximately equal to the effect of cutting the compressor speed in half.

Design options	Fresh food mode COP increase
Double evaporator area	5.5%
Double condenser area	7.0%
Double evaporator fan speed	6.9%
Double condenser fan speed	6.9%
Cut compressor speed in half	**22.0%**

Table 2.1 Options for improving fresh food mode COP

Finding an optimal balance between adding more evaporator and condenser areas and speeding up the fans in the fresh food mode depends on specific cost considerations, space allocation and noise calculations that are beyond the scope of this study.

Nevertheless, significant energy savings can be achieved by simply reducing the compressor speed by a factor of two while the system is running in the fresh food mode. Table 2.2 shows that even with this relatively small turndown ratio, the overall system energy use can be cut by 8-10% over the entire range of typical ambient temperatures. What is remarkable is that greater savings are achieved at higher room temperatures, which is exactly where they are most welcome.

Ambient temperature, F	System energy use, kW-hr/yr		Predicted energy Savings, %
	Conventional	Dual-temp.	
70	525	480	8.5
90	833	756	9.2
110	1223	1105	9.7

Table 2.2 Predicted overall energy savings

Chapter 3

Evaporator design

3.1 General design considerations

In a dual-temperature evaporator system, the evaporator should be located in a place where the amount of ductwork required to sequentially cool the freezer and the fresh food compartments is minimized. The ductwork itself should be laid out in such a way that the total air pressure losses are minimized and the required evaporator fan power is reasonably small. Finally, the control system and the mechanical valves responsible for redirecting the air to the appropriate compartments should be kept as simple as possible and introduce minimum pressure losses or undesired heat transfer.

In the original 25 ft^3 side-by-side Amana test unit, the evaporator was located on the back wall of the freezer section. The cold air flow was directed upward and then pushed through a set of small slots. The air was then re-circulated through a grille near the bottom of the evaporator. Part of the air flow passed through a damper near the top of the freezer and entered the fresh food section. However, only about 6% of the air flow was directed into the fresh food compartment, since the desired temperature there was higher than in the freezer. It would have been very impractical to keep the evaporator in the same location when the entire air flow have to be directed into each compartment at some point in the cycle. For one thing, the pressure losses while operating in the fresh food mode would be extremely high. Also, it would be undesirable to put the control valves in the freezer where the risk of frosting is higher.

Three alternative locations for the evaporator were considered. Due to the danger of freezing the controls, the new prototype evaporator had to be installed on the fresh food side. Another common feature of all the proposed designs was that the evaporator would be mounted near the top the compartment, so that the natural convection would help distribute the cold air downward. Also, this would help to reduce the fan power, taking advantage of buoyant forces that bring the warm air back up near the top of the refrigerator compartments.

The first option was to mount the evaporator on the mullion which is located between the compartments. This way, the distance the air has to flow to enter either section would be minimal and therefore the air pressure drop could be very low. The biggest drawback of this design is that the evaporator would occupy part of the most valuable space up front near the refrigerator door.

The second approach was to locate the evaporator along the back wall of the fresh food compartment. This way the evaporator would only take up the least desirable and hard to reach space behind the shelves. However, the ductwork and the damper configuration for such a design is much more complex and less accessible than that for the one discussed above.

Finally, the third option was to attach the evaporator to the mullion, making its face area nearly square instead of rectangular so that it doesn't extend far toward the front of the compartment. This design combines the advantages of the previous two. In addition, the dimensions could be selected so that the air flow contraction before it enters the fan would be more gradual and would introduce less pressure drop. The final design was based on this last approach and is shown in Figure 3.1.

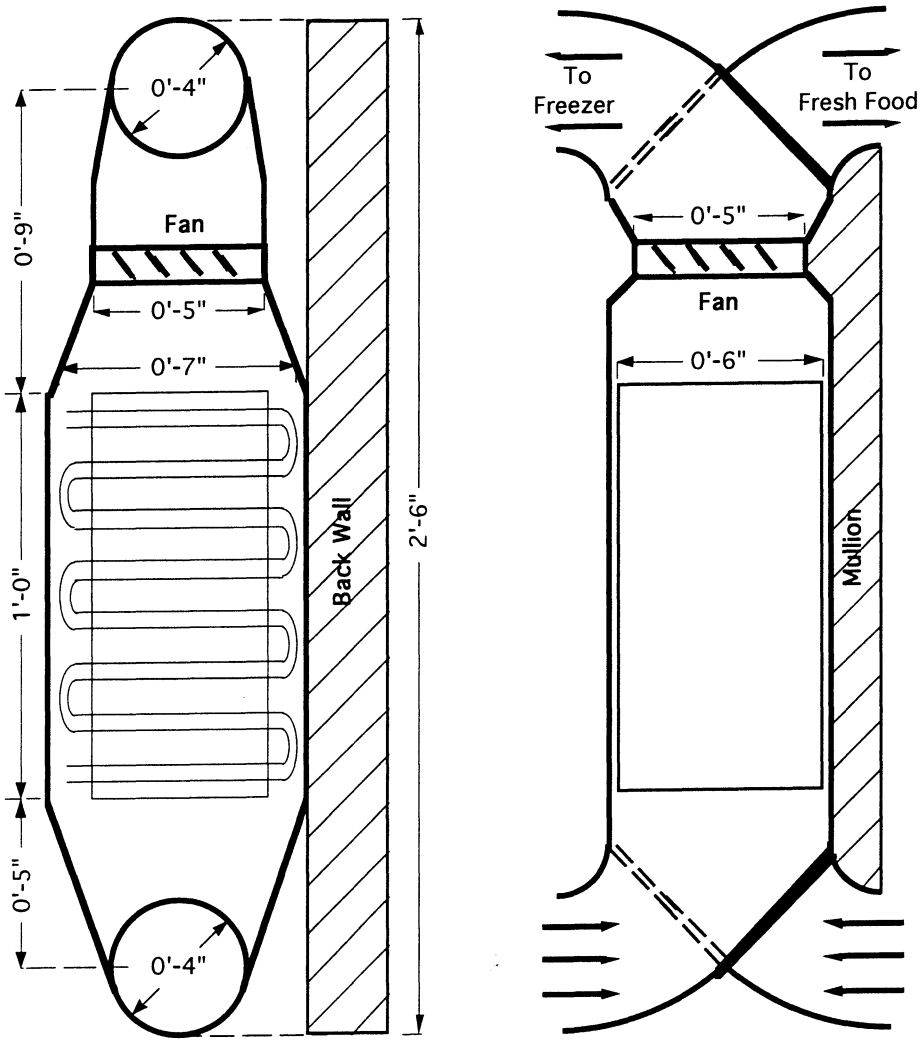

Figure 3.1 Evaporator coil and ductwork diagram

Figure 3.2 shows schematically where the original and the new evaporators were placed. The ductwork is not shown and the space requirements for the complete installation are therefore higher than indicated below.

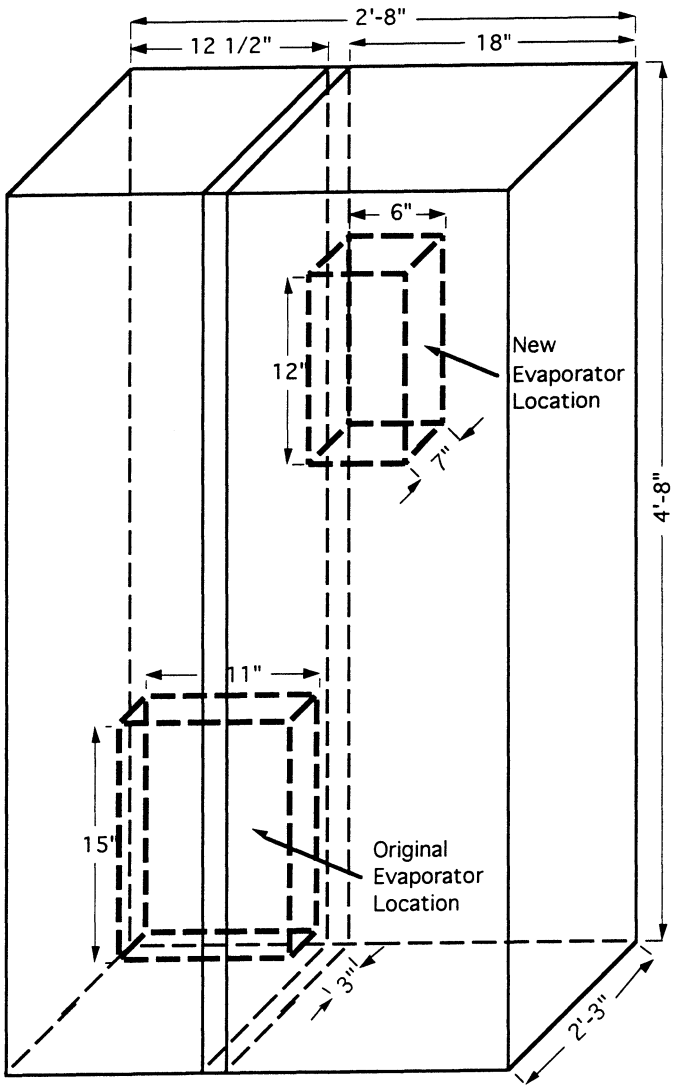

Figure 3.2 Evaporator location diagram

The evaporator fan has to be installed above the evaporator to protect it from melted ice dripping off the coil. The distance between the evaporator and the fan should be such that the sudden contraction of the flow cross sectional area would not introduce excessive pressure losses. This means that the evaporator cannot be located right at the top of the compartment.

3.2 Prototype coil configuration

In order to build a heat exchanger of the unconventional cross section (7" deep and 6" wide), three 2" thick coils were manufactured and joined together by Peerless of America. However, these coils had to have different tube spacing and fin pitch than the mass-produced ones. A variety of fin efficiency, heat transfer and head loss calculations were done to determine these parameters prior to prototype construction, as described later in this chapter.

The tubes in the new heat exchanger were circuited in a different way than in the original coil, as shown in Figures 3.3 and 3.4. While, the same kind of standard 5/16" aluminum tubing was used in both cases, the original evaporator used 0.007" thick aluminum fins which were replaced by somewhat lighter 0.00575" in the new coil. Finally, the tube bend diameters were unchanged so that the new prototype unit could be easily manufactured using standard tools for tube bending. Air flow was upward in both cases.

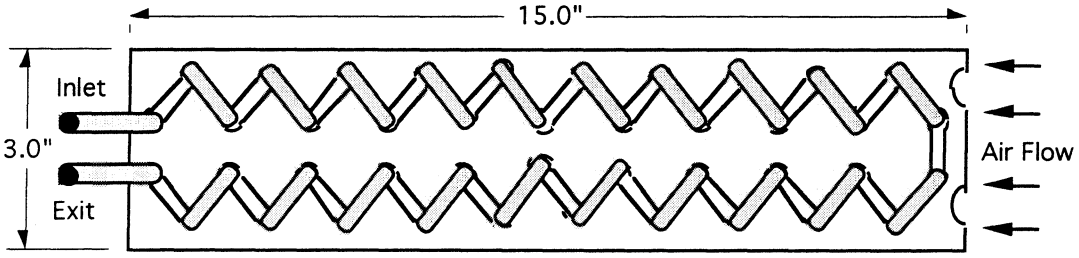

Figure 3.3 Original evaporator coil circuiting

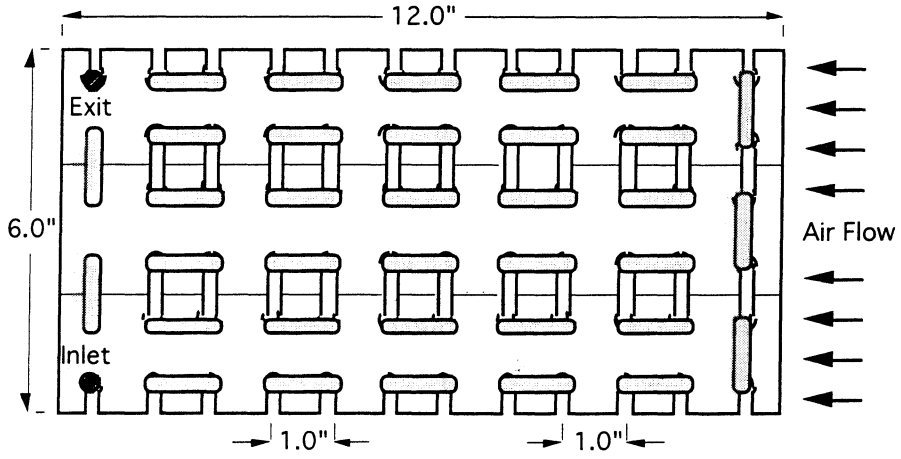

Figure 3.4 New evaporator coil circuiting

The fin pitch has been cut in half since the new fresh food air defrosting mechanism should be capable of preventing frost formation effectively and can remove frost more frequently. The new fin density was set at 10 fins per inch, compared to 5 fins per inch for the original coil. Since considerable frost accumulation could still occur during the longest on-cycles, particularly near the bottom of the coil where the moisture might concentrate, the 5 fins per inch density was used for the fins around the two bottom rows of tubes.

The new evaporator is twice as thick as the original coil (6" vs. 3"). However, since it is shorter (12" vs. 15") and narrower (7" vs. 10"), the overall volume of the new coil is only slightly larger than that of the original one. The finned volumes of these coils are essentially equal (around 360 in^3).

3.3 Evaporator tube spacing

It was desirable to keep the fin efficiency the same as in the original design. The Gardner equations (1945) modified by Schmidt for a staggered tube arrangement (1949)) were used to find how the tube spacing influences heat exchanger effectiveness. Complete guidelines on the use of these correlations were given by Korte and Jacobi (1997).

The average distance between the tubes of the existing evaporator was roughly 1.15 inches. This distance was calculated as the geometric mean of the tube spacing in the direction normal to air flow and the spacing in the flow direction. It was estimated that the fin efficiency of the original design was about 92%. If the number of tube passes was cut in half, the fin efficiency would be only 81%, providing about 12% less effective heat transfer compared to the base case. Figure 3.5 shows how the average tube spacing affects the fin performance.

It is obvious that in order to keep the fin efficiency around the industry standard 85-95%, the tube spacing should have been held roughly the same as in the original coil. In other words, if the thickness of the evaporator was to be doubled, the number of tube passes should have been at least doubled as well in order to avoid a serious degradation of fin performance.

In fact, the new design takes advantage of an even closer tube spacing of about 1.0 inch, which brings the fin effectiveness up to 95%. The tradeoffs associated with this comparatively tight spacing are discussed in the next section when the pressure drop over the tube bank is calculated.

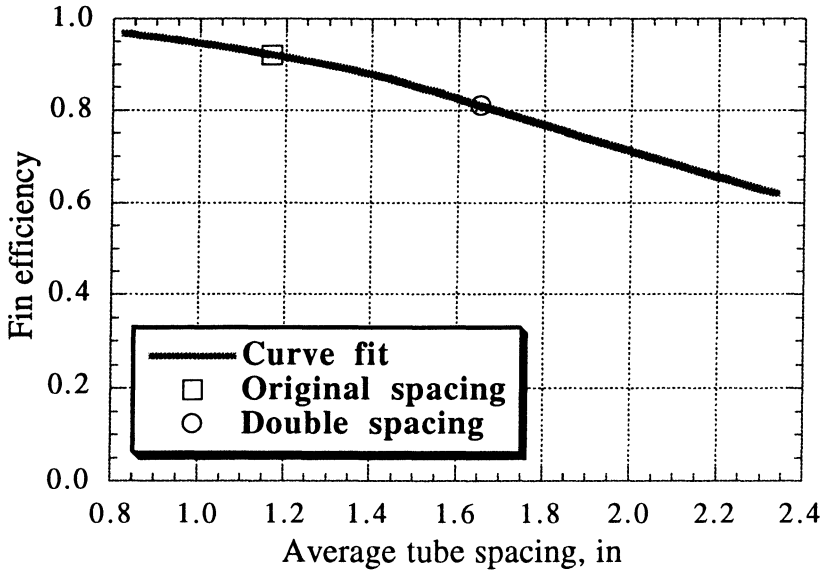

Figure 3.5 Evaporator fin efficiency vs. tube spacing

3.4 Air-side pressure drop calculations

First it was necessary to estimate the pressure losses in the original design. The goal while designing the new coil was to keep the pressure losses approximately equal to those of the original design, to ensure that the fan energy usage was not increased dramatically. Secondly, the relative contribution of the losses in the ductwork and those in the evaporator coil were evaluated. The new evaporator was designed so that the minimum number of fins and tubes provide adequate heat transfer yet do not block the flow and do not create unnecessary pressure drops.

3.4.1 Pressure losses in the ductwork

About 94% of the air flow was originally directed into the freezer compartment. The total flow rate was assumed to be 44.5 cfm as estimated by Srichai and Bullard (1997) using data obtained over a wide range of operating conditions. It was impractical to calculate the pressure losses for the air flowing into the fresh food compartment due to the fact that the ductwork was sealed into the mullion. However, this air flow was only about 1/17 of the total, and the length of the fresh food duct was much longer than that for the freezer section. Therefore, the actual overall losses were probably higher than if all the air were directed into the freezer. For our design evaluation the pressure drop was calculated conservatively, as if the entire flow was directed into the freezer.

The head losses consist of the major losses due to pipe friction h_f, and the minor losses due to pipe transitions and fittings h_m, and can be calculated using the following two equations (Ahmed, 1987):

$$h_f = f\frac{LV^2}{8Rg}, \tag{3.1}$$

where

f is the friction factor,
L is the piping length,
V is the flow velocity,
R is the hydraulic radius of the pipe;

and

$$h_m = \sum_i K_i \frac{V^2}{2g}, \tag{3.2}$$

where

K_i is a loss coefficient.

It should be noted that the calculation of frictional losses as defined above should be modified to account for the fact that the flow was not fully developed as the total duct length was only a few times larger than the duct hydraulic radius. However, such modification was not done because the duct frictional losses make only a relatively small contribution to the overall pressure drop.

Since not all the air reached the top of the chamber, L was set equal to about half of the total distance between the evaporator and the highest slot through which air entered the chamber. The same was done to estimate the average velocity. For a rectangular pipe, the hydraulic radius is calculated as:

$$R = \frac{ab}{2(a+b)}, \tag{3.3}$$

where a and b are the cross sectional dimensions.

Two contractions were considered. The first one was at the points where the air flowed around the evaporator and entered the piping. The second contraction was where the air entered the freezer compartment.

The above equations were used to calculate the total head loss. It turned out that the only significant head loss occurred at the point where the flow entered the chamber and was undergoing a sudden contraction. Using the loss coefficients of 0.4 to 0.5 from Ahmed, the total head loss was roughly estimated to be 0.038 inches of water. The losses due to flow contractions and pipe bends were about two orders of magnitude larger than

frictional losses. The flow in the duct was laminar with $Re \approx 2700$ which made frictional losses negligible compared to the losses due to flow contractions and turns which were both sudden and sharp.

The same kind of loss calculations as presented above were applicable to the new design. It was desirable to use circular piping at the point where the air goes through the mullion, in order to ensure smoother flow. The minimum diameter of this opening was selected in such a way that the total new estimated head loss was lower than that for the original design by at least 30%. This brought the total head loss down to roughly 0.027 inches of water.

Based on the above considerations, the radius of the opening in the mullion was selected to be 2". The opening for the air going into the fresh food compartment was made exactly the same due to symmetry. Again, the only significant duct loss occurred when the air flow was going through the contraction and made a 90° turn before it passed through the opening in the mullion.

3.4.2 Pressure losses over the evaporator coil

The pressure drop correlations by Gray and Webb (1986) were used to approximate the head losses associated with the flow over the evaporator coil. The flow rate was again assumed to be 44.5 cfm.

The pressure drops due to the fins and the tubes were estimated separately and then superposed, as it is usually done in the literature. The pressure drops were calculated using the following equation

$$\Delta p_f = f_f \frac{A_f}{A_{\min}} \frac{G^2}{2\rho} \tag{3.4}$$

and

$$\Delta p_t = f_t \frac{\rho V^2}{2} N_t, \tag{3.5}$$

where

Δp_f and Δp_t are the pressure drops due to fins and tubes respectively,
f_f and f_t are the appropriate friction factors obtained from correlations below,
A_r and A_{min} are is the fin heat transfer areas and the minimum flow area,
V and G are the flow velocity and the mass flux,
ρ is the average air density,
N_t is the total number of tube passes.

The following calculations depend on the Reynolds number as defined below:

$$\mathrm{Re} = \frac{D_{eff} G}{\mu}, \tag{3.6}$$

where

D_{eff} is the hydraulic diameter of the tubing,
μ is the kinematic viscosity of air at the average temperature

The friction coefficient due to fins (f_f) was found as:

$$f_f = 0.508\,\mathrm{Re}^{-0.521}\left(\frac{S_t}{D_{eff}}\right)^{1.318}, \tag{3.7}$$

where

S_t is the tube spacing normal to flow.

For *Re* on the order of 1000 a curve fit of a graph presented by Zukauskas (1972) was used to estimate the friction coefficient due to tubes (f_t) as follows:

$$f_t = 2.0\,(1.0736\,C^{-0.7338}), \tag{3.8}$$

with a dimensionless parameter C that is defined as

$$C = \left(\frac{S_t}{D_{eff}} - 1\right)\left(\frac{S_l}{D_{eff}} - 1\right), \tag{3.9}$$

where

S_l is the tube spacing in the air flow direction.

The base case evaporator had a staggered tube arrangement. Therefore, tube spacing S_l and S_r, as defined above, did not make physical sense. Instead, the number of tube passes per row (N) could be assumed to be either 2 or 4, with appropriate tube spacing value adjusted separately for each case. Depending on the assumption, the above correlations gave substantially different results. The actual pressure drop lies somewhere between the two estimates, perhaps closer to the 2 tube passes assumption.

The new evaporator design had 6 inline tube passes and evaluating the pressure drop over this coil was more straightforward than for the original one. A simple computer program was used to calculate all the parameters presented in Table 3.1.

	Pressure drop [inches of H_20]			Reynolds	Min. flow area
	due to tubes	due to fins	total	number	[in^2]
Original (N_t=2)	0.21	0.14	0.35	1120	19.0
Original (N_t=4)	0.38	0.12	0.50	1510	14.1
Original (average)	0.30	0.13	0.42	1315	16.6
New design	0.32	0.13	0.45	1125	20.7

Table 3.1 Pressure drop over the evaporator coil

In spite of the fact that the total fin area almost doubled due to closer fin pitch and the total number of tube passes was increased by about 60% (from 42 to 72), the overall pressure drop over the coil was not increased substantially. This can be explained by the fact that the face velocity decreased by about 20% due to the larger cross sectional area of the evaporator. The pressure drop has a quadratic dependence on the velocity, which leads to a lot smaller losses than one might expect. Also, the new unit was shorter, which further reduced the head losses.

3.4.3 Final pressure drop considerations

On one hand, the head losses in the ducts were reduced by 30%. On the other hand, the losses over the evaporator coil were kept about the same. Therefore the goal of decreasing the total pressure losses was achieved, while a lot smoother flow due to improved duct design was ensured. Better heat exchanger performance could also be achieved due to larger number of tubes and fins in an evaporator of roughly the same volume. This effect is discussed in the next section.

3.5 Air-side heat transfer coefficient

The purpose of this section is to verify that the redesigned evaporator had equal or better heat transfer characteristics than the original one. Calculations below were done to confirm that the new geometric arrangement with larger flow face area and more fins could in fact provide enhanced heat transfer.

A dimensionless parameter used in the heat transfer correlations available in the literature is called the Colburn or *J-factor*, which is defines as:

$$J = St \cdot \mathrm{Pr}^{2/3}, \tag{3.10}$$

where

St is the Stanton number,
Pr is the Prandtl number,

which are in turn found as:

$$St = \frac{h}{G C_p} \tag{3.11}$$

and

$$\Pr = \frac{\mu C_p}{k}, \tag{3.12}$$

where

C_p is the specific heat of air,
h is the heat transfer coefficient.

For a heat exchanger with four passes per row of tubes ($N = 4$), the *J-factor* can be estimated using the following correlation by Gray and Webb:

$$J_4 = 0.14\,\mathrm{Re}_{Deff}^{-0.328}\left(\frac{S_t}{S_1}\right)^{-0.502}\left(\frac{s}{D_{Eff}}\right)^{0.0312}, \tag{3.13}$$

where

s is the spacing between adjacent fins,
D_{eff} is the hydraulic diameter of the tubing.

The Gray and Webb correlation for heat exchangers with the number of tube passes other than four is based on the above correlation for J_4. However, a correction factor, referred to as *R-factor* is introduced in such a way that

$$J_N = J_4 \cdot R, \tag{3.14}$$

where

$$R = 0.991\left[2.24\,\mathrm{Re}_{Deff}^{-0.092}\left(\frac{N}{4}\right)^{-0.031}\right]^{0.607(4-N)}. \tag{3.15}$$

Just like for the pressure drop estimates presented in the previous section, the heat transfer coefficient of the original evaporator was first estimated for a 2 tube passes case and then for a 4 tube passes case. Using the above correlations for these two cases, the overall heat transfer coefficient was found to lie between 1.14 Btu/h/°F and 2.39 Btu/h/°F. The simple average of the two is 1.77 Btu/h/°F and the actual experimentally estimated value was 1.56 Btu/h/°F. For comparison purposes this kind of accuracy seems rather adequate.

The heat transfer coefficient was also found for the new evaporator. It was estimated to be 1.74 Btu/h/°F, which means that the heat transfer coefficient of the new coil should be very similar to that of the originally installed unit.

Chapter 4

Compressor selection

4.1 Selection criteria

The compressor selection process for a dual-temperature evaporator refrigerator system is somewhat different from that for a conventional system. First of all, in order to get the desired energy savings while operating in the fresh food mode, the compressor should be operating at a lower speed than in a conventional system. This means that a dual- or a variable-speed unit is required. The higher the turndown ratio, the better operating efficiency is expected.

Secondly, if the compressor speed is adjusted while operating in the freezer mode, system performance can be further improved. In order to provide such precise control over the system operation it is desirable that the compressor speed could be controlled continuously over the entire range of compressor speeds.

On one hand, the compressor pull down capacity, that is its ability to provide enough flow at extreme ambient conditions, should be adequate. On the other hand, the compressor should not be oversized. If it is, then while operating under "typical" ambient conditions the system would not work efficiently because the runtime fraction of the refrigerator operating in the fresh food mode would be very low. If the compressor speed cannot be turned down to effectively increase this runtime fraction, the cycling losses might be extremely high.

The originally installed compressor is an Americold model RV800, rated at 800 Btu/hr nominal capacity at 2400 rpm. This rating point corresponds to a condition with -10°F condensing temperature and 130°F evaporating temperature. This compressor could only be set to operate at 2400 or 3600 rpm. Unfortunately, this particular unit turned out to be significantly bigger than the one required for the new system.

The alternative choices were unit #1 which is rated at 670 Btu/hr (about 84% of the capacity of the original compressor) and unit #2 with 420 Btu/hr capacity (about 53% of the size or the original compressor). Without losing lubrication, both compressors can be turned down to operate at a minimum speed of 1800 rpm, about half of the 3600 rpm nominal maximum speed.

4.2 Performance evaluation

The maximum ambient temperature at which a compressor can still maintain the set temperature of 5°F in the freezer and 45°F in the fresh food compartments simultaneously was first estimated. A conventional system model was used to calculate this temperature for each compressor running at the maximum operating speed non-stop (with the runtime fraction equal to 1.0). It turned out that the original unit and unit #1 were capable of operating around 110°F and 106°F respectively, while unit #2 provided enough capacity to keep the compartments cool only at temperatures below 95°F. It should be noted that it might take a very long time to actually cool the system under these extreme conditions.

Capacity rating, Btu/hr	Compressor power, Watts	Max. ambient temperature, °F	Overall COP
800	174	110	0.82
670	146	106	0.92
420	92	95	1.20

Table 4.1 Maximum pull down temperatures

Due to the fact that the dual-temperature evaporator system should have higher overall COP than the conventional one described above, the next step was to calculate the combined runtime for the freezer and the fresh food modes as compared to the mixed air case. Table 4.2 shows that 4 to 8% of the runtime could in fact be used for the evaporator defrost with the warm fresh food air flow over the coil. These results were computed for the 800 Btu/hr compressor, but similar runtime reduction could be achieved for the other two compressors. Alternatively, the dual-temperature system could pull down at a slightly higher maximum ambient temperature than indicated in Table 4.1.

Ambient temperature , °F	Runtime				Percent usage
	Fresh food	Freezer	Total	Mixed air	
60	0.03	0.27	0.30	0.32	96
90	0.11	0.50	0.61	0.67	92
110	0.20	0.72	0.92	1.00	92

Table 4.2 Compressor usage vs. ambient temperature

Each compressor was further evaluated to estimate the runtime fractions required to cool each compartment separately at two ambient conditions, 60°F and 90°F. These results are presented in Table 4.3.

Operating condition	Capacity rating, Btu/hr	3600 rpm		1800 rpm	
		Runtime	COP	Runtime	COP
Fresh Food 90° ambient	800	0.11	1.40	0.15	1.78
	670	0.12	1.50	0.17	1.86
	420	0.15	1.76	0.22	2.02
Fresh Food 60° ambient	800	0.03	1.76	0.05	2.25
	670	0.04	1.90	0.06	2.34
	420	0.05	2.23	0.08	2.36
Freezer 90° ambient	800	0.50	0.97	0.70	1.23
	670	0.54	1.05	0.77	1.27
	420	0.68	1.22	-	-
Freezer 60° ambient	800	0.27	1.30	0.37	1.60
	670	0.29	1.39	0.42	1.64
	420	0.36	1.59	-	-

Table 4.3 Compressor runtimes at 3600 and 1800 rpm

At 90°F unit #1 operating at 1800 rpm needed 0.17 runtime to cool the fresh food compartment and an additional 0.77 runtime to cool the freezer. This means that even under the more efficient low speed operation this compressor had sufficient capacity to be used at this ambient temperature. Unit #2 required 0.22 runtime for fresh food operation at 1800 rpm and 0.68 runtime for the freezer at 3600 rpm. This compressor was not capable of cooling the system unless the speed was set close to the maximum in the freezer mode.

In all the cases considered, the overall steady state COP was improved by at least 4 to 8% over the original compressor when unit #1 was used. Unit #2 would have brought the steady COP up by additional 10-15% as compared with unit #1.

Ideally, unit #1 with larger turndown ratio would make a perfect fit. However, under the circumstances, even though this unit might not provide the advantage of running the system efficiently over the entire range of ambient temperatures, it would provide the pull down capacity essential for the refrigerator operation. Therefore, the 670 Btu/hr unit was selected (model RV670-1, serial number A-7926 B-2157).

Chapter 5

Capillary tube selection

5.1 Performance requirements

The dual-temperature evaporator system has very dissimilar operating conditions while cooling the freezer or the fresh food compartments and has to be separately optimized for each mode. One way of making sure that the system operates efficiently in both modes is by varying the compressor operating speed, as demonstrated in Chapter 2. However, the compressor selected for the prototype refrigerator, as described in Chapter 4, has an inadequately limited turndown.

This means that even by turning the compressor down to the minimum operating speed during the fresh food mode operation, it would not be possible to bring the refrigerant mass flow rate down low enough to match the mass flow rate of the system operating in the freezer mode at full compressor speed. In order to deal with different flow rates in each mode, separate capillary tubes are required to be used exclusively during freezer as opposed to fresh food cooling.

An inexpensive solenoid valve can be used to switch the refrigerant flow at the same time as the air valves redirect the air flow. In the future, as compressors with wider range of operating speeds become available, the requirement for having two separate capillary tubes can be eliminated, as demonstrated later on in this chapter.

In order for the condenser to perform most efficiently, it is desired that only a few degrees of subcooling would be present at the condenser exit. Depending on the captube design, the conditions at this exit can be widely different. The goal of the following optimization was to make sure that at the design point of 5°F and 45°F freezer and fresh food temperatures respectively with 90°F ambient, the subcooling was present in both modes but did not exceed 10-20°F.

It was also important not to select excessively long captubes, which would lead to higher subcooling and lower mass flow, thereby causing a reduction in the overall refrigerator COP. Finally, the optimum refrigerator charge for both modes had to be the same, which was an additional design constraint. Alternatively, an accumulator or a receiver could be used to temporarily store the excess charge during the freezer mode operation. However, selecting and installing one of these devices would require transient system behavior analysis, which could not be done using the ACRC steady state model.

5.2 Freezer mode operation

In its original configuration, the side-by-side refrigerator test unit had 2-phase flow at the condenser exit over the entire range of normal operating conditions. The new dual-temperature evaporator design was expected to provide similar performance while operating in the freezer mode to that of the original system. Therefore, it was necessary to redesign the captube in such a manner that would force the system to have subcooling at least in a part of the range of typical operating conditions. Only points having measurable subcooling can be used to develop compressor maps and the inability to reach subcooling could cause problems with the map accuracy, as described in Appendix E.

The two ways to make sure that the system achieves condenser exit subcooling is either by decreasing the captube diameter or by increasing its length. The original system was equipped with a 10 foot long captube with 0.037" internal diameter. Captubes are also available with 0.031" and 0.028" internal diameters. Standard captubes are sold in 10 or 12 foot sizes but other lengths could be obtained if necessary.

C.T. dia., in	0.037			0.031			0.028		
Captube length, ft	**Condenser**		**System charge, oz**	**Condenser**		**System charge, oz**	**Condenser**		**System charge, oz**
	ΔT_{sub}, °F	**exit quality**		**ΔT_{sub}, °F**	**exit quality**		**ΔT_{sub}, °F**	**exit quality**	
6	0	0.27	3.53	0	0.13	4.33	0	0.07	4.93
8	0	0.19	3.90	0	0.07	4.99	0	0.02	5.95
10	0	0.14	4.24	0	0.03	5.71	***4***	***0.00***	***6.71***
12	0	0.10	4.55	0	0.01	6.28	***12***	***0.00***	***7.43***
14	0	0.07	4.87	4	0.00	6.70	18	0.00	8.47
16	0	0.05	5.20	9	0.00	7.11	22	0.00	9.45
18	0	0.04	5.57	14	0.00	7.66	25	0.00	10.17
20	0	0.02	5.84	17	0.00	8.36	28	0.00	10.68
22	0	0.01	6.11	20	0.00	9.03	30	0.00	11.08
24	1	0.00	6.42	23	0.00	9.59	32	0.00	11.38
26	3	0.00	6.57	24	0.00	10.03	34	0.00	11.63
28	6	0.00	6.74	26	0.00	10.39	35	0.00	11.84

Table 5.1 Captube performance in freezer mode

In the original system the suction line heat exchanger was located 4.45 feet downstream of the end of the liquid line and was 4.96 feet long. The outlet section of the captube leading to the evaporator was 0.67 feet long. While keeping the heat exchanger and outlet sections the same length as before, a variety of inlet section sizes were examined. This was done for each one of the three captube diameters available.

Table 5.1 shows the condenser exit conditions predicted by the ACRC simulation model as well as the suggested amount of refrigerant charge for a range of combinations of captube lengths and diameters. In each case it was assumed that the evaporator was fully utilized and was operating with 5°F of superheat at the exit. Also, these results have to be viewed as preliminary estimates because they were calculated using approximate parameters to characterize the evaporator and the compressor.

If either of the thicker captubes was installed in the system, it had to be considerably longer than the original 10 foot tube in order to produce subcooling. However, the captube with 0.028" diameter was found to be capable of forcing the flow to become subcooled even with only 10 or 12 feet of length. The new system has to be charged with about 7 ounces of refrigerant, exceeding the original requirement of 5.1 ounces by more than 30%.

5.3 Fresh food mode operation

It turns out that it would be easier to achieve subcooling at the condenser exit while operating in the fresh food mode. In fact, any of the two smaller captube diameters could be used. Table 5.2 shows all the options.

C.T. dia., in	0.037			0.031			0.028		
Captube length, ft	**Condenser**		**System charge, oz**	**Condenser**		**System charge, oz**	**Condenser**		**System charge, oz**
	ΔT_{sub}, °F	**exit quality**		**ΔT_{sub}, °F**	**exit quality**		**ΔT_{sub}, °F**	**exit quality**	
6	0	0.13	4.63	0	0.03	5.48	0	0.03	5.47
8	0	0.06	5.10	4	0.00	6.23	***19***	***0.00***	***7.42***
10	0	0.02	5.57	***14***	***0.00***	***6.89***	31	0.00	9.07
12	0	0.00	5.98	22	0.00	7.77	39	0.00	10.10
14	5	0.00	6.25	29	0.00	8.73	45	0.00	10.74
16	10	0.00	6.56	34	0.00	9.53	50	0.00	11.19
18	14	0.00	6.90	39	0.00	10.13	55	0.00	11.48

Table 5.2 Captube performance in fresh food mode

In order to select the captube length for the fresh food mode operation it was essential to make sure that the optimal refrigerant charge should be similar to that for the captube selected for the freezer mode. Therefore, the two options are a 10 foot long 0.031" diameter captube and an 8 foot long 0.028" diameter one. The advantage to using a thicker captube would be that it would have roughly the same length as the one used for the freezer operation, making it easier to run the two alongside of each other.

Additionally, a thicker captube would be less likely to suffer from clogging. Therefore a 0.031" diameter captube was selected to be used in this mode.

As an academic exercise, it can be shown that if the compressor operating speed range (max. speed / min. speed) could be boosted from a factor of 2 to a factor of 5, it would be possible to use the same captube in both modes. Table 5.3 shows the fresh food mode condenser exit subcooling as a function of the compressor turndown ratio. All the calculations were done for a 12 foot long 0.028" captube, just like the one that was selected for the freezer mode.

Compressor turndown ratio	**Condenser**		**System charge, oz**
	ΔT_{sub}, °F	**exit quality**	
0.50	39	0.00	10.10
0.45	35	0.00	9.94
0.40	32	0.00	9.74
0.35	27	0.00	9.30
0.30	25	0.00	9.38
0.25	19	0.00	8.89
0.20	***14***	***0.00***	***8.21***

Table 5.3 Captube performance vs. compressor turndown

The 0.20 turndown has a reasonable amount of subcooling and a total optimal system charge that is only slightly higher than that for the freezer operation in Table 5.1. Therefore, it would be highly advantageous to install a compressor with wider operating range since that would not only contribute to better performance, but would also allow for use of a single captube.

Chapter 6

Current and future experimental work

6.1 Experimental setup

Our experimental unit, an Amana side-by-side refrigerator, was heavily modified in order to be transformed into a dual temperature evaporator system. While most of the system's insulation and structural design was kept intact, many of the vital internal components were completely redesigned and replaced. The refrigerator was fully instrumented, as described in Appendix G.

6.1.1 Evaporator sub-system

The new evaporator coil was installed near the top of the fresh food compartment, as specified in Chapter 3. Figure 6.1 shows a picture of the new coil.

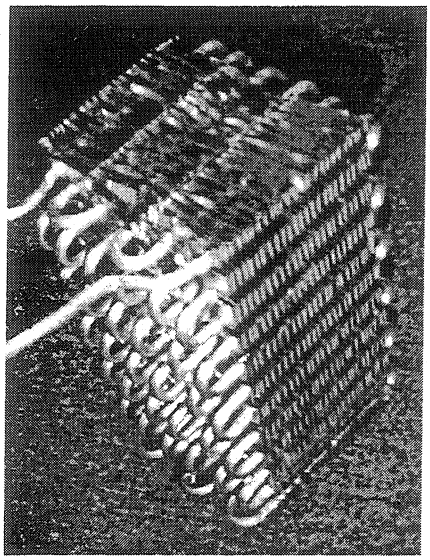

Figure 6.1 Redesigned evaporator coil

The coil was enclosed into an assembly built by Siebe Controls. This assembly consisted of a box with a transparent removable front panel and a system of two interconnected dampers that control the air flow. A photograph of the evaporator enclosure is shown in Figure 6.2

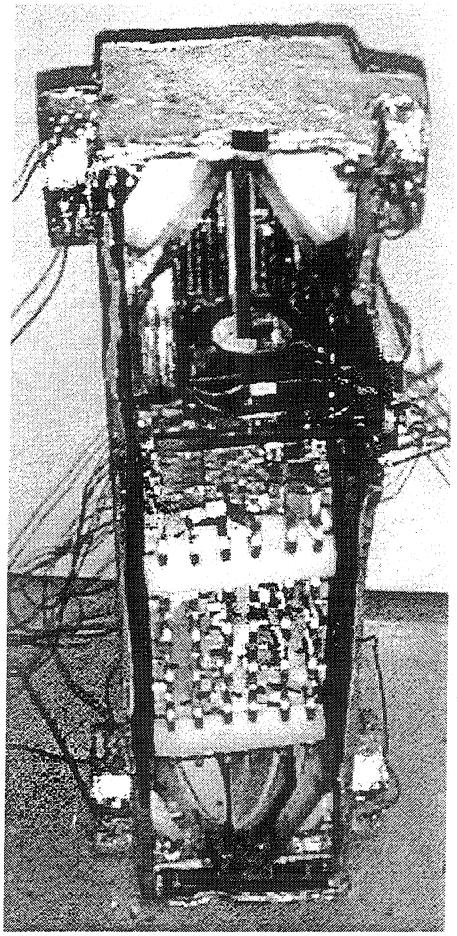

Figure 6.2 Evaporator air flow switching assembly

The damper at the bottom of the box controls warm air flow from one compartment into the evaporator while the damper at the top of it directs the cooled outlet air out into the same compartment. The two dampers are operated simultaneously by a remote switch which powers a single stepper motor mounted on the front panel. The switching controller was designed in such a way that the evaporator fan operation is stopped while the dampers are moving. This was done to prevent air flow from interfering with damper operation and to avoid air mixing between compartments.

A variable speed fan manufactured by Nidec (model TA500DC) was used to provide the flow over the coil. This fan is rated at 150 cfm while operating at its maximum speed when powered by 48 Volts DC. Lower speeds can be achieved by turning the voltage down.

The fan was mounted onto a removable plate above the evaporator coil, as pictured in Figure 6.3.

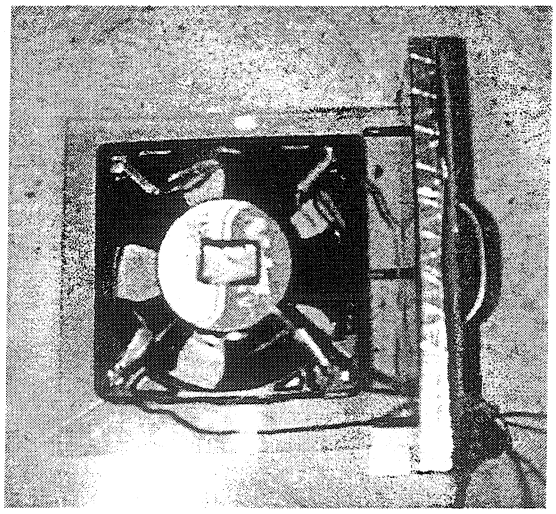

Figure 6.3 Evaporator fan

6.1.2 Captube sub-system

In order to allow flexibility in using capillary tubes of different diameters and lengths, the outlet sections of four parallel captubes were brazed to a the suction line for a length of 5 feet. The adiabatic inlet section of each captube can be "snipped" to provide optimal flow expansion.

A series of solenoid valves was used to direct the flow into an appropriate tube. Two of the captubes had internal diameter of 0.028 inches and initial lengths of 10 feet each. The third captube was the same length but measured 0.031 inches in diameter. Finally, the fourth captube was even thicker, being rated at 0.040 inches ID and longer, having 12 feet in length.

Figure 6.4 schematically shows locations of all the captubes and solenoid valves. By default, both of the on-off valves (denoted "In" and "Out") are closed. This way all the air can be evacuated out of the captubes after each snipping without having to recharge the entire system. In order for the system to operate, these two valves have to be actuated. Additionally, three Y-valves (also called three-way valves) were used to select the active captube. If none of them are actuated, the flow is directed into the first captube. If valve #1 is actuated, the flow is switched to the third captube. Depending on the position of valve #1, the other two Y-valves (#2 and #3) can be used to direct the flow into the second and the fourth captube respectively, if actuated. All valves are wired to be remotely controlled from a single console that can be used from outside of the environmental chamber.

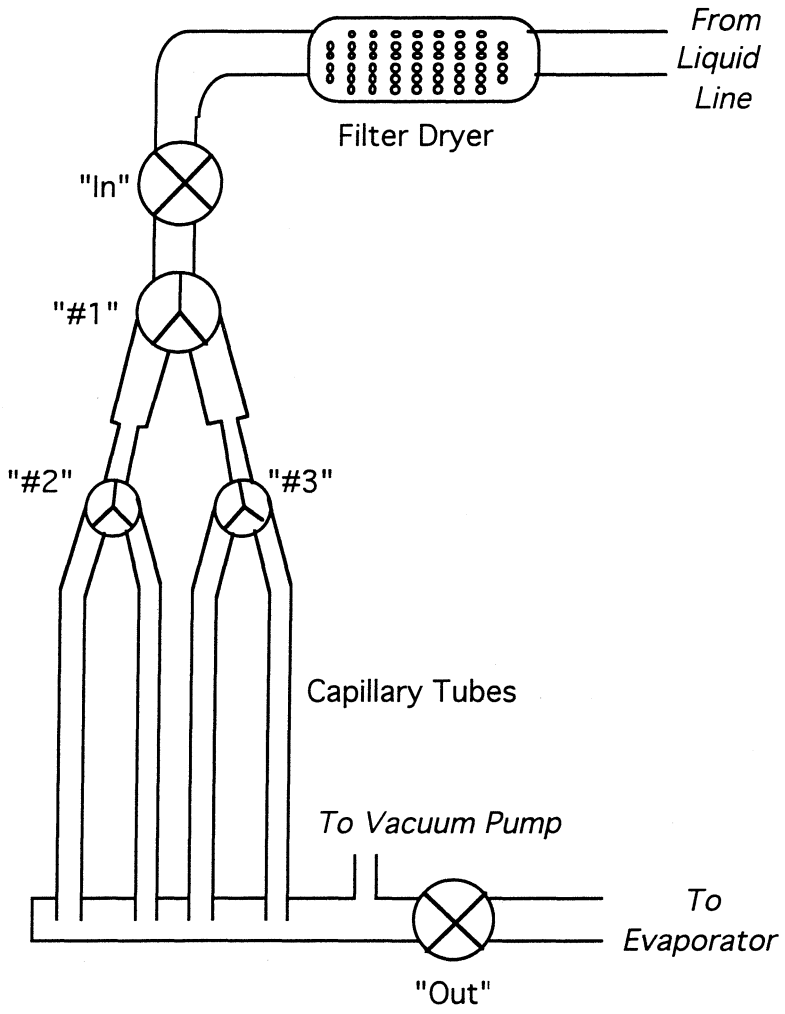

Figure 6.4 Capillary tubes configuration

In should be noted that in a production design only two captubes and a single solenoid valve could be necessary. The only reason this fairly complicated system was assembled was to provide extra flexibility necessary for performance optimization.

6.1.3 Other components

The new compressor was selected and installed based on the considerations described in Chapter 4. The compressor was hooked up to a controller that is capable of slowing it down by a factor of two.

The condenser coil and fan were retained from the original Amana refrigerator because simulations showed that they would provide adequate performance for the new design. See Chapter 2 for details.

6.2 System optimization

6.2.1 Captube snipping

Ideally, the first and the second captubes were intended for use during freezer operation, while the other two were meant for fresh food operation. However, before the system can be operating properly in each mode, snipping might be required.

Fresh food operation optimization should be done at the lowest compressor speed, while freezer cooling should be performed at the maximum setting. The optimization should seek to achieve about 5°F subcooling at the standard DoE test conditions. This will allow for accurate calculation of refrigerant mass flow at the most common operating conditions. It is also desired to provide measurable subcooling over a wider range of ambient and compartment temperatures that must be included in the comprehensive test matrix. This can be achieved by varying the compressor speed after the captube length has been finalized.

It would be extremely difficult to optimize captube lengths for both operating modes at the same time. Therefore, optimization should be performed for each compartment individually. In order to do that, the system should be brought to steady state with the entire evaporator air flow directed into the same compartment for an extended period of time. The freezer should be tested at 5°F and the fresh food at 45°F, both running in a 90° chamber.

First, the captube length and the refrigerant charge should be optimized for freezer compartment cooling. While doing that, the heater installed in the fresh food compartment should be turned off and the fresh food temperature should be allowed to stabilize at some value below ambient.

At each captube length, optimization should start with an overcharged system, having more refrigerant than suggested in Chapter 5. An overcharged system will typically have high condenser subcooling and low or non-existent evaporator superheat. The charge should be slowly reduced in an attempt to lower subcooling to about 5°F. If this is not possible, the captube should be snipped and the entire process repeated.

Once the first captube is selected, the amount of refrigerant charge that was shown to be optimal for freezer operation should be used during fresh food mode captube snipping. Again, the goal is to achieve low subcooling.

Whenever either the first or the second captube was cut down so that it provides adequate performance in the freezer mode, the switch for solenoid #2 should be set to direct the flow into this captube. The same goes for solenoid #3 that should be fixed for the fresh food operation. After this is done, only solenoid #1 will be used to control the refrigerant flow and must be flipped whenever the air flow is redirected into the appropriate compartment.

6.2.2 Compressor speed selection

After the captube length have been chosen, altering the compressor speed will become the main optimization technique. This flexibility can be used to control the operation effectiveness at the off-design points.

In particular, if at a lower ambient temperature it is shown that both compartments can be cooled down in less than 100% of runtime, the compressor can be slowed down while cooling the freezer. This way transient losses might be reduced, resulting in greater overall performance.

On the other hand, while operating at a high ambient temperature condition, cooling might become very inefficient. If this is the case, the compressor should be running at a higher speed during fresh food operation in order to provide greater overall cooling capability over time. The simulations in Chapter 3 have predicted that if the compressor is set at its maximum speed the system can be managed to operate even at ambient temperatures as high as 106°F.

6.2.3 Evaporator fan speed selection

Evaporator fan speed can be controlled using the variable voltage power supply that powers the evaporator fan installed in the system. By reducing the voltage over the fan, the evaporator air flow can be cut by a factor of about 2 or 3. The fan can still run, albeit very slowly, at voltages as low as 15 Volts DC, with 48 Volts being the maximum setting.

At each data point where the evaporator is not fully utilized, the evaporator fan can be turned down in order to reduce the overall UA of the coil. This would be an effective way to control the evaporator performance for experimental purposes and, particularly, the amount of superheat at the evaporator exit. However, such a strategy may not be optimal for a production refrigerator because the energy savings due to increased two phase area may be canceled by the loss of the air side heat transfer coefficient.

If evaporator de-superheating is observed (as described in Appendix B), it can be possible to enlarge the two-phase region of the evaporator by blowing less air over the coil. Under same conditions it might be possible to increase the runtime fraction

6.3 Desired results

For experimental performance evaluation the best approach would be to follow the same test matrix that was used while testing the system before it was altered. However, in order to achieve the desired compartment temperatures in both compartments at the same time, constant manual switching will be required between the two operating modes. This will involve switching the air flow into the appropriate compartment, the refrigerant flow into the correct captube and setting the compressor speed. The switching frequency should be determined experimentally in order to provide relatively stable temperatures in both compartment while not introducing excessive cycling losses.

For this design to be ultimately successful it must be demonstrated that it can provide energy savings at every typical operating condition. Therefore, a careful comparison of the energy consumption data should be done between the original system and the modified dual temperature design.

Nevertheless, it is most important to show that this particular design can indeed compare favorably in performance at the test condition prescribed by the Department of Energy. This is why the above optimization techniques were geared towards using the most care at this operating condition.

Such a direct comparison might not, however, reveal all the advantages of the new design. Additional savings could result from evaporator coil frost removal techniques using the warm fresh food compartment air.

It must also be realized that this particular refrigerator's cabinet insulation was not optimized to perform well under this new setup and additional improvements could be made if the entire refrigerator were designed from the ground up. Additionally, using multi-speed compressors with wider speed range could provide extra performance boost and/or simplify the design by eliminating the need for separate captubes.

Chapter 7

Summary and conclusions

7.1 Dual-temperature evaporator system design

The idea behind a dual-temperature evaporator system is that the same evaporator is sequentially used first to cool the freezer compartment, then the air flow is switched to cool fresh food compartment.

7.1.1 Design optimization

While a dual-temperature refrigerator is running in the fresh food mode, the lower temperature lift can raise the steady state COP by as much as a factor of two. This could improve the overall system COP by up to 20%. Also, using fresh food compartment air to defrost the evaporator during the off-cycle can be more energy efficient than employing auxiliary power sources.

If a single-speed compressor were used in a dual-temperature evaporator system, it would pump nearly twice as much mass flow in the fresh food operating mode than in the freezer mode. Unless there is a way to reduce capacity by slowing down the compressor while cooling the fresh food compartment, larger heat transfer areas or faster fan speeds would be required for efficient operation. However, shorter runtime fractions associated with larger evaporator and condenser UA's could lead to higher transient losses. Also, increasing the size of either heat exchanger would have only a marginal effect on the system performance but could be quite costly.

On the other hand, slowing the compressor down by a factor of four or five will result in energy savings approaching the theoretical maximum. However, with a current limitation of only a factor of two turndown, about 22% fresh food mode COP boost is expected. Over the entire range of typical operating conditions the overall energy savings are anticipated to be around 8-10%.

7.1.2 Evaporator coil and ductwork

In the original test refrigerator, the evaporator was located near the bottom of the freezer section next to the back wall. Only about 6% of the air flow over the coil was used to cool the fresh food section while the bulk of the air was recirculating in the freezer compartment.

With the new design it was important to minimize air side pressure losses during both freezer and fresh food mode operation. Therefore, the coil had to be moved

elsewhere. After carefully analyzing all the options, it was decided to mount the redesigned evaporator in the fresh food compartment. The face area of the new coil was made nearly square instead of rectangular, which was helpful in both straightening the flow and reducing the head losses.

The volume occupied by the evaporator coil was maintained roughly the same as that of the original unit. The fin pitch was cut in half because it was believed that the new fresh food air defrosting mechanism should be very effective in preventing frost formation. Finally, the tube spacing was slightly reduced to improve the fin efficiency.

The ductwork was completely redesigned utilizing smother bends and transitions which lead to an estimated 30% head loss reduction in the ductwork. Pressure losses over the evaporator coil were kept about the same as before. Finally, it was estimated that the air-side heat transfer coefficient of the new evaporator should be very similar to that of the original unit.

7.1.3 Compressor selection

Selecting a compressor required a balance between the need for adequate pull down capacity and the desire to reduce the mass flow while operating in the fresh food mode. Since this compressor's turndown ratio was limited to a factor of two, a careful analysis was necessary to consider the tradeoffs between the higher COPs associated with installing a smaller compressor and a requirements for the refrigerator to be able to operate at ambient temperatures up to 110°F.

The final selection was a compressor similar to the originally installed unit but about 84% of the size with correspondingly lower mass flow for any given conditions.

7.1.4 Capillary tube sizing

In order to deal with different flow rates in the freezer and fresh food cooling modes, two separate capillary tubes were required. The newly selected captubes had to be longer and thinner than the one originally installed in the system.

It was essential that condenser subcooling of at least a few degrees would be achieved over a wide range of operating conditions. This was needed to make sure that accurate compressor maps could be developed from the calorimetry data obtained from the system. Simulations predicted that it would be a lot easier to achieve subcooling at the condenser exit while operating in the fresh food mode.

To make sure that the evaporator would be fully utilized it was desirable to limit the evaporator superheat. Also, the optimal evaporator refrigerant charge had to be approximately equal in both operating modes.

Afterwards, it was demonstrated that if the compressor turndown ratio would be as high as a factor of five, it could be possible to use the same captube in both modes.

7.2 Multiple circuit heat exchanger design

This study concentrated on the effects of using multiple circuits in both condenser and evaporator on the system performance. The advantage of employing multi-circuited coils is that the total effective heat transfer area per unit mass of refrigerant is increased and the total amount of charge in the system can be reduced. The main benefits of a low charge system are:

1. Smaller cycling losses than in a conventional system due to limited vapor migration during off-cycle and faster charge redistribution after startup.
2. Quicker response to the changes in the environment.

To ensure that the calculations were realistic, the evaporator and condenser pressure drops were unchanged, and the total length of tubing was held constant so that the material cost would not increase. The resulting tube diameters were smaller, so refrigerant-side surface-to-volume ratio increased and the charge inventory decreased accordingly.

It was predicted that if 3 condenser circuits and 5 evaporator circuits were used instead of 1 in each, the total charge inventory would be decreased by nearly a factor of two. Halving the system charge inventory halves the time needed for the refrigerant to travel around the loop and contributes to cycling loss reduction.

Robustness of a low charge system was a very important concern. However, refrigerator simulations were used to show that this ultra-compact system could maintain its capacity and COP essentially as well as its conventional counterpart. This fact was established over the ambient temperature range from 60°F to 110°F, with the multi-circuited system performing particularly well at higher ambient temperatures.

7.3 Evaporator de-superheating phenomenon

The original-equipment evaporator had both counterflow and parallel flow passes with respect to the air stream. In the initial modeling of this evaporator it was assumed that no more than half of the evaporator could be superheated. However, experiments showed that this was not always the case. In order to adequately monitor the temperature and phase changes occurring inside the coil, 12 surface thermocouples were mounted on the evaporator return bends.

It was observed that when most of the evaporator was filled with two phase liquid, the amount of heat conduction along the fins was almost negligible. On the other

hand, the experimental results also indicated that heat conduction plays an extremely significant role when more than half of the evaporator is filled with superheated vapor.

The heat transfer along the fins from the superheated zone near the evaporator exit to the two phase zone at the inlet could lead to effective de-superheating of the refrigerant. This was particularly noticeable at lower ambient temperatures.

7.4 Dual-speed compressor efficiency

Two sets of data were obtained from a refrigerator system with a reciprocating compressor running at 2400 and 3600 rpm respectively. The data was taken and analyzed for a variety of ambient conditions as well as cabinet temperatures. However, there was no way to experimentally control the inlet and outlet conditions of the compressor. Even when the surrounding air temperatures were identical, the actual refrigerant pressures and temperatures were generally different when operating at different speeds. This was due to the fact that the condenser heat rejection rate depends on the operating speed.

It was verified experimentally that the compressor isentropic efficiency did not depend on the compressor inlet conditions and that the compressor outlet pressure was virtually the same for both operating speeds at a given ambient temperature. These observations made it possible to compare directly paired data points having the same room and cabinet air temperatures.

Unexpectedly, the isentropic efficiencies of the compressor operating at these two speeds were within 3% of each other for all the data points. Therefore it was concluded that the efficiency of this particular dual-speed compressor was not strongly dependent upon the operating speed.

7.5 Metastable behavior in capillary tubes

The results obtained in earlier experiments were used to support the hypothesis that metastable behavior can have significant effect on the mass flow rate when condenser subcooling is relatively small. This effect was demonstrated to cause up to 30% higher mass flow rates than predicted by an equilibrium model.

Additional system tests were also conducted. This time the data for every point was taken at a steady condition so that transient effects could no longer be confused with metastable behavior. No particular trend could be found, but the mass flow rate instabilities and the non-repeatability phenomenon were observed once again.

Mass flow variations for given air temperature conditions could make it difficult to properly control a system equipped with a variable-speed compressor. These

observations could also serve as an explanation for poor agreement between experimental data and steady state system models.

References

Ahmed N., Fluid Mechanics, Engineering Press, San Jose, pp. 327-335, 1987.

Cavallaro, A.R., and C.W. Bullard, "Effect of Variable-Speed Fans of Refrigerator Component Heat Transfer," ASHRAE Transactions, Vol. 101, Pt. 2, pp. 1218-1224, 1995.

Dautel, T., personal communication, 1997.

Gray, D.L., and R.L. Webb, "Heat Transfer and Friction Correlations for Plate Finned-Tube Heat Exchangers Having Plain Fins," Proceedings of Eighth Intl. Heat Transfer Conference, San Francisco, pp. 2745-2750, 1986.

Kim, K., B. Kopko, and R. Radermacher, "Application of Tandem System to High-Efficiency Refrigerator/Freezer," ASHRAE Transactions, pp.1239-1247, 1995.

Korte, C.M., and A.M. Jacobi, "Condensate Retention and Shedding Effects on Air-Side Heat Exchanger Performance." ACRC TR-132, University of Illinois at Urbana-Champaign, 1997.

Lavanis, M., I. Haider, and R. Radermacher, "Experimental Investigation of an Alternating Evaporator Duty Refrigerator/Freezer," ASHRAE Transactions, Vol. 104, Pt. 2, 1998.

Lee, H.M., H.W. Lee, and J.H. Lim, "High Efficiency Multi-Evaporator Cycle and Control of a Refrigerator," Samsung, Suwon City, Korea, 1997.

Liu, Y., and C.W. Bullard, "An Experimental and Theoretical Analysis of Capillary Tube-Suction Line Heat Exchangers," ACRC TR-109, University of Illinois at Urbana-Champaign, 1997.

Meyer, J., and Dunn W.E., "New Insights into the Behavior of the Metastable Region of an Operating Capillary Tube, "International Journal of HVAC&R Research, Vol. 4 Pt. 1, pp. 105-115, 1998.

Srichai, P.R., and C.W. Bullard, "Two-Speed Compressor Operation in a Refrigerator/Freezer," ACRC TR-121, University of Illinois at Urbana-Champaign, 1997.

Sweedyk, J.M., "Capillary Tubes - Their Standardization and Use," ASHRAE Transactions, Vol. 87, Pt. 1, 1981.

Zukauskas, A., "Heat Transfer from Tubes in Cross Flow,", Advances in Heat Transfer, ed. J.P. Hartnett and F. Irvine, Jr., Vol. 8, pp. 93-160, Academic Press, New York, 1972.

Woodall, R.J., and C. W. Bullard, "Development, Validation, and Application of a Refrigerator Simulation Model," ACRC TR-99, University of Illinois at Urbana-Champaign, 1996.

Woodall, R.J., and C. W. Bullard, "Simulating Effects of Multispeed Compressors on Refrigerator/Freezer Performance," ASHRAE Transactions, Vol. 103, Pt. 2, pp. 630-639, 1997.

Appendix A

Compact heat exchanger design

A.1 Introduction

A.1.1 Multiple-circuit design

This Appendix explains the tradeoffs associated with the use of compact, multiple-circuit heat exchangers as refrigerator evaporators and condensers.

Multiple-circuit heat exchangers are currently widely used in air conditioning systems to enhance heat transfer and provide better overall efficiency. This concept can be extended to home refrigerator systems as well. Figure A.1 is a simple sketch of a multiple-circuit component.

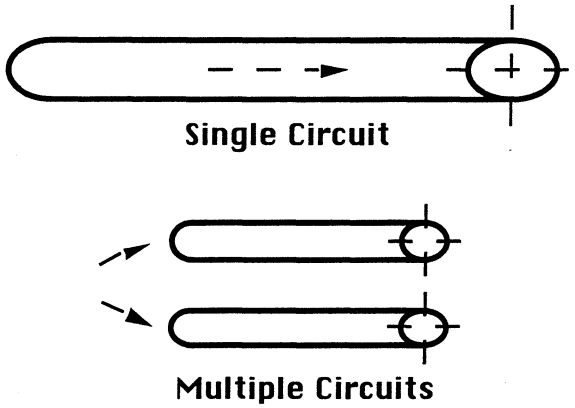

Figure A.1 Schematic multiple circuit diagram

When multiple circuits are implemented in a heat exchanger, the total effective heat transfer area per unit mass of refrigerant can be increased. Therefore the amount of charge needed for the heat exchanger to operate can be reduced. If this approach is applied to both major heat exchangers in a refrigerator, condenser and evaporator, the total charge inventory in the system can be reduced substantially.

The most important benefit of a low charge system is that it has much lower cycling losses than a conventional one. When such a system is being restarted, it takes significantly less time to redistribute the charge and to cool it down to the optimal operating temperature. Furthermore, a compact system has quicker response to the changes that occur in the environment, since there is less thermal inertia associated with it.

A.1.2 Design obstacles

One of the major drawbacks of a compact system is its initial cost. Although there is less refrigerant required, the number of metal parts and their connections is definitely a major contribution to the cost. Also, the more circuits in the condenser, the more difficult it might be to attach the fins.

There are a few fluid flow considerations too. First, the flow should be evenly distributed between the circuits, which is difficult to achieve for a large number of circuits. Second, the pressure drop associated with more contact area can go up, requiring more power to pump the refrigerant.

Finally, for some systems it might happen that a compact design would not provide required robustness over the entire operating conditions range. The performance of a compact system should be examined at a variety of ambient temperatures to ensure acceptable performance at the off-design points.

The ultimate goal is to prove that for every compact system, it is possible to find the optimal number of circuits in each heat exchanger in such a way that the cycling loss reduction benefit is not canceled by the cost increase and flow considerations.

A.2 Modeling assumptions

A.2.1 System parameters

The ACRC refrigerator simulation model is capable of modeling multiple-circuit systems at steady state conditions. It allows to test the performance of a refrigerator for any combination of condenser and evaporator circuits.

The so called "design mode" was initially used to optimize the system. The model was employed to simulate the standard Department of Energy refrigerator test condition, which is 90°F ambient air temperature, 40°F in the fresh food and 5°F in the freezer compartments. The geometry of the freezer and fresh food compartments was unchanged and experimentally estimated cabinet conductances were used to calculate the evaporator load.

In order to make a fair comparison between a conventional and a multiple-circuit system, the diameter of each circuit was selected so that the pressure drop across the heat exchangers was unchanged. The number of degrees of superheating at the exit of the evaporator and subcooling at the exit of the condenser were also kept constant. In other words, the goal was to maintain the heat exchanger performance as close to that of the original system as possible by fixing the inlet and outlet conditions for each heat exchanger, while, ideally, maintaining the same refrigerant flow rate.

Air side heat transfer areas and frontal air flow areas were set to be equal to those of the original components as well. This could be achieved physically by adding a proper number of fins or wires on the air side of the heat exchangers. Air side heat transfer coefficients were also assumed to be the same as in the conventional design. They complete the list of vital performance characteristics that were maintained.

The above mentioned constraints were sufficient to make sure that at that at least at a single operating condition the newly redesigned heat exchangers would provide performance characteristics very close to those of the original components, while saving valuable space and reducing charge inventory. The performance of the new system at other temperature conditions was also considered, as described later in this Appendix.

It should be noted, that in the design mode, the effectiveness of the suction line heat exchanger was set as an input. While doing so, it was understood that the length and the diameter of the captube could be adjusted at the final stage of the design process. All other system components, most notably the compressor, did not have to be redesigned in any way.

A.2.2 Additional constraints

Two different approaches were selected to further describe the geometry of the new heat exchangers. They are hereafter referred to as Case 1 and Case 2.

Case 1: The total length of the heat exchanger tubing was kept constant in order to make sure that the cost of the compact system is comparable to that of the conventional one. For example, in a three circuit system the length of each circuit was three times less than that in the original design.

It must be understood, however, that the total amount of materials used will still change due to the change in the tubing diameters. For example, when going to 6 parallel circuits, the total refrigerant side tube area will be cut by roughly a factor of 2. The resulting tube areas for this and other cases are shown in Figure A.2.

The thickness of the tube material might be adjusted as well. In fact, the amount of material used for tubing can be further reduced by making thinner tube walls, if it is deemed appropriate from the strength of materials standpoint. However, if the resulting increase in the air side heat transfer coefficient does not offset the loss of air side tube area, additional fins or wires have to be added. The tradeoff analysis between adding material to increase the refrigerant side and the air side areas can be done similarly to that for conventional single circuit heat exchangers.

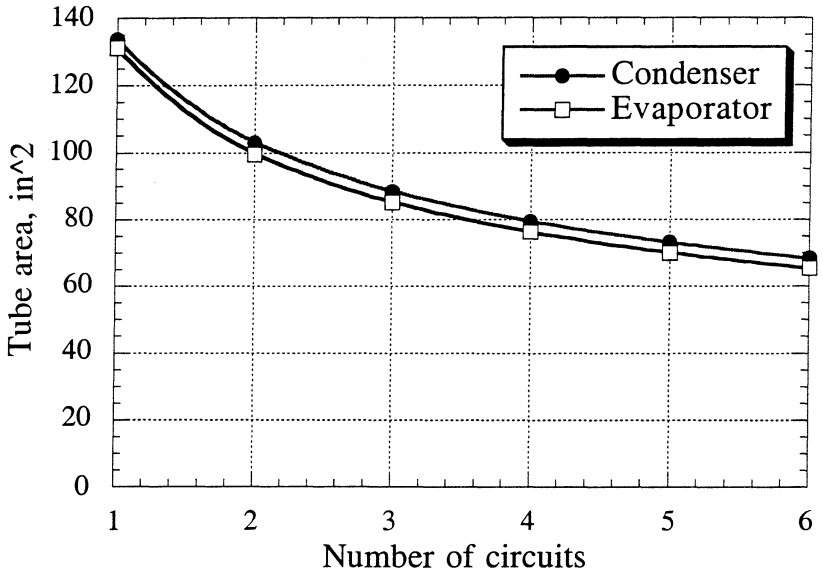

Figure A.2 Internal tube areas for Case 1

Case 2: The second approach was to set the length of each circuit so that the refrigerant side tubing area was the same as originally. While the cost of production might go up due to an increase in total length of tubing and in the fin-tube connection costs, a more efficient system with nearly identical performance characteristics could be designed.

Figure A.3 presents sample inside tube diameters for such systems. The original diameters are shown for the single circuit point on the left of the graph. The length of the tubing is inversely proportional to the tube diameter and as the diameters are cut in half for the 6 parallel circuit case, the length of tubing has to be doubled.

In this case, the increase in the surface to volume ratio leads to more effective heat transfer through the tube walls. This allows to reduce the requirement for fin or wire area needed to keep the heat transfer coefficient the same as in the base case.

Ideally, there might be a design that incorporates the advantages of the two cases considered above. However, for simplicity, the feasibility of each individual case was analyzed instead.

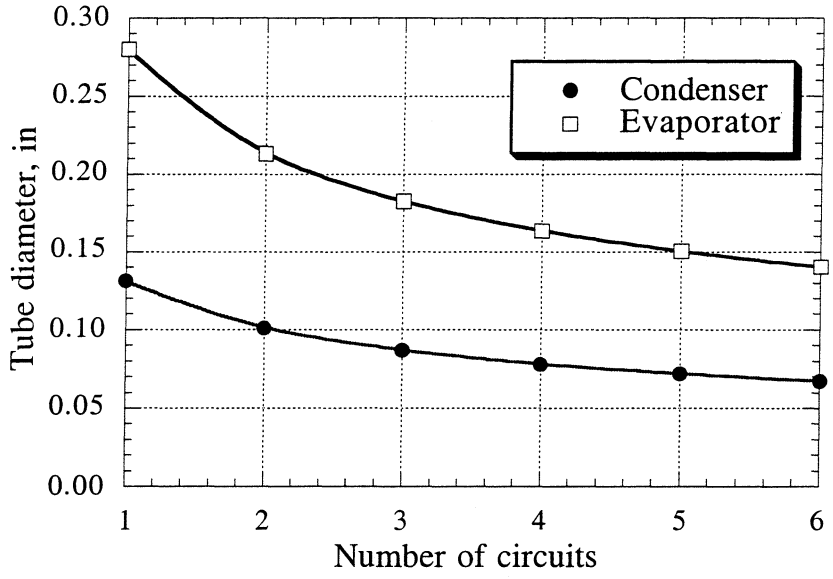

Figure A.3 Heat exchanger tube diameters for Case 2

A.2.3 Design variables

By maintaining the pressure drops, subcooling and superheating constant, as described above, all the steady state refrigerant temperatures were kept within 1°F and pressures within 2% of their base case values throughout the system.

However, the refrigerant distribution in the system was altered, resulting in a reduced fraction of the refrigerant residing in the smaller heat exchangers of a compact system. The total refrigerant inventory and the corresponding refrigerant mass flow rate were computed using the ACRC model for each combination of the numbers of parallel circuits.

In order to maintain the exact set temperatures in both compartments, the fractions of evaporator air flow to freezer and fresh food were adjusted. All the heat transfer rates in the system were calculated for the new heat exchanger geometry and the refrigerant inventory. Required power consumption was also determined. Run time fraction was estimated as the ratio of the total system load to the system capacity.

Finally, the two most important performance characteristics - COP and annual steady-state energy usage were computed based on the above information.

A.3 Modeling results

A.3.1 Charge inventory

Dozens of modeling runs were made for a variety of heat exchanger configurations. Figure A.4 shows the amount of charge required for different combinations of condenser and evaporator circuits in Case 1. The first bar on these graphs represents the base case with one circuit in each heat exchanger. The heavily shaded bars show the benefit of eliminating the liquid line mullion heater, which is commonly referred to as the post condenser loop.

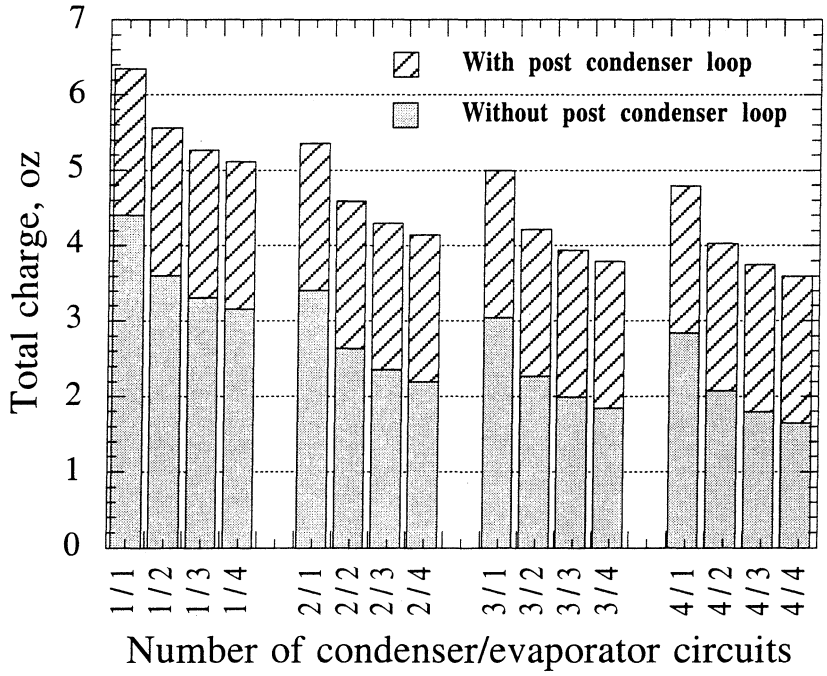

Figure A.4 Charge inventory for Case 1

By going to 4 circuits in the condenser and 4 circuits in the evaporator in a system with a post condenser loop, the total charge inventory can be decreased by nearly a factor of two. In the absence of the mullion heater, the same effect can be achieved with only 3 and 2 (or 2 and 3) circuits respectively.

In the base case (one circuit in each heat exchanger) the refrigerant travel time around the entire loop, calculated as the total mass over the mass flow rate, was

approximately 3 minutes. This number can be decreased to 1 minute and 40 seconds or less, with the introduction of the compact heat exchangers. It can be further reduced to 50 seconds if the mullion heater is eliminated.

The time it takes for a system to reach steady state EER is directly proportional to the refrigerant travel time above, thus suggesting a clear cycling loss reduction benefit of such systems over the conventional ones. Figure A.5 is similar to Figure A.4 and provides the refrigerant charge data for Case 2. Since these heat exchangers are larger, they do not give the same dramatic inventory reduction as the Case 1 models.

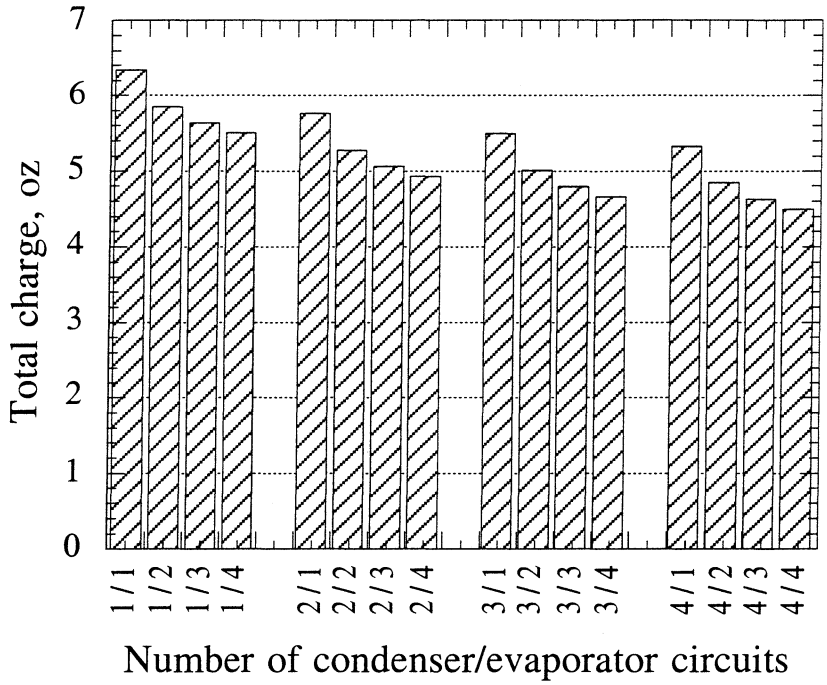

Figure A.5 Charge inventory for Case 2

A.3.2 System optimization

Although the cycling losses can be reduced dramatically, as shown in the previous section, there might be a tradeoff with the steady state performance in Case 1 due to the system's somewhat lower capacity which results from smaller refrigerant mass flow rates. Figure A.6 clearly shows the effect of adding extra circuits on the system steady state COP. This graph shows the reduction in COP caused by adding circuits in one heat exchanger at a time, while keeping the conventional design for the other one.

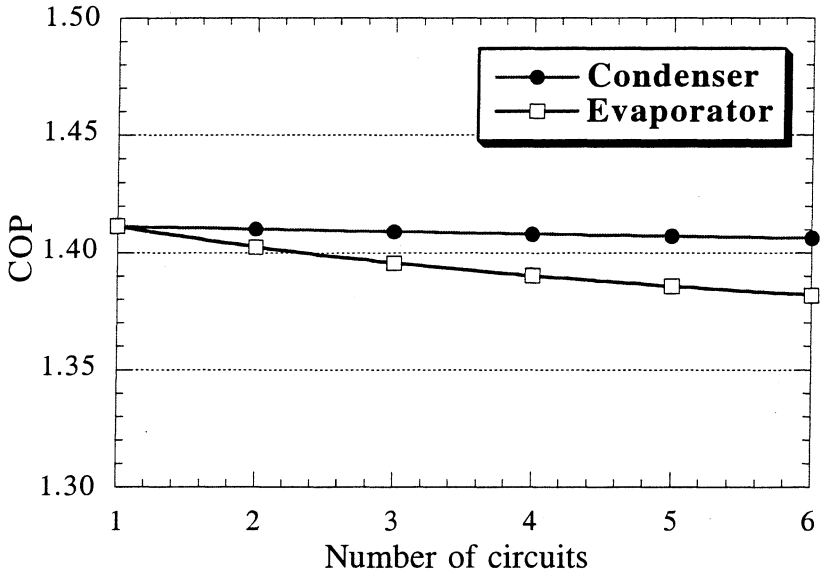

Figure A.6 Effect of circuiting on steady state COP for Case 1

Figure A.6 indicates that adding the condenser circuits does not have a very significant effect on the performance, while the evaporator redesign can lead to a fairly small 2 % reduction in the steady state COP. It is not unreasonable to expect that the reduction in the cycling losses can bring the actual overall COP to the levels higher than that of the original system, compensating for the minor steady state performance reduction.

For the Case 2 the COP is virtually unaltered no matter how many circuit are added to the heat exchangers.

Aside from performance issues, the other important consideration is the complexity of the system design and the cost of production associated with it. In Case 1, the cost does not increase a lot, while the same might not be true for Case 2.

At this point, considering the cost of materials, extra welding requirements and the relatively small charge inventory reduction of a compact heat exchangers designed based on the constant area criterion (Case 2), it becomes clear that such an approach is not very practical. From this point on only the case based on the constant length criterion approach (Case 1) is considered.

Some of the Case 1 multiple circuit system designs with the corresponding numbers for the refrigerant charge residing in each heat exchanger and the refrigerant

mass flow rates are shown in Table A.1 The heat transfer loads for the condenser and the evaporator are also shown.

Number of condenser circuits	Number of evaporator circuits	Charge in condenser, oz	Charge in evaporator, oz	Total charge, oz	Mass flow, lbm/hr	Condenser load, Btu/hr	Evaporator load, Btu/hr
1	1	2.32	1.65	6.35	10.82	914.8	765.4
1	2	1.33	1.65	5.36	10.82	914.3	765.1
1	3	0.97	1.65	4.99	10.82	913.7	764.8
1	4	0.77	1.65	4.79	10.82	913.2	764.5
1	5	0.65	1.65	4.67	10.82	912.8	764.3
1	6	0.57	1.65	4.58	10.82	912.3	764.0
1	1	2.32	1.65	6.35	10.82	914.8	765.4
2	1	2.31	0.88	5.55	10.67	902.6	755.4
3	1	2.29	0.61	5.27	10.55	893.3	747.8
4	1	2.28	0.47	5.11	10.46	885.9	741.7
5	1	2.27	0.38	5.02	10.39	879.8	736.7
6	1	2.26	0.33	4.95	10.32	874.7	732.5
1	1	2.32	1.65	6.35	10.82	914.8	765.4
2	2	1.33	0.88	4.59	10.67	902.0	755.1
3	3	0.96	0.61	3.93	10.56	892.3	747.2
4	4	0.76	0.47	3.60	10.47	884.5	740.9
5	5	0.64	0.38	3.38	10.39	878.0	735.7
6	6	0.55	0.32	3.24	10.33	872.4	731.3

Table A.1 Performance results summary for Case 1

For the particular system under consideration, the point with 3 condenser circuits and 5 evaporator might be selected as the optimum design for minimizing charge, as shown in Figure A.7. In this graph the lines are the "lines of constant number of condenser circuits." Along each line, every point represents the performance of the system with different number of evaporating circuits, going from 1 on the far right to as many as 7. This graph was used to demonstrate that increasing the number of circuits in either heat exchanger above a certain number would not provide any significant charge reduction. Instead adding too many circuits would hurt the system efficiency and add unnecessary cost and complexity.

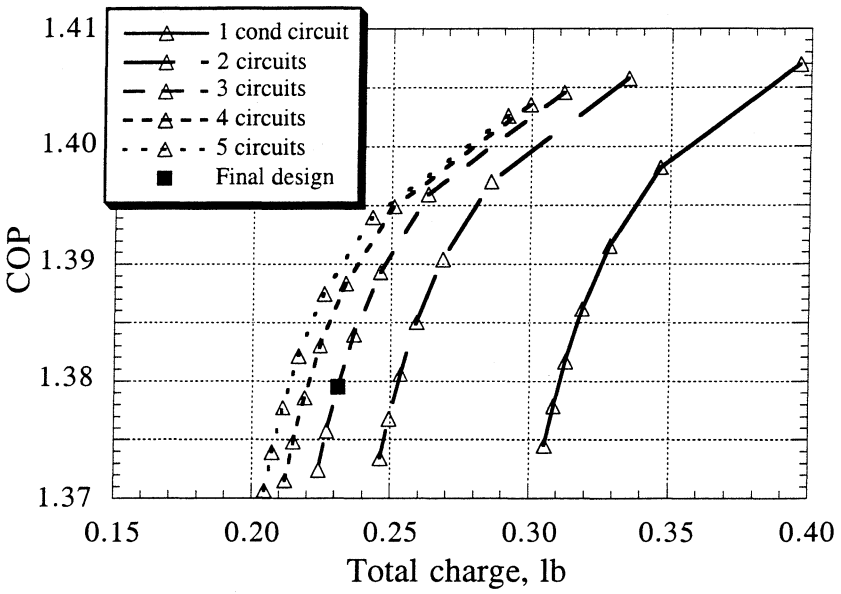

Figure A.7 System COP for different heat exchanger configurations

Obviously, the "optimum point" shown above was selected somewhat arbitrarily and no actual cost calculations were done. The number of circuits that is optimal for other similar systems can depend on a variety of considerations specific to those systems. However, the particular selection procedure presented in this section might provide a good example of an optimization methodology that could be used for charge minimization.

A.3.3 System robustness

In order to make sure that the optimized low charge system would perform adequately under a variety of typical refrigerator operating conditions, its performance should be tested at different ambient air temperatures. This was done using the "simulation mode" of the ACRC solver.

In this mode, the optimum number of circuits and corresponding refrigerant charge are now set as inputs, while all the pressures and temperatures as well as performance characteristics of the system are estimated for each ambient air condition. The effectiveness of the captube suction line heat exchanger is computed, rather than assumed as in the "design mode."

The steady state COP of the new design at each temperature was compared to that of the base case system and presented in Figure A.8.

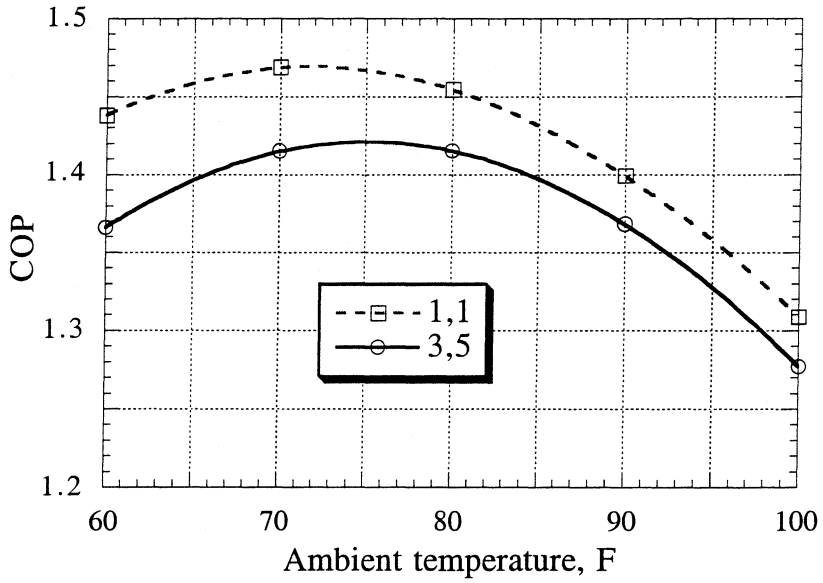

Figure A.8 Compact system robustness

The numbers for the COP of the system at 90°F differ slightly from those in Figure A.6 due to the fact that the models inputs and outputs were switched around and the effectiveness of the captube suction line heat exchanger (CTSLHX) was calculated more precisely than before.

Figure A.8 shows that the steady state COP of the compact system is lower than that of a conventional system by 2-5%. Nevertheless, this effect should prove to be small compared to the savings gained due to the cycling loss reduction.

It could have been possible to further optimize the capillary tube suction line heat exchanger to improve the system performance across the board. This might potentially help to further reduce the performance loss associated with the compact system. The compressor could have also been re-sized to provide higher mass flows at the new operating conditions.

The fact that the steady state COP reduction was pretty small, especially at higher ambient temperatures is very encouraging. It allows us to conclude that construction of a compact system with less than half of the refrigerant inventory of the "base case" system is feasible without significantly sacrificing performance at any of the typical operating conditions.

Appendix B

Evaporator zones modeling

B.1 Theoretical considerations

B.1.1 Introduction

In order for an evaporator to be properly modeled it usually has to be divided into a number of zones. Typically, as the refrigerant exits the capillary tube and enters the evaporator it is in the state of a two phase liquid-vapor mixture. For the simplest case, as the refrigerant flows along the evaporator tubes it gains energy and the quality of the mixture steadily increases along the path. If the evaporator is undersized it might be possible that the refrigerant remains two phase even at the evaporator outlet, in which case there is no need to divide it into zones. Alternatively, and more typically, the evaporator exit is superheated, and two zones, namely the two phase zone and the superheated zone, have to be considered separately.

This simple modeling scheme can only be used to describe either parallel flow or counterflow evaporators. However, many modern units, like the evaporator originally installed in the our side-by-side test refrigerator, have both counterflow and parallel flow configurations with respect to the air stream. This results in some interesting behavior that was first observed by Srichai and Bullard (1997).

However, Srichai has done only a limited number of experiments and was taking just a few thermocouple measurements from the surface thermocouples placed on the evaporator fins. This did not provide enough information to facilitate a full understanding of all the temperature changes on the refrigerant side of the evaporator. A more clear picture have emerged after some additional instrumentation was done. These new findings are presented in this Appendix.

B.1.2 Evaporator configuration

During the initial modeling it was assumed that the evaporator would consist of 3 zones as shown in the Figure B.1 on the left. Under normal operating conditions, the superheated part of the evaporator should be relatively small compared to the overall size of the unit. This follows from an observation that little heat transfer occurs in the vapor only region, which implies that the evaporator should be sized in a manner that ensures that most of the tube volume is filled with two phase refrigerant. The overall

effectiveness of the evaporator could be compromised if the superheated zone takes up a larger part of the tubing. However, Srichai has demonstrated that under many actual experimental conditions more than half of the evaporator can become superheated, as shown on the right of the Figure B.1. The next section describes the reasoning behind dividing the evaporator into the 4 zones, as shown below:

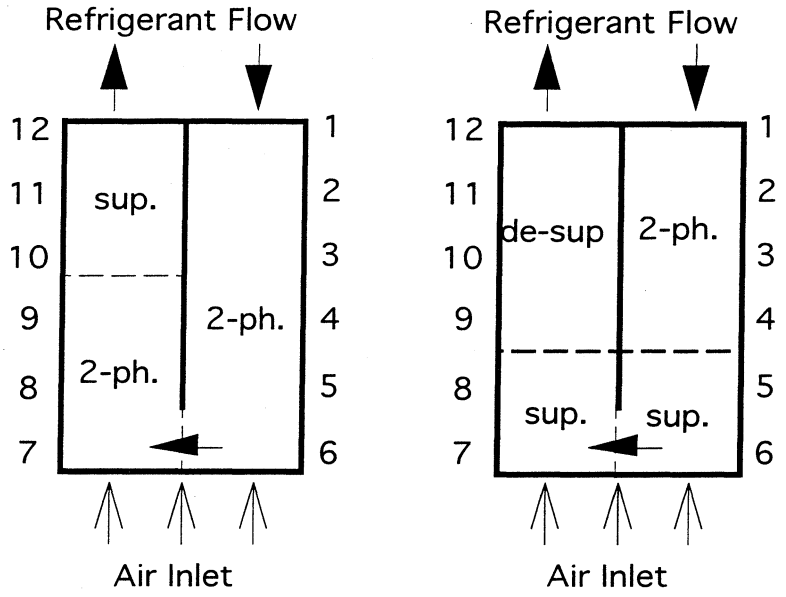

Figure B.1 Evaporator zones schematic diagram

In order to monitor the refrigerant state, surface thermocouples were mounted on the evaporator return bends at locations schematically indicated by numbers 1 through 12 in the Figure B.1.

Ideally, all the thermocouples except for the one or two placed near the evaporator exit should be reading similar temperatures equal to the saturation temperature for the pressure at each point. Since the pressure drop in the evaporator was estimated to be on the order of 1 psi, the temperature variation should have been about 2-3°F, uniformly decreasing along the tubing. This would have indicated that the evaporator was fully utilized and the superheated region was relatively small.

B.1.3 Heat conduction along the fins

If most of the evaporator is filled with refrigerant whose temperature varies only by a few degrees due to the pressure drop, the amount of heat conduction along the fins cannot possibly be a major consideration. On the other hand, it can have a more

noticeable effect as the superheated region becomes larger. Furthermore, as our experimental results indicate, this phenomenon can play an extremely significant role when more than half of the evaporator gets filled with superheated vapor.

Obviously, there is virtually no heat transfer along the fins that connect the regions of the tubing where the refrigerant is two phase on both sides. Therefore, in the 3 zone model the only significant heat conduction along the fins is between the superheated zone and the top of the two phase zone. This conduction can cause the amount of superheating at the exit to drop as compared to that somewhere in the middle of the superheated zone. Nevertheless, in order to ensure that even the comparatively small fin conduction effects at the bottom of the evaporator are accounted for, Srichai's equations always include this term for every fin both at the top and at the bottom of the coil.

When analyzing the heat transfer to and from the refrigerant in the superheated region, many thermodynamic effects have to be considered together. First of all, the air flow near the top of the evaporator is relatively cool compared to the bottom, as the air has already traveled along the coil. Therefore, the rate of convective heat transfer from the airflow to the coil decreases along the air flow. Secondly, the temperature of the refrigerant in the superheated region is also higher than that in the two phase region, which further reduces the heat transfer rate. Finally, as the temperature of the refrigerant rises, so does the amount of heat that propagates along the fins to the two phase region near the inlet.

At the point in the flow where the amount of heat conduction along the fins becomes greater than the heat transfer from the air, the refrigerant can start to cool back down. Therefore, this effect is referred to as "de-superheating."

For the cases where the size of the superheated region is relatively large, the amount of heat that can be transferred along the fins can increase dramatically. In fact, if more than half of the evaporator is filled with vapor, such transfer effectively occurs along all the fins. Naturally, the most significant conduction still takes place near the top of the coil where the temperature difference between the two refrigerant flows reaches its maximum.

De-superheating can start anywhere along the tubing. It is only for modeling convenience that the region of the vapor flow opposite the two phase region on the other side of the coil is denoted as the de-superheating zone. However, it is indeed more likely that de-superheating will begin somewhere in this evaporator zone rather than in the region below.

B.2 Experimental results

Data were taken for a wide range of temperature settings to demonstrate how the behavior of the evaporator differs for various running conditions. An example of a case where there was almost no de-superheating was the standard DoE test condition with 90° room temperature and cabinet temperatures of 5° and 45° in the freezer and fresh food compartments respectively. The Figure B.2 below shows the actual thermocouple readings obtained at this condition.

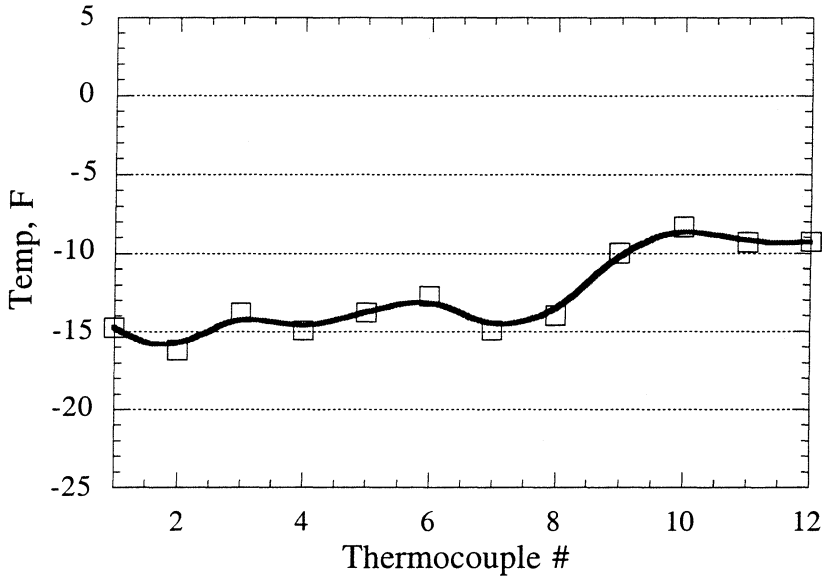

Figure B.2 Evaporator thermocouple readings at 90°F ambient

Figure B.3 presents the data for a case where almost exactly half of the evaporator was filled with two phase liquid, while the other half was all vapor. The compartment temperatures were still held at 5° and 45°, as in the case above, but the room temperature was decreased to 75°F.

Finally, Figure B.4 demonstrates an extreme case when more than half of the evaporator was all vapor. The cabinet temperatures were the same as in the examples above, but the room temperature was a relatively low 60°F.

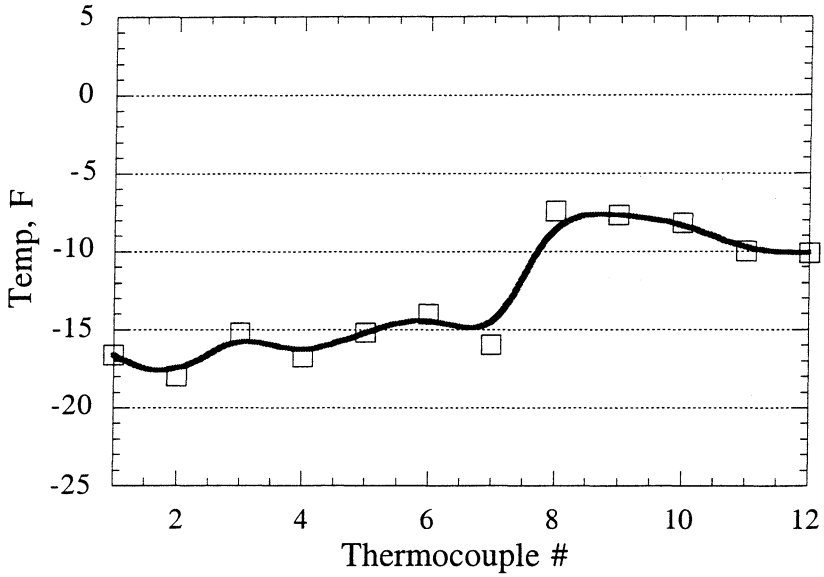

Figure B.3 Evaporator thermocouple readings at 75°F ambient

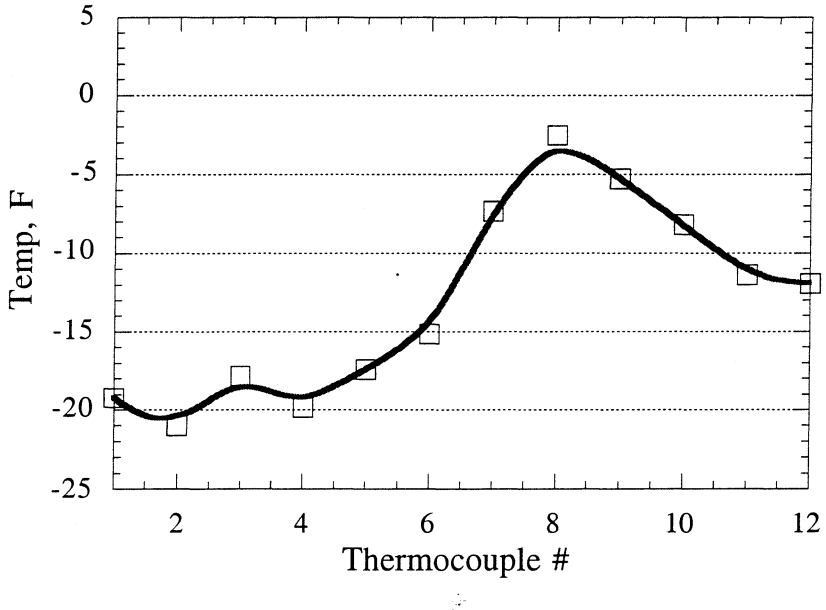

Figure B.4 Evaporator thermocouple readings at 60°F ambient

B.3 Conclusions and observations

As demonstrated by the thermocouple data, the heat transfer effect along the fins can alter the downstream evaporator temperature profile quite dramatically. In fact, our experiments have shown that inlet and exit measurements typically done in a "conventional" coil instrumentation cannot possibly give a complete picture of what is happening on the refrigerant side.

The apparent superheat at the exit of the evaporator was only 5-10°. For a simple parallel flow or counterflow coil this suggests that only a small part of the evaporator is superheated. However, in more complex geometries, such as the one described above, the exit condition measurement might not contain any useful information on the positions and relative sizes of the different evaporator zones.

In other words, the de-superheating effect was shown to be responsible for "concealing" huge degrees of superheat which lead to low heat transfer rates. Under low ambient temperature conditions the evaporator was in fact oversized for the application. This could lead coil manufacturers to design bigger than necessary units based on the improper notion that the amount of superheat at the evaporator exit is a good indicator of the relative size of the superheated zone.

Appendix C

Isentropic efficiency of a dual speed compressor

C.1 Problem definition

In order to fully understand the advantages and disadvantages associated with using a dual (or multiple) speed compressor, its efficiency operating with different speeds should be measured. If there is a significant dependence of compressor efficiency on the speed, a system model should take that into account. On the other hand, if there is a range of speeds where there is no such dependence, that range should be determined. This appendix presents the data and results obtained for an Americold RV800 compressor operating in a side-by-side Amana refrigerator with at two speeds - 2400 rpm and 3600 rpm. This unit was originally designed to operate at the latter speed and therefore was expected to perform best while operating around 3600 rpm.

A typical compressor in a domestic refrigerator has a significant heat transfer to the environment that is hard to estimate experimentally and therefore a first law energy balance for the compressor cannot be easily written. This explains why direct measurements of the inlet and outlet conditions of the compressor do not provide enough information to calculate the power requirements per unit mass flow rate. Instead, the overall power consumption of the compressor is measured directly.

The isentropic efficiency is determined as the ratio of enthalpy change required for an ideal compressor to operate over the actual energy input:

$$\eta_{isentropic} = \frac{\dot{m} \cdot \Delta h_{ideal}}{W_{actual}}, \tag{C.1}$$

where $\dot{m}$ is the mass flow rate of the refrigerant in the system.

An ideal isentropic compressor is defined as one that operates under the same inlet temperature and pressure conditions and has the same pressure drop as the actual one but the outlet temperature is calculated to be such that there is no entropy change between the inlet and the outlet. Therefore, the enthalpy change in the numerator of the equation above can be written as:

$$\Delta h_{ideal} = h(p_2, s_1) - h(p_1, T_1), \tag{C.2}$$

where state 1 is located at the inlet and state 2 at the outlet of the compressor.

The mass flow rate $\dot{m}$ is determined using a compressor map provided by the compressor manufacturer. A compressor map relates the flow rate to the saturation

temperatures of refrigerant at inlet and outlet pressures of the compressor. These temperatures are conventionally denoted T_c and T_e respectively, because they roughly correspond to the pressures at the inlet of the condenser and at the outlet of the evaporator. This compressor map is based on calorimeter data obtained at 90°F ambient for a typical compressor of this model and uses a bi-quadratic curve fit with 9 coefficients.

For positive displacement compressors, like the one used in this experiment, the mass flow rate is directly proportional to the operating speed, and therefore the mass flow rate map can be scaled up or down for any given speed. For the purpose of this experiment, the compressor map that was initially developed for 3600 rpm operation can be scaled down by a factor of 1.5 to be used for the 2400 rpm case.

It should be noted, that the power map cannot be scaled down in the manner described above, due to the fact the friction losses are not directly proportional to the speed. If simple scaling was possible, there would be no need to conduct this experiment in the first place. In fact, the power can be found using the following relation:

$$W_{total} = \int_1^2 \dot{V}\, dP, \qquad \text{(C.3)}$$

where $\dot{V}$ (P,T) is different at every point inside the compressor and cannot be measured directly.

C.2 Experimental results and analysis

Two sets of data were taken and analyzed for the refrigerator system running under a variety of ambient conditions as well as cabinet temperatures. However, there was no way to experimentally set the inlet and outlet conditions of the compressor, so the actual refrigerant pressures and temperatures were generally different for 2400 and 3600 operation, even when the surrounding air temperatures were identical.

A special program was written for the step by step data reduction. First, all the temperatures were obtained from direct thermocouple measurements. The compressor inlet pressure was found as the evaporator exit pressure less the pressure drop in the suction line. Since the compressor outlet pressure measurement was gauge, the measured atmospheric pressure was added to it.

In addition to the straight forward calculations described above, the amount of subcooling in the liquid line was also calculated. It was determined as the difference between the saturation temperature at the pressure at the liquid line exit and the actual measured refrigerant temperature at that point. This pressure was equal to the pressure at

the compressor outlet less the pressure drops in the condenser and the liquid line. It was found that there was no subcooling at the exit of the liquid line for all the data points in both data sets.

Figure C.1 shows how the compressor efficiency depends on the condenser inlet saturation temperature (T_c).

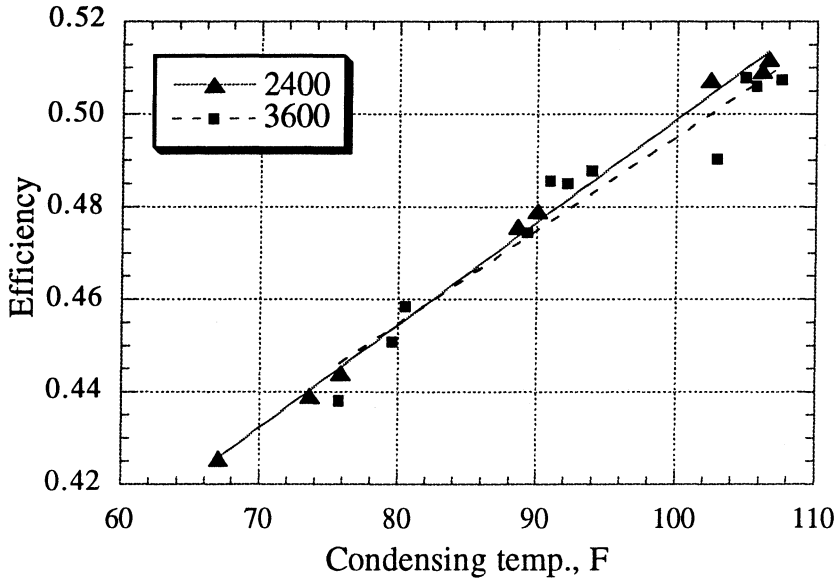

Figure C.1 Compressor efficiency vs. condensing temperature

The linear fits for the 2400 case and for the 3600 are almost identical. The difference of less than 5% at higher T_c can be attributed to the uncertainty in the measurements.

Clearly, the compressor operates up to 15% more efficiently under higher condensing pressures and temperatures. This means that this compressor has better performance when the ambient temperatures are higher regardless of the operating speed.

Figure C.2 shows that there is virtually no effect of the evaporator outlet saturation temperature (T_e) on the compressor efficiency. In fact, the lines of constant efficiency are nearly horizontal (shown are lines with efficiencies of 0.51, 0.48 and 0.45), which means that efficiency only depends on the compressor outlet pressure and temperature, and not on the inlet conditions. Again, this observation can be made based on either the 2400 or 3600 rpm data set alone, or on the combination of the two, like in the graph below.

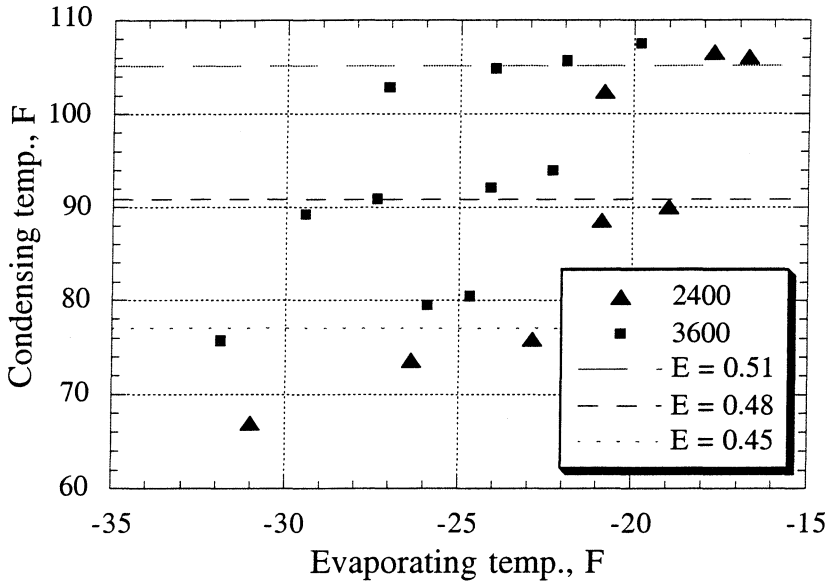

Figure C.2 Compressor efficiency vs. evaporating temperature

Due to the fact that the efficiency doesn't depend on the compressor inlet conditions and the fact that the compressor outlet pressure is virtually the same for both operating speeds at a given ambient temperature, it is possible to compare directly paired data points having the same room and cabinet air temperatures. The sample table below provided a simple way to match compressor efficiencies.

Temperature,°F			Efficiency	
Ambient	**Fresh Food**	**Freezer**	**2400 rpm**	**3600 rpm**
90	45	5	0.51	0.51
75	45	5	0.48	0.49
60	45	5	0.44	0.45

Table C.1 Typical isentropic compressor efficiencies

The efficiencies were within 3% of each other for all the data points. This data clearly indicates that the efficiency of this particular dual speed compressor is not strongly dependent upon the operating speed.

Appendix D

Captube flow analysis

D.1 Introduction

D.1.1 Captube test stand results review

The purpose of this Appendix is to confirm some of the results obtained by Liu and Bullard (1996) in their work on non-adiabatic flows of R-134a in capillary tubes, and to analyze the metastable behavior they have observed experimentally.

Liu has conducted a series of experiments on a stand-alone refrigerant test loop. A diaphragm pump was used to drive pure refrigerant flow. Test stand experiments were performed for three different captube and suction line geometries. The condensing temperatures were held constant at 90, 110 and 130°F. A more detailed setup description can be found in their report.

Liu's captube line heat exchanger data is used later in this Appendix to analyze the accuracy of the newly modified ACRC stand-alone capillary tube suction line heat exchanger (CTSLHX) model.

In their work, Liu and Bullard have demonstrated that under a given capillary tube inlet pressure and suction line superheat, mass flow depends on whether captube subcooling is increasing or decreasing. However, it was found that this hysteresis effect was not repeatable. One of the main difficulties running the loop was the inability to precisely control both inlet conditions of the captube and the suction line at the same time.

More repeatable results were achieved in an earlier work by Meyer and Dunn (1996), while dealing with adiabatic captubes. A very clear mass flow hysteresis was observed as the captube subcooling was increased and then decreased while keeping the refrigerant pressure constant. It was demonstrated that the location of the flash point in the capillary tube depends on how the particular state point was achieved. Therefore, it was shown that for a given level of subcooling there exists a range of possible mass flow rates, not just one correct value.

D.1.2 System test approach

The second stage of Liu's and Bullard's experimental work was done on a fully-instrumented Whirlpool refrigerator. The subcooling at the capillary tube inlet was

determined from the measured condenser exit pressure and temperature and was controlled by varying the evaporator air inlet temperature.

It was observed that for a given evaporator inlet air temperature ($T_{a\ evap\ in}$), the amount of subcooling depended on whether $T_{a\ evap\ in}$ was increasing or decreasing. The system COP for the points on the increasing $T_{a\ evap\ in}$ path was shown to be consistently lower than for those on the decreasing $T_{a\ evap\ in}$ path. It should be noted that the refrigerator compartment conditions were constantly changing, making the system operate in a transient regime. Nevertheless, the results were subsequently interpreted using a quasi-steady state analysis, making it hard to distinguish between metastable behavior and transient effects.

In order to confirm Liu's results, a series of new experiments was conducted on a newly instrumented side-by-side Amana refrigerator. This system was instrumented in basically the same way as the Whirlpool used in earlier tests. However, a slightly different approach was taken in the measurement techniques.

The new series of experiments, while using similar experimental techniques, was conducted in such a way that a few intermediate points were brought to the steady state and the data were obtained only at those points. This eliminated transient effects that could be otherwise confused with system's inherent metastable behavior.

D.2 CTSLHX model validation

This section addresses the ACRC model's ability to simulate the performance of Liu's "Tube B" which had dimensions virtually identical to those of the captube installed in the instrumented Amana test unit.

The dimensions of the captube were determined from laminar water tests and direct measurements by Dautel (1997) to a high degree of accuracy. The most sensitive parameter, the capillary tube diameter, was found to be 0.0362 ± 0.0002 inches.

Two sets of data from Liu and Bullard (1996) are presented here. Both experiments were conducted at 110°F condensing temperature. The amount of superheat was manually held nearly constant at 24 ± 4°F and 18 ± 4°F for the first and the second tests respectively.

Figures D.1 and D.2 present the experimental results for the mass flow rate, as well as those predicted by the CTSLHX model from the measured captube and suction line inlet conditions.

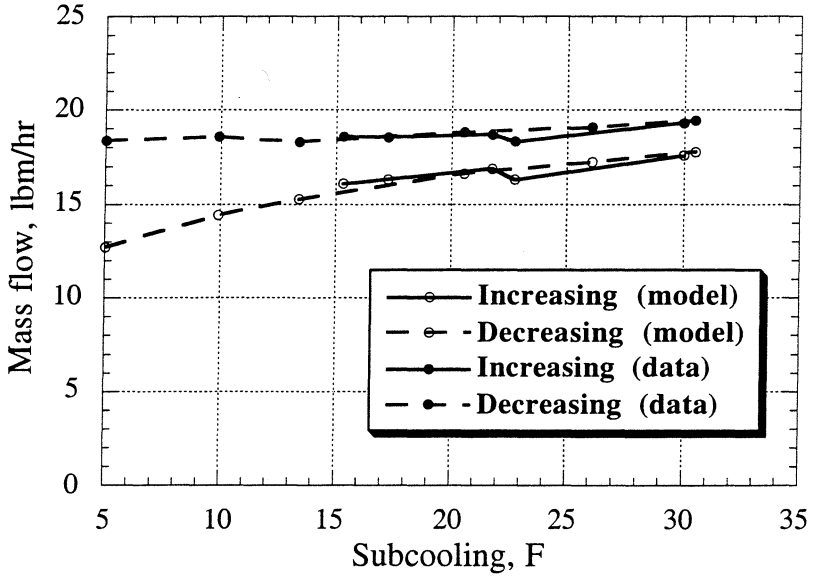

Figure D.1 Mass flow rates for loop test 1

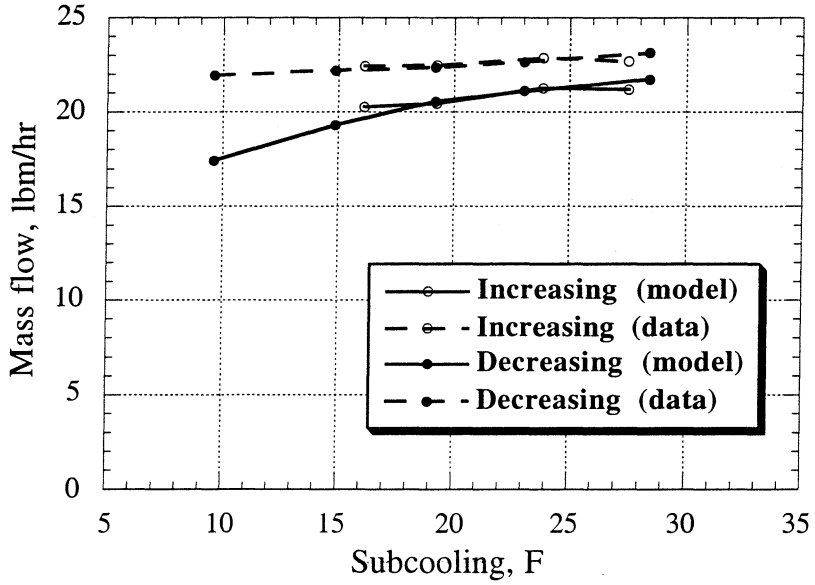

Figure D.2 Mass flow rates for loop test 2

In all cases the ACRC model predicted a lower mass flow rate than what was experimentally measured. Model predictions differed from the experiment by as much as 31% for Test 1 and by up to 21% for Test 2. The mass flow was measured with a mass flow meter that has a ±0.15 lbm/hr accuracy, which could lead to only about 1% uncertainty.

It should be noted that model predictions were much more accurate for high subcooling points than for those with a low degree of subcooling. In fact, only 6 to 8% mass flow underprediction was observed for 30°F subcooling cases.

Initially it was presumed that an incorrect estimate of the tube roughness could affect the mass flow rate. Unfortunately, the laminar water flow tests yielded no roughness information because friction is independent of roughness. Instead, a value of roughness was chosen from the middle of the range measured by Sweedyk (1981). However, Figure D.3 shows that, according to the CTSLHX model, there should be very little dependence of mass flow rate on the absolute tube roughness coefficient.

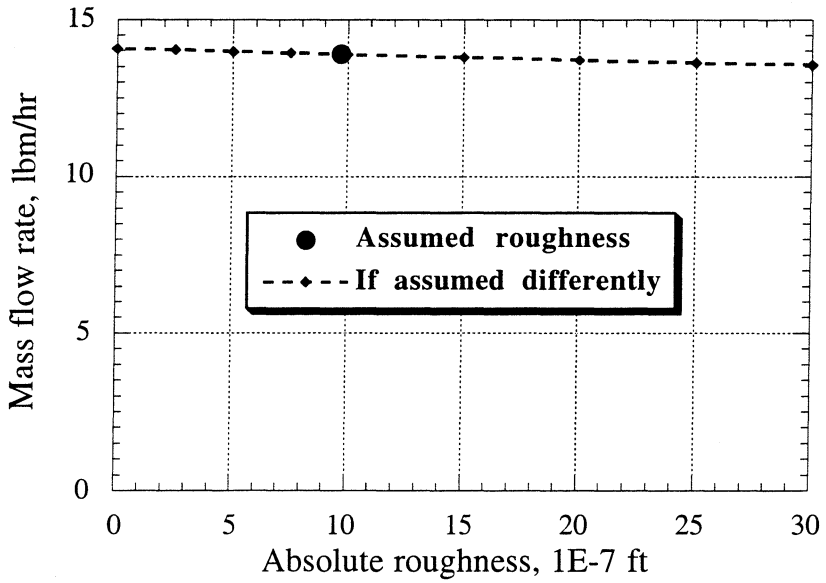

Figure D.3 Roughness effect on mass flow rate

It is clear that even if the absolute captube roughness was decreased from the currently used value of $9.71 \cdot 10^{-7}$ ft to zero (perfectly smooth tube assumption), the mass flow rate would increase only by 1.3%. This indicates that there must have been another problem with the model. It was concluded that the most likely cause of the mass flow

underprediction is the metastable effect and it might be necessary to add a metastable correction to the CTSLHX model.

The refrigerant temperature at the compressor inlet ($T_{comp\ in}$) was used to determine the amount of heat transfer in the suction line. Figures D.4 and D.5 show that the CTSLHX model gives a very close prediction for this temperature for all but the lowest subcooling points.

Particularly, for points with subcooling of 15°F or more, the error was no more than 2°F. However, $T_{comp\ in}$ for 5°F subcooling was underpredicted by as much as 6°F, which could lead to an underestimation of heat transfer by as much as 13% operating over an approximately 45°F temperature increase in the suction line.

All these results support the hypothesis that there is significant metastable behavior when subcooling is relatively small. This effect causes higher mass flow rates and correspondingly greater heat transfer then predicted by the equilibrium model.

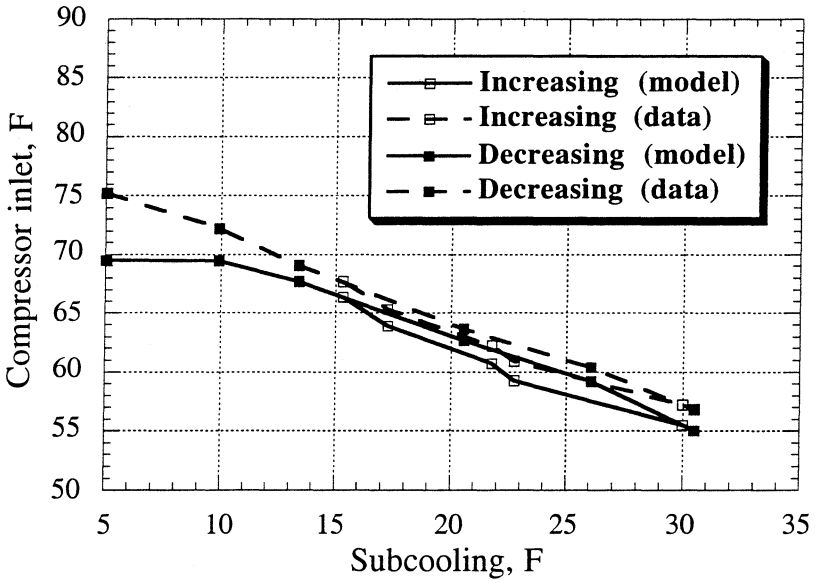

Figure D.4 Compressor inlet temperatures for loop test 1

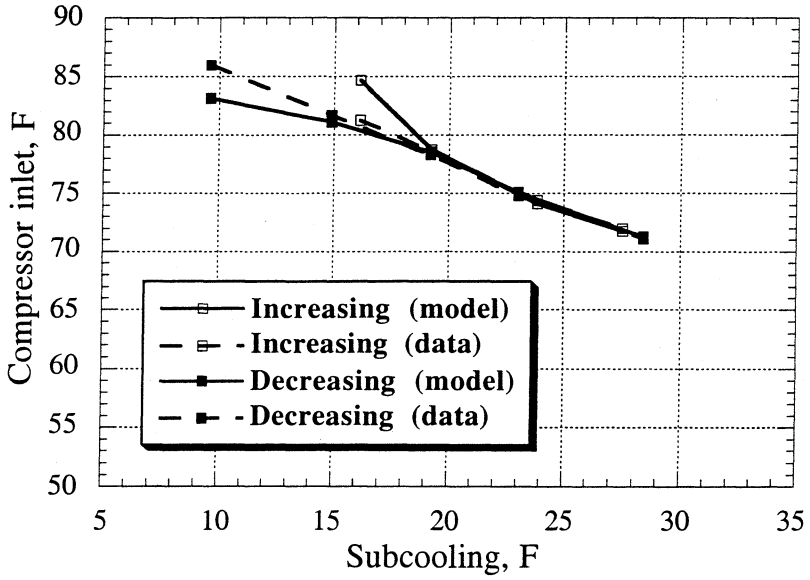

Figure D.5 Compressor inlet temperatures for loop test 2

D.3 Amana system tests

D.3.1 Experimental test conditions

The Amana side-by-side system was tested at 60°F ambient temperature. At this particular ambient setting, the range of cabinet temperatures where the system exhibits liquid line subcooling was the fairly wide. It should be noted that at higher temperatures where a refrigerator would normally operate, the Amana unit didn't have any subcooling, unless overcharged.

The temperatures of the freezer and fresh food compartments were first set to very low values to ensure that there was no subcooling in the liquid line. The schedule in Table G.1 was used to bring the mixed evaporator air inlet temperature up from 5-8°F to 46-49°F and back down. It took at least 30 hours to complete each cycle because it was necessary to reach steady state condition at every point to avoid any undesirable transient effects.

Data point	1	2	3	4	5	6	7
Freezer, °F	0	15	30	45	30	15	0
Fresh Food, °F	40	45	50	55	50	45	40

Table D.1 Cabinet temperatures for the system tests

Temperature and pressure data were collected at each point. The amount of subcooling was determined as the difference between the measured refrigerant temperature at the condenser exit and the saturation temperature corresponding to the measured pressure at this point. Similarly, the amount of superheat at the evaporator outlet was calculated as the saturation temperature corresponding to the evaporator exit pressure less the temperature directly measured at this point. Finally, the mass flow rate was estimated using the compressor map based on the condensing and evaporating temperatures. A simple computer program was used to reduce the data.

D.3.2 System test results

The subcooling was very small at the low temperature points, making the experimental results hard to interpret. Furthermore, the data was not repeatable much in the same way as it was observed by Liu. It should be realized that on a test stand it was possible to hold superheat constant while varying only the subcooling. In an actual system, everything changes simultaneously which made it harder to interpret the data.

It should be realized that on a test stand it was possible to hold superheat constant while varying only the subcooling. In an actual system, everything changes simultaneously which made it harder to interpret the data.

Figures D.6 and D.7 show the mass flow rate in the system calculated based on the compressor map. No particular trend can be found, but it is clear that metastable behavior was observed. The mass flow fluctuation of as much as 2 lbm/hr cannot be attributed to any other factor and is too large to be caused by a measurement error.

Figures D.8 and D.9 show the amount of subcooling obtained in the experiments during the same two runs. Any number below 2°F was treated as an indication that no subcooling was present.

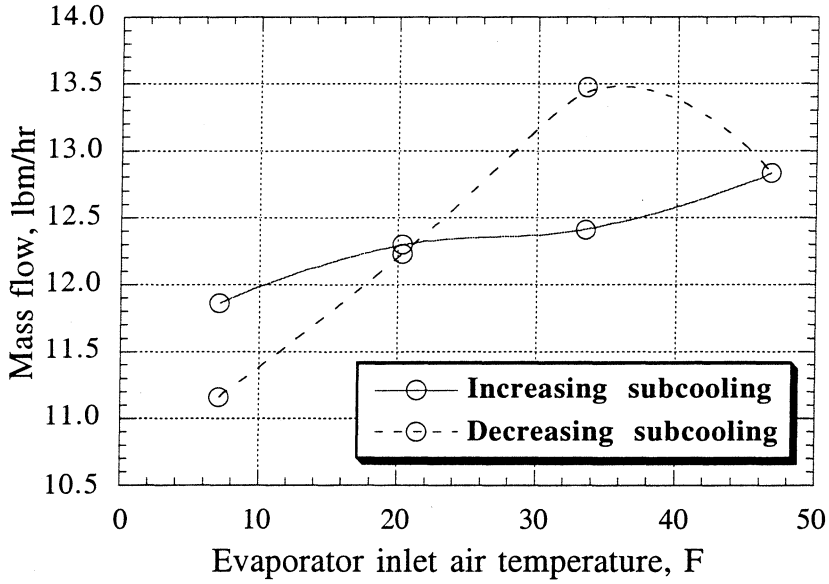

Figure D.6 Mass flow rates for system test 1

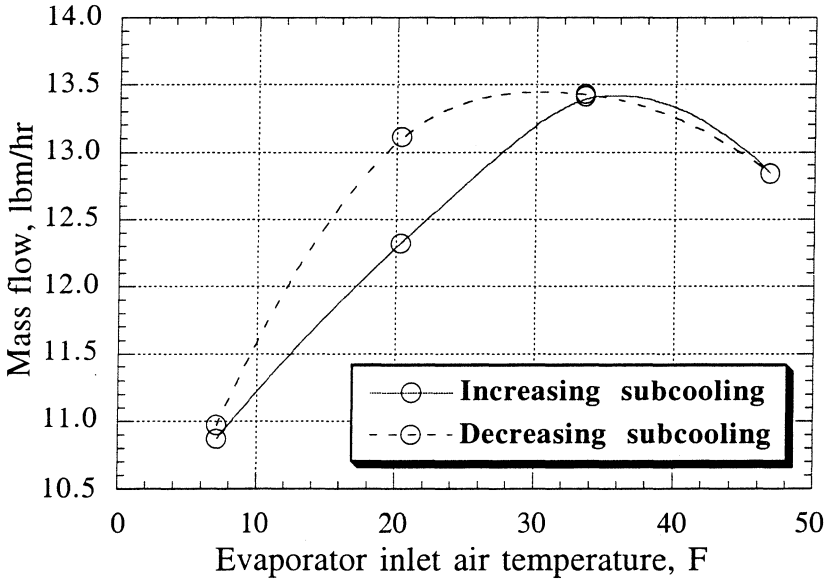

Figure D.7 Mass flow rates for system test 2

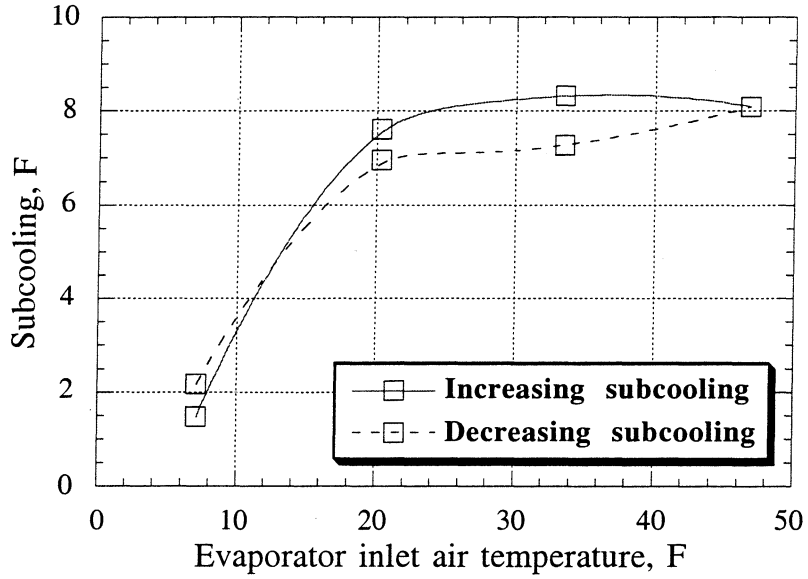

Figure D.8 Captube subcooling for system test 1

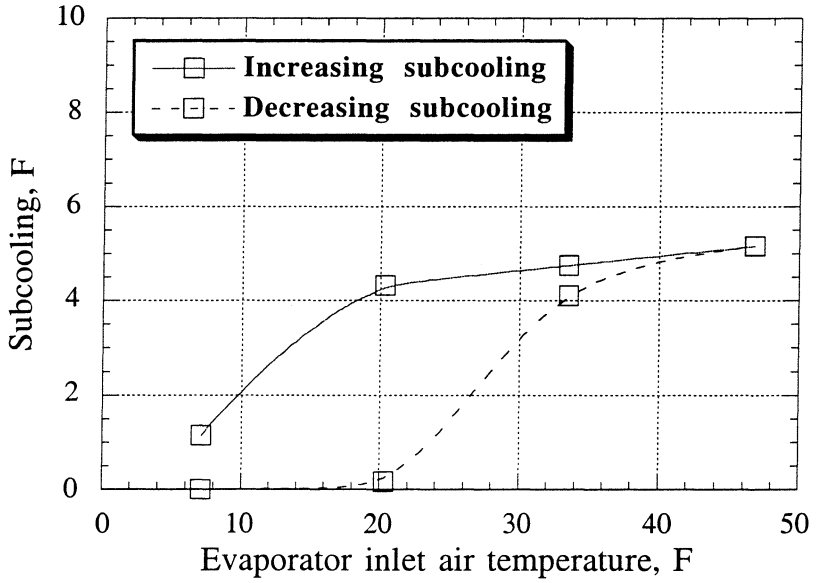

Figure D.9 Captube subcooling for system test 2

The existence of mass flow instability was obvious and this behavior should be further investigated. However, the system test results were not repeatable, as shown in

the Figures above. A variety of additional factors, such as accumulation of frost on the evaporator and variations in ambient humidity could have contributed to the non-repeatability of this kind of an experiment.

Table D.2 summarizes the actual evaporator and condenser temperatures observed during the experiments.

Evaporator	TEST 1		TEST 2	
Exit, °F	Subcooling, °F	Superheat, °F	Subcooling, °F	Superheat, °F
7.08	*None*	*None*	*None*	*None*
20.31	7.61	12.21	4.33	11.41
33.54	8.32	21.96	4.75	18.23
46.77	8.09	32.78	5.15	31.44
33.54	7.27	17.86	4.11	18.08
20.31	6.95	12.07	*None*	3.42
7.08	*None*	*None*	*None*	*None*

Table D.2 Subcooling and superheat results for the system tests

D.4 Conclusions

The instabilities observed in Liu's loop tests could support the hypothesis that significant metastable behavior was observed. The variations in compressor and evaporator inlet temperatures were particularly noticeable when the captube subcooling was relatively small. By analyzing Liu's test stand data it was shown that this behavior could lead to higher refrigerant mass flow rates and correspondingly to greater suction line heat transfer than predicted by the equilibrium model.

However, both the captube subcooling and the refrigerant mass flow rate were also not repeatable in the new system tests. Since the data for every point was taken at a steady condition, transient effects could no longer be blamed for the non-repeatability. There was a clear variation between the data taken for the two new tests as well as fluctuations in the data as the captube subcooling was increased and decreased within a given test. The source of described non-repeatability is still unknown and the physical causes of the metastable behavior remain unclear.

In addition to that, since there were no clear repeated "patterns" formed in any of the graphs above, both in the loop tests and the system tests, this phenomenon cannot be described as hysteresis.

Non-repeatability was observed by Liu and Bullard (1996) both during system tests and loop tests and confirmed in the new system tests on a different refrigerator.

This leaves no doubt to whether the data was incorrect due to a simple measurement error or a faulty sensor.

Clearly, captube behavior is affected by some operating conditions that are not reflected in simple pressure and temperature data. Such conditions might include refrigerant-oil mixture solubility and viscosity being altered over time. Changing humidity and the resulting frost formation on the evaporator coil could also affect the test results during a system test.

The instabilities observed could be large enough to make designing a system control system very difficult, because the actual state of the system cannot be determined by just a few measurements to reliably predict the rest.

The biggest obstacle for effective control of such systems might be that, as experiments presented abo make it difficult to design an efficient control system for a multiple speed compressor. Such control system would have to self-compensate for the instabilities in the captube's behavior.

Appendix E

Parameter Estimations

E.1 Motivation

Several months have elapsed since Srichai's (1997) Amana refrigerator instrumentation work was completed. In order to check if the parameter estimates that were done immediately after the instrumentation were still valid, a new set of experiments was necessary. This need became particularly evident when the RFSIM simulation model started to no longer provide reasonable accuracy in predicting the actual behavior of the refrigerator system. These simulations, based on the newly estimated parameters, were intended to provide a baseline for comparison with the performance of a dual-use evaporator system that was subsequently built.

E.2 Evaporator related parameters

E.2.1 Air flow rate over the coil

In order to determine the flow rate ($\dot{V}_{evap}$) over the evaporator coil independently of the air split fraction f_z, both fresh food and freezer compartment temperature controllers were set equal. This was the only way to ensure that the two air streams from the compartments had the same temperatures and therefore the temperature of the mixed air as it enters the evaporator grille did not depend on the volumetric flow rate fractions of the air from each compartment. However, in reality there was always a 5-10°F difference between the two compartment temperatures because the heaters had difficulty compensating for stratification and the fact that a lot more cooling was done in the freezer compartment as compared to the fresh food. Special care should be taken in order to avoid such problems in the future.

The air flow rate calculations were performed using the technique originally developed in by Robert Srichai (1997). The system schematically shown in Figure E.1 was considered.

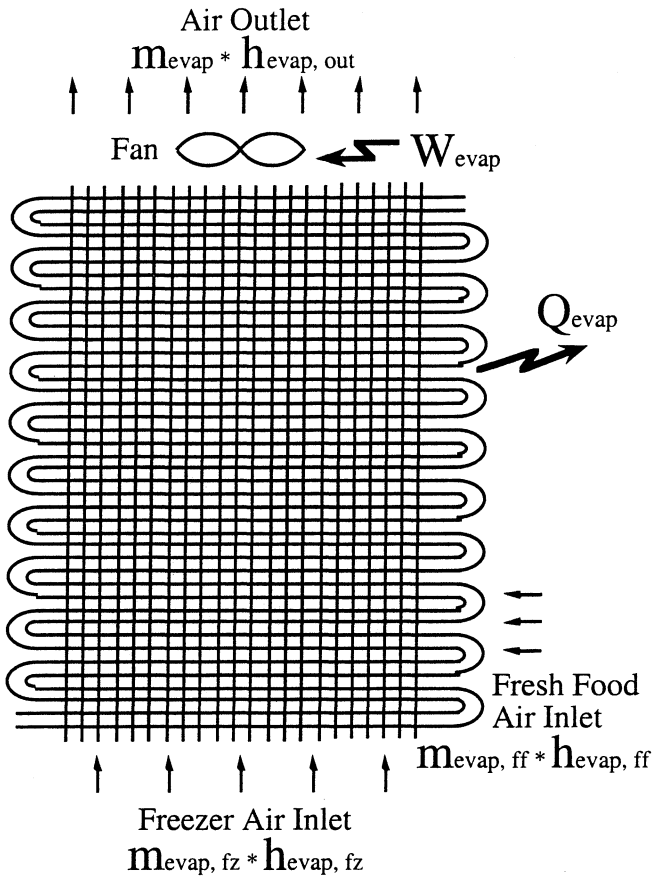

Figure E.1 Frontal view of the evaporator

The energy balance for the air flow over the coil and the fan, as shown in the diagram above, can be written as:

$$\dot{m}_{evap,fz} \cdot h_{evap\,in,fz} + \dot{m}_{evap,ff} \cdot h_{evap\,in,ff} + \dot{W}_{evap\,fan} = \dot{m}_{evap} \cdot h_{evap\,out} + \dot{Q}_{evap}, \qquad \text{(E.1)}$$

where the evaporator load can be determined as:

$$\dot{Q}_{evap} = \dot{Q}_{frez} + \dot{Q}_{frig} + UA_{frez} \cdot \left(T_{amb} - T_{az}\right) + UA_{frig} \cdot \left(T_{amb} - T_{af}\right) + \dot{W}_{evapf\,an} \qquad \text{(E.2)}$$

It should be noted that if the evaporator load from this equation is substituted into the energy balance above, the fan power term cancels out. This can be explained by the fact that the energy difference between the air inlet and outlet flows already takes heating due to the fan into account.

Mass flow rates for the energy balance equation can be calculated based on the volumetric air flow rates. For example, the flow rate out of the evaporator can be calculated as:

$$\dot{m}_{evap} = \frac{\dot{V}_{evap} \cdot 60}{\upsilon\left(T_{evap\,out}, P_{atm}\right)} \tag{E.3}$$

Similar equations can be written for each of the inlet flows. Also, mass conservation has to be observed:

$$\dot{m}_{evap} = \dot{m}_{evap,fz} + \dot{m}_{evap,ff} \tag{E.4}$$

Finally, by definition of the air split fraction:

$$\frac{f_z}{(1-f_z)} = \frac{\dot{V}_{evap,fz}}{\dot{V}_{evap,ff}} \tag{E.5}$$

Only four test runs were performed under these conditions, yielding an average $\dot{V}_{evap}$ value of 58.4 cfm. It is obvious from the above equations that the calculation of this value is based on the cabinet conductances which have to be determined independently using the reverse heat leak test, which is described later in this Appendix.

The calculation uncertainty due to the unequal compartment return air temperatures is on the order of ±2 cfm. This uncertainty should be considered in addition to significant data scatter, as indicated by 5 cfm standard deviation. This adds up to the total air flow rate uncertainty of about 12%. Table E.1 shows all the relevant results for each data point.

Temperature, F			Heaters powers, W		Evaporator	Air flow
Freezer	Fresh food	Ambient	Freezer	Fresh food	fan power, W	rate, cfm
45.9	50.0	60.4	195.1	17.0	5.4	53.7
53.6	62.8	90.5	194.8	17.0	5.3	65.0
46.0	59.5	90.8	137.2	17.6	5.3	57.0
51.1	61.4	90.8	151.6	17.6	5.3	58.0

Table E.1 Air flow rates over the evaporator

E.2.2 Air split fraction

After the value for the air flow rate have been determined using the data presented in the previous section, it was possible to use experimental data for the refrigerator with different temperature settings in the two compartments to determine the air split fraction.

This new data set consisted of nine data points. The temperatures of the freezer and fresh food compartments were set at 5°F and 45°F respectively. Using the same equations as before, the value of f_z was estimated to be 0.94, which is very different from Srichai's estimate of 0.82. In fact, this implies that the flow rate into the fresh food compartment is by about a factor of two smaller than the one initially reported.

There is very little scatter in the air split fraction estimate and the standard deviation is less than 0.01. However, this seemingly small variation translates into a fairly significant 15% uncertainty in the flow rate into the fresh food flow compartment. Table E.2 shows the operating conditions and results for each of the 17 data points used.

Temperature, F			Heaters powers, W		Evaporator	Air split
Freezer	Fresh food	Ambient	Freezer	Fresh food	fan power, W	fraction
3.3	47.5	91.1	23.4	24.3	4.8	0.937
2.9	44.4	91.1	30.8	21.9	5.2	0.921
3.3	46.7	76.0	40.8	40.4	4.9	0.943
2.9	46.2	75.7	34.2	44.5	5.1	0.927
2.6	44.4	75.8	44.5	36.9	5.2	0.929
3.4	46.0	61.0	55.1	53.2	5.0	0.948
3.0	45.6	60.6	50.5	60.4	5.2	0.927
2.3	44.2	60.7	64.9	51.6	5.2	0.937
1.1	44.6	91.0	16.6	17.7	5.0	0.941
10.0	49.6	91.0	32.8	25.9	5.1	0.941
20.0	55.6	90.7	47.1	30.8	5.1	0.938
1.4	45.2	75.8	26.4	36.6	5.0	0.944
10.2	50.1	75.7	42.8	43.1	5.0	0.943
19.8	54.6	75.4	59.4	47.8	5.1	0.938
1.3	45.1	60.5	37.0	51.3	5.0	0.947
10.0	49.4	60.6	50.3	55.9	5.0	0.947
19.8	52.9	60.8	67.2	58.3	5.0	0.946

Table E.2 Air split fractions in the evaporator

Please note that in the above table 4 points, out of the 21 point set used in many subsequent parameter estimations, were skipped because of a faulty air side thermocouple reading.

It might have been possible to obtain more accurate estimates for the air flow rate and the air split fraction by estimating them simultaneously. A method for doing this was perfected by Robert Srichai (1997).

E.3 Cabinet conductances

The reverse heat leak test method was originally described by Paul Krause (1996) for use with the Whirlpool top-mount refrigerator. This method was subsequently adopted by Robert Srichai (1997) for the Amana side-by-side refrigerator. The Amana tests were repeated again to make sure that the cabinet conductances of the test unit have not changed significantly after more than a year of heavy modification and experimental use.

For the duration of these experiments, the compressor was disconnected from its power source and the heaters were turned on, just like in the earlier experiments. The cabinet temperatures were kept at virtually equal temperatures that were about 40-50°F above the chamber temperature.

A schematic drawing of the refrigerator heat transfer during a reverse heat leak test is shown in Figure E.2.

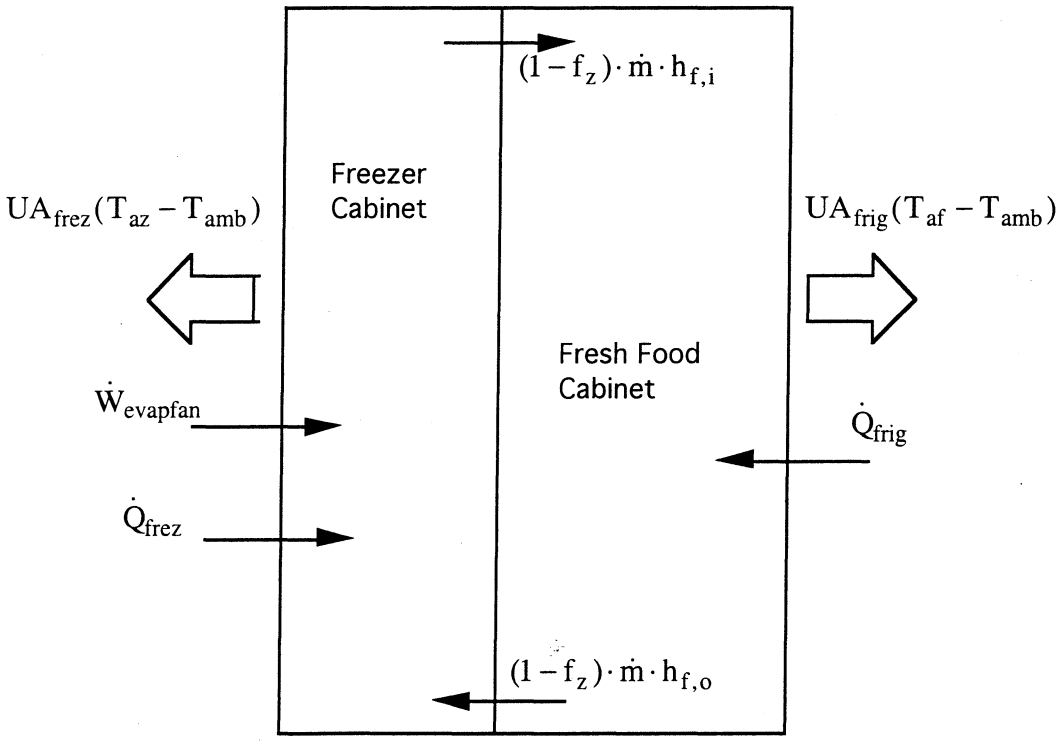

Figure E.2 Control volume for cabinet conductances on a refrigerator

The only modification to the original technique was that in all of the new experiments both the evaporator and the condenser fans were turned on, while in the earlier experiments only the evaporator fan was working. This was done to ensure that the air flow over the condenser was generating the same amount of forced convection as it does in all the experiments in which the refrigerator is running. The power was provided directly to the evaporator fan in order to bypass the refrigerator's built-in control system which does not start running the fan until the compressor have been on for a pre-programmed amount of time.

The freezer heater and the evaporator fan generate heat that "leaks" through the walls out into the chamber. Also, there is a small amount of heat exchange between the compartments due to the difference in temperatures between the air flow in and out of each compartment. The overall heat balance for the freezer can be written as follows:

$$\dot{Q}_{frez} + \dot{W}_{evapfan} = UA_{frez} \cdot \left(T_{az} - T_{amb}\right) + \dot{Q}_{flow} \tag{E.6}$$

An almost identical energy balance can be written for the fresh food compartment. The only difference is the absence of the evaporator fan. However, there are two muffin fans installed in the fresh food compartment to prevent stratification, but they are powered in parallel with the heater and their power consumption is included within the heater measurement. This relation is shown below:

$$\dot{Q}_{frig} = UA_{frig} \cdot \left(T_{af} - T_{amb}\right) - \dot{Q}_{flow} \tag{E.7}$$

The heat transfer due to the flow between the compartments is:

$$\dot{Q}_{flow} = \left(1 - f_z\right) \cdot \dot{m}_{air} \cdot \left(h_{f,i} - h_{f,o}\right) \tag{E.8}$$

Three data sets were used to calculate the *UA's*. The first data set consisted of six data points with temperature settings identical to those used by Srichai. These points had compartment temperatures of 90, 95, and 100°F and ambient settings of 50 and 55°F. The second set had five data points with compartment temperatures ranging from 80 to 105°F and an ambient temperature of 50°F. Finally, the third set had four data points with compartment temperatures of 90 to 110°F and ambient settings of 50 and 60°F.

For the last test, the compartment temperature settings were slightly adjusted in order to minimize the return air temperature difference as it flows back from the

compartments to the evaporator inlet. This was done to make sure that the uncertainty in the air flow rate and air split fraction did not affect the conductance estimates.

Each set used its own calibration values to ensure consistency. All the data points are shown in Table E.3.

Temperature, F			Heaters powers, W		Evaporator	Conductances	
Freezer	Fresh food	Ambient	Freezer	Fresh food	fan power, W	Freezer	Fresh food
98.2	96.8	55.8	41.0	35.2	2.9	0.967	0.928
88.9	87.3	51.0	37.1	33.5	3.2	0.985	1.006
98.2	96.6	50.9	45.0	38.9	3.3	0.949	0.926
88.5	87.2	55.6	29.2	24.2	3.0	0.909	0.835
93.8	92.5	55.5	35.5	30.3	2.9	0.938	0.886
93.7	92.3	50.5	40.0	32.2	3.0	0.928	0.838
103.2	101.8	50.5	52.6	42.7	4.3	1.018	0.893
98.2	97.0	50.4	47.4	39.3	4.0	1.017	0.902
93.5	92.6	50.3	41.4	37.1	4.2	1.014	0.914
88.3	87.0	50.2	36.7	30.1	4.2	1.013	0.877
83.2	82.0	50.2	31.1	27.1	4.3	1.018	0.910
108.9	107.1	51.3	63.3	40.4	3.3	1.013	0.870
106.3	107.0	51.2	55.5	42.6	3.5	0.964	0.870
96.8	97.3	61.0	32.0	27.8	3.1	0.907	0.843
101.6	102.0	56.2	44.5	35.7	3.2	0.948	0.880

Table E.3 New values for cabinet conductances

Table E.4 shows the *UA's* found in the experiments done by Robert Srichai, as compared to those based on the new data:

Conductances	Previous estimate	New estimate	Increase, %
Freezer	0.879	0.973	10.6
Fresh food	0.800	0.892	11.5

Table E.4 Cabinet insulation wear over time

The new compartment conductances were found to be about 10 to 12% higher than the previous estimates. It is very likely that these changes are caused by door gasket wear or age related degradation of the cabinet insulation, which may have been accelerated by the large number of hours the test unit was operated at high ambient temperatures.

It must be understood how important it is to estimate the *UA's* precisely. In fact, the majority of other parameter estimations are based on them. Also, the compressor maps are developed assuming that the cabinet conductances are known and the accuracy of these maps is very dependent on the accuracy of the conductance estimates.

This is why it was essential to carefully calibrate the data sensing equipment before using the reverse heat leak data. The calibration is done using the so called soaked data, which consists of thermocouple and transducer readings taken while the refrigerator is off and in thermal equilibrium with its surroundings. The difference between a particular thermocouple reading and the average of all thermocouple readings in the set is used as the calibration value that is added to steady state data. The power transducer data is calibrated by subtracting the measured power while the system is idle from the steady state data.

Since the power of each heater in reverse heat leak tests does not exceed 50 Watts, a 5 Watt error in the calibration would have at least a 10% effect on the *UA* estimate. In fact, such relatively large calibration errors have been observed when an inconsistency between the soaked data points taken at different times.

It was also necessary to iterate back and forth between the compartment conductances and the evaporator parameters, the air split fraction and the flow rate, as described in the previous section. This was the only way to make sure that all the parameter estimates were consistent with each other.

E.4 Compressor related parameters

E.4.1 Compressor maps

RFSIM model requires two compressor maps - one for the *mass flow* that the compressor provides under different temperature conditions and one for the *power* required for the compressor to operate.

All the maps below are nine coefficient bi-quadratic curve fits in the following standard form:

$$w \text{ (or } P \text{)} = a_1+a_2 \cdot t_e+a_3 \cdot t_e^2+(b_1+b_2 \cdot t_e+b_3 \cdot t_3^2) \cdot t_c+(c_1+c_2 \cdot t_e+c_3 \cdot t_e^2) \cdot t_c^2, \quad \text{(E.9)}$$

where

t_e is the refrigerator evaporating temperature,
t_c is the refrigerator condensing temperature,
w is the refrigerant mass flow in lbm/lb,
P is the compressor power in Watts.

This particular curve fit was found to approximate the compressor data more accurately than other 9 or 10-coefficient fits, particularly those that involve third powers of either temperature.

The Ameritech RV800 compressor can operate at two discrete speeds - nominally 3600 and 2400 rpm. The actual operating speeds were measured with an accelerometer and were found to be 3770 ± 70 and 2470 ± 30 rpm respectively (Srichai, 1997). All the maps described in this section are for the higher speed setting, although they can be scaled down linearly to model the slower speed operation.

The mass flow was calculated from cabinet calorimetry and the refrigerant side flow energy change between the compressor inlet and the capillary tube inlet using the following simple energy balance:

$$w_{map} = \frac{\dot{Q}_{evap}}{h_{comp\,in} - h_{captube\,in}}, \qquad \text{(E.10)}$$

where, unlike other parameter estimates, evaporator load includes the post condenser loop heat transfer, in addition to cabinet loads, heater powers and evaporator fan power.

Captube inlet subcooling of at least 5 to 10°F was required to reliably predict the refrigerant condition at the captube inlet. In order to get subcooling, the system was overcharged for a few special *in situ* calorimetry tests, to have 8.64 oz (245 grams) of R-134a. This is 100 grams more than the factory charge. In addition to that, a big household cooling fan was installed behind the condenser to increase the air flow over it.

The maps for this compressor were originally presented by Srichai (1997). These maps were based on a total of 27 data points all of which were obtained from system tests done at ACRC. These data ranged from 70 to 120°F condensing temperature and from -30 to 0°F evaporating temperature. Unfortunately, Srichai's original maps could not be reliably extrapolated because all the points on each line of constant condensing temperature were bunched closely together. Extrapolation, however, is needed for certain model runs, particularly for fresh food operation of a dual temperature evaporator system.

Since a power map can be developed based on direct transducer measurements at any condition, 40 of the new non-subcooled data points were used in addition to the original data to produce a wider set of compressor conditions. The condensing and evaporating temperatures for all of these data points are shown in Figure E.3. Only the data from the experiments with 3600 rpm compressor speed are included.

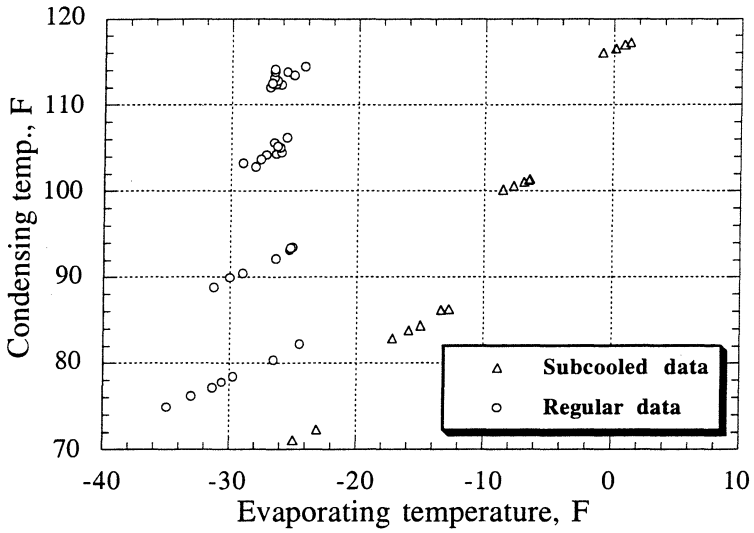

Figure E.3 Compressor power map data

The coefficients for the power map were found to be:

a_1 = 1.3572e+2 a_2 = 3.2577e-1 a_3 = -2.2990e-4
b_1 = 6.4766e-1 b_2 = 1.5888e-2 b_3 = -3.2767e-4
c_1 = 2.8471e-7 c_2 = 2.5648e-5 c_3 = 3.7599e-6

The final map is shown in Figure E4.

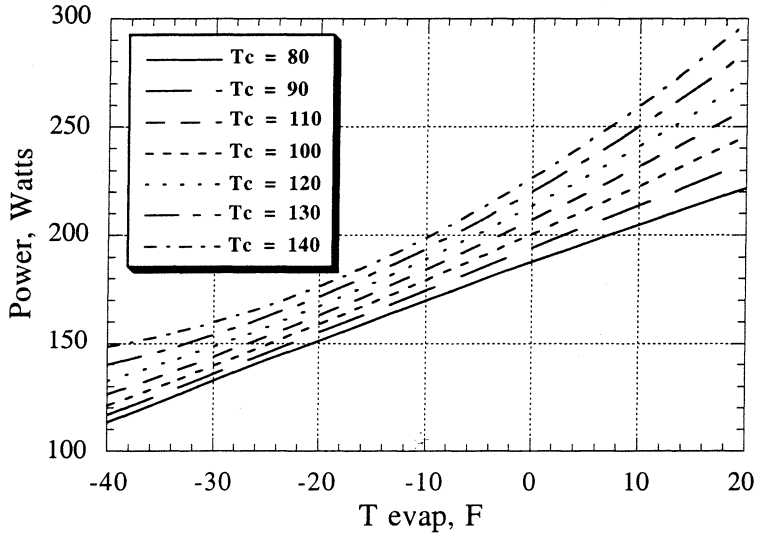

Figure E.4 New compressor power map

The power map was verified using the newest data. It was shown that this map consistently underpredicts the current data by an average of 5 Watts. However, this difference is within the power measurement uncertainty range. In fact, the power is calculated as the total system power measurement less the two fan power measurements. Each of these values can have up to 2 Watt variation, resulting in a 6 Watt total uncertainty for the compressor power.

A different approach was taken to expand the data set for the mass flow map. In addition to the original data for the 3600 rpm speed, 16 data points for the 2400 rpm compressor operation were taken. The mass flow for these data points was multiplied by a factor of 1.53, which is the ratio of the actual measured operating speeds. The range of temperature conditions for these data points is demonstrated in Figure E.5.

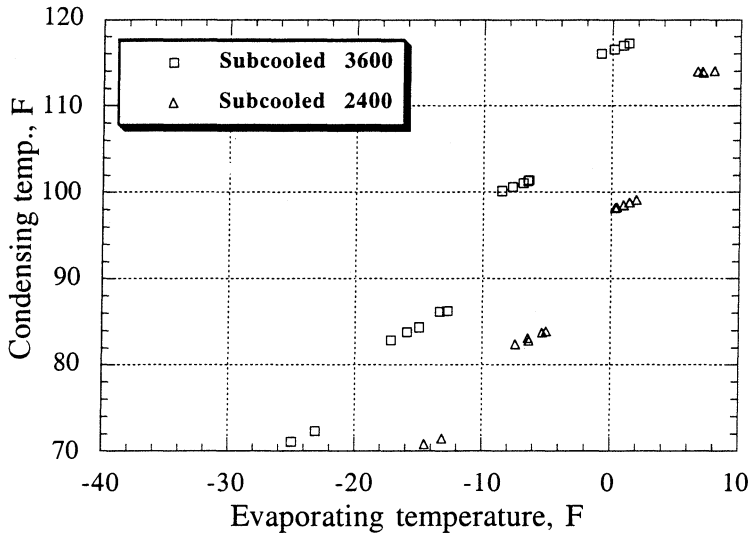

Figure E.5 Compressor mass flow map data

The coefficients for the mass flow map were found to be:

a_1 = 1.2262e+1 a_2 = 5.5723e-2 a_3 = -2.2046e-3
b_1 = 3.1840e-1 b_2 = 7.8738e-3 b_3 = -3.7171e-5
c_1 = -2.2600e-3 c_2 = -1.7409e-5 c_3 = 1.0184e-6

Finally, the map itself is shown in Figure E.6.

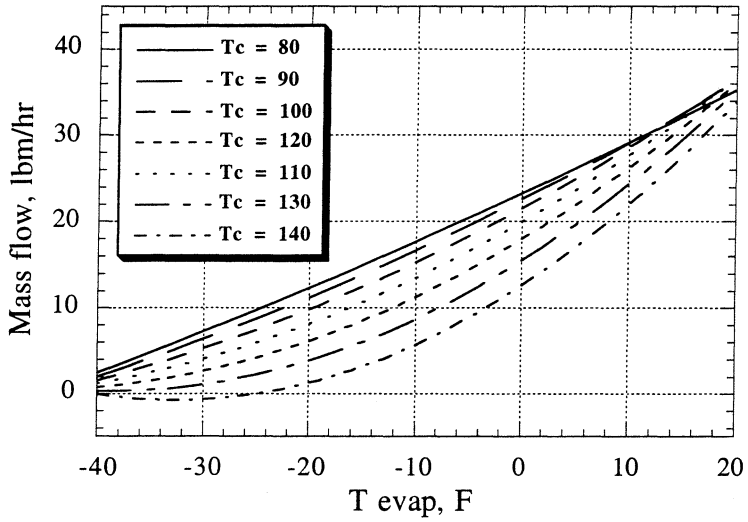

Figure E.6 New compressor mass flow map

There is no way to verify this map using the current data, but since the power map was shown to be fairly accurate, there is no reason to suspect that the mass flow map have changed since the subcooled data was taken.

E.4.2 Overall compressor heat transfer coefficient

The compressor heat loss is simulated using an air side heat transfer coefficient that has to be determined experimentally.

First the evaporator load is found as:

$$\dot{Q}_{evap} = \dot{Q}_{frez} + \dot{Q}_{frig} + UA_{frez} \cdot \left(T_{amb} - T_{az}\right) + UA_{frig} \cdot \left(T_{amb} - T_{af}\right) + \dot{W}_{evap\,fan} \qquad \text{(E.11)}$$

and along with the heat generated inside the compressor itself it is rejected in the condenser and the compressor:

$$\dot{Q}_{evap} + \dot{W}_{comp} = \dot{Q}_{cond} + \dot{Q}_{comp}, \qquad \text{(E.12)}$$

where the compressor power is found as:

$$W_{comp} = W_{total} - W_{evap\,fan} - W_{cond\,fan} \qquad \text{(E.13)}$$

The energy rejected by the compressor can be written as:

$$\dot{Q}_{comp} = W_{comp} + w \cdot (h_{comp\,in} - h_{comp\,out}), \tag{E.14}$$

on the refrigerant side and

$$\dot{Q}_{comp} = hA_{comp} \cdot (T_{comp\,shell} - T_{over\,comp}) \tag{E.15}$$

on the air side.

$T_{over\ comp}$ in the equation above is the temperature of the air flowing around the compressor which can be estimated if the heat capacity of air is assumed constant as it flows over both the compressor and the condenser:

$$T_{over\,comp} = \frac{\dot{Q}_{cond} \cdot T_{cond\,fan} + \dot{Q}_{comp} \cdot T_{grille\,in}}{\dot{Q}_{cond} + \dot{Q}_{comp}} \tag{E.16}$$

Table E.5 shows soluttions to the above equations for a set of 21 data points.

Temperature, F					Mass flow,	Comp. H.T.C.,
Freezer	Fresh food	Ambient	Comp. shell	Over comp.	lbm/hr	Btu/hr-F
4.8	46.8	91.5	153.5	97.2	7.771	6.922
4.5	46.2	75.5	138.7	82.4	8.427	6.053
4.1	45.9	61.0	117.2	67.0	8.027	6.413
4.3	47.9	90.9	152.2	95.7	6.447	7.021
3.3	47.5	91.1	152.4	96.4	6.212	6.877
2.9	44.4	91.1	153.3	96.3	6.792	7.095
3.3	46.7	76.0	135.0	81.9	6.544	6.622
2.9	46.2	75.7	134.9	81.0	6.731	6.630
2.6	44.4	75.8	134.3	81.3	7.420	6.870
3.4	46.0	61.0	118.1	67.1	6.088	6.554
3.0	45.6	60.6	117.8	66.2	6.310	6.685
2.3	44.2	60.7	118.0	66.8	7.511	6.605
1.1	44.6	91.0	153.6	96.3	5.581	6.694
10.0	49.6	91.0	154.7	96.7	6.033	6.711
20.0	55.6	90.7	155.6	96.7	6.273	6.650
1.4	45.2	75.8	134.7	81.0	5.483	6.456
10.2	50.1	75.7	135.3	81.3	6.151	6.399
19.8	54.6	75.4	136.6	81.4	6.619	6.349
1.3	45.1	60.5	116.9	65.8	4.764	6.402
10.0	49.4	60.6	117.5	66.1	5.375	6.377
19.8	52.9	60.8	118.1	66.5	5.692	6.351

Table E.5 Compressor heat transfer coefficients

The average heat transfer coefficient hA_{comp} was estimated to be 6.61 Btu/hr-°F with a standard deviation of about 4%. The new estimate for the heat transfer coefficient is just over 20% higher than the 5.50 Btu/hr-°F value reported by Srichai.

One possible explanation of such a significant discrepancy is that the four thermocouples that measure the compressor shell temperature are not as closely attached to the surface as before or the insulation around them has gradually degraded due to high temperatures and constant air flow over them. This means that it only appears as if the heat transfer coefficient has increased while in fact the measured temperature difference between the shell and the air flow is just a few degrees lower.

E.4.3 Compressor shell vs. discharge curve fit

The above effect can be demonstrated if the relationship between the compressor shell temperature and the discharge temperature is plotted, as shown in Figure E.7.

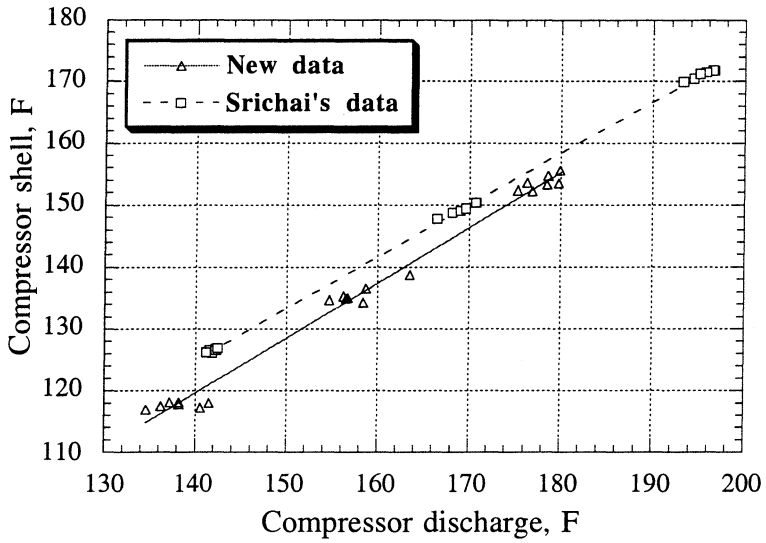

Figure E.7 Compressor shell vs. discharge

The new linear fit, which is the one used in the RFSIM simulation model, is based on the new data in the graph above:

$$T_{shell} = 0.892 \cdot T_{comp\,out} - 5.32 \qquad \text{(E.17)}$$

It can be observed that the newer points in this set have lower shell temperature corresponding to a given discharge temperature than older ones, which creates significant scatter. This also indicates that the shell temperature measurement degradation is a consistently observed phenomenon, not just a coincidence.

Under similar refrigerant side conditions the new fit gives a consistently lower value for the shell temperature than the one reported by Srichai. The difference of 5-7°F accounts for about 10-15% of the total temperature difference between the air flow and the compressor shell. This effect is at least partially responsible for the apparent difference between the two estimates of hA_{comp}, as described in the previous section.

E.5 Condenser related parameters

E.5.1 Air flow rate over the coil

As in the previous sections, the refrigerant side energy balance is:

$$\dot{Q}_{evap} + \dot{W}_{comp} = \dot{Q}_{cond} + \dot{Q}_{comp}, \tag{E.18}$$

where the evaporator and the compressor heat transfer can be found the same way as in the hA_{comp} parameter estimation.

In addition, the total heat transfer on the air side can be estimated as:

$$\dot{Q}_{cond} + \dot{Q}_{comp} + W_{cond\ fan} = \dot{m}_{cond} \cdot (h_{cond\ fan} - h_{grille\ in}), \tag{E.19}$$

where, by definition:

$$\dot{m}_{cond} = \frac{\dot{V}_{cond} \cdot 60}{\upsilon \cdot (T_{cond\ fan}, P_{atm})} \tag{E.20}$$

The new flow rate estimate is 124.6 cfm with a 5% standard deviation, which is somewhat larger than Srichai's 116.4 cfm, a 7% change. However, the uncertainty in two of the air flow temperatures measurements is about 0.5°F, so the temperature change of the air flow can be only estimated with a 1.0°F accuracy. This corresponds to a 10 -15% total uncertainty which alone could easily cause this estimate to change. In other words, this difference is most likely a result of measurement uncertainty, rather than an actual fan performance change.

It should be mentioned that Srichai was using the average specific heat of air on the air side multiplied by the temperature change, rather than the actual enthalpy difference, which is responsible for only about a 0.5% difference between the two estimates.

The results for each of the 21 data points are shown in Table E.6.

Temperature, F					Condenser	Cond. air flow
Freezer	Fresh food	Ambient	Grille in	Cond. fan	fan power, W	rate, cfm
4.8	46.8	91.5	90.8	100.4	10.0	125.5
4.5	46.2	75.5	75.7	85.4	9.5	115.6
4.1	45.9	61.0	60.8	69.5	8.6	124.0
4.3	47.9	90.9	90.3	98.9	8.8	128.0
3.3	47.5	91.1	91.1	99.4	8.5	135.0
2.9	44.4	91.1	90.0	99.8	8.8	119.5
3.3	46.7	76.0	76.6	84.5	7.8	136.3
2.9	46.2	75.7	75.4	83.8	8.1	127.5
2.6	44.4	75.8	75.1	84.4	8.2	119.7
3.4	46.0	61.0	62.0	69.5	7.3	136.3
3.0	45.6	60.6	60.8	68.8	7.7	128.9
2.3	44.2	60.7	60.5	69.6	7.6	119.0
1.1	44.6	91.0	90.8	99.5	9.2	125.4
10.0	49.6	91.0	90.8	99.9	9.3	124.7
20.0	55.6	90.7	90.6	100.0	9.4	123.4
1.4	45.2	75.8	75.7	83.8	8.4	123.6
10.2	50.1	75.7	75.7	84.2	8.4	123.2
19.8	54.6	75.4	75.4	84.4	8.5	121.2
1.3	45.1	60.5	60.7	68.5	7.9	120.4
10.0	49.4	60.6	60.8	68.9	7.8	119.8
19.8	52.9	60.8	61.0	69.2	7.8	119.7

Table E.6 Air flow rates over the condenser

E.5.2 Air side heat transfer coefficient

Assuming that the heat transfer resistance due to the wall tubing is negligible, the effectiveness-NTU method was used to estimate the air side resistance of the condenser coil. Unlike the data used in Srichai's estimations, no subcooling was observed in the new experiments. The condenser had only two zones - superheated and two phase regions. However, the conductance equations for each of the two zones are identical to those presented in his work.

In the absence of subcooling, the actual thermodynamic state is unknown at the two phase outlet of the condenser. Therefore, the heat transfer in the condenser had to be estimated similarly to that for the air flow rate over the coil estimate above, as the evaporator load less the heat rejected in the compressor. This heat transfer is distributed

over both condenser regions with only 20-25% of the heat rejected in the vapor region, which was 10-12% of the total condenser tubing length.

The two regions had independently calculated effectivenesses, as described by Srichai. The total heat transfer and the outside tubing area had to add up as shown below:

$$\dot{Q}_{cond} = \dot{Q}_{cond\,\mathrm{sup}} + \dot{Q}_{cond\,2p} \tag{E.21}$$

and

$$A_{cond} = A_{cond\,\mathrm{sup}} + A_{cond\,2p} \tag{E.22}$$

When doing the calculations it was noted that there was an inconsistency between the amount of energy rejected in the condenser and compressor combined verses the evaporator load estimated based on cabinet calorimetry .

The compressor inlet refrigerant state in the equation below was obtained experimentally and the map was developed as described earlier in this appendix:

$$\dot{Q}_{evap} = w_{map} \cdot (h_{comp\,in} - h_{cond\,out}) \tag{E.23}$$

If this energy balance is used to solve for the condition at the exit of the condenser, it would indicate that there is a significant subcooling at this point. However, the subcooling was not detected by measurements. The fact that for each data point the measured temperature was equal to the saturation temperature at the measured pressure makes this observation extremely trustworthy. Many of the possible explanations for this phenomenon are discussed in the following section.

Since, due to the confusion described above it was impossible to actually calculate the condenser exit condition, this condition had to be guessed. The calculations below are based on an assumption that there is a quality of 0.0 or 0.1 at the condenser exit. In addition, for another estimate the map was "adjusted" by multiplying it by a factor of 1.4 in order to ensure that a quality exit condition was predicted for all the points. These three estimates are compared to each other to get a feel for the range of values that the heat transfer coefficient might have. The average of the three values is arbitrary taken as the final estimate.

Table E.7 shows the results for each of the 21 data points used. The average results for the assumed condenser exit quality cases were 4.44 and 4.33 Btu/hr-ft^2-°F for 0.0 and 0.1 qualities respectively and 4.27 Btu/hr-ft^2-°F for the "fudge factor" case. The final estimate, which is an average of the three is 4.35 Btu/hr-ft^2-°F. This is about 15%

higher than 3.74 Btu/hr-ft^2-°F, as reported by Srichai. This might indicate that exit qualities are on average even higher than 0.1.

	"Adjusted" map			Exit quality of 0.0		Exit quality of 0.1	
Basic map, lbm/hr	Map lbm/hr	Cond. exit quality	H.T.C. Btu/hr-ft^2-F	Map lbm/hr	H.T.C. Btu/hr-ft^2-F	Map lbm/hr	H.T.C. Btu/hr-ft^2-F
7.77	10.88	0.22	4.40	8.98	4.68	9.74	4.56
8.43	11.80	0.39	3.39	8.12	3.74	8.83	3.66
8.03	11.24	0.32	3.60	8.28	3.84	9.03	3.77
6.45	9.03	0.17	4.49	7.80	4.71	8.46	4.58
6.21	8.70	0.11	5.12	7.93	5.29	8.60	5.14
6.79	9.51	0.13	4.53	8.52	4.70	9.24	4.57
6.54	9.16	0.18	4.61	7.85	4.82	8.54	4.70
6.73	9.42	0.21	4.29	7.79	4.52	8.48	4.41
7.42	10.39	0.25	4.03	8.25	4.28	8.98	4.19
6.09	8.52	0.14	4.24	7.55	4.36	8.23	4.27
6.31	8.83	0.15	4.09	7.74	4.21	8.44	4.13
7.51	10.52	0.27	3.63	8.16	3.83	8.90	3.76
5.58	7.81	0.07	4.89	7.36	5.00	7.99	4.85
6.03	8.45	0.09	4.74	7.88	4.86	8.55	4.72
6.27	8.78	0.11	4.50	8.01	4.64	8.69	4.52
5.48	7.68	0.11	4.53	6.99	4.65	7.61	4.54
6.15	8.61	0.17	4.38	7.43	4.56	8.08	4.45
6.62	9.27	0.21	4.09	7.73	4.30	8.41	4.20
4.76	6.67	0.01	4.11	6.59	4.12	7.20	4.03
5.38	7.53	0.10	3.93	6.87	4.02	7.50	3.93
5.69	7.97	0.12	3.98	7.15	4.08	7.80	3.99

Table E.7 Condenser heat transfer coefficients

Appendix F

Sources of inaccuracies

F.6 Reasons for suspicion

As mentioned in the previous sections, it was virtually impossible to reliably model the behavior of both the condenser and the evaporator. In the first case, if a refrigerant side energy balance in conjunction with the compressor mass flow map were used to find the exit state of the condenser, it would predict that there should have been a substantial amount of subcooling at this point. This contradicts the fact that all the experimental measurements subsequent to Srichai's development of the compressor map indicated a two phase exit. In the second case, a similar calculation based on the amount of superheat at the evaporator exit would have predicted a subcooled inlet while, according to the experimental data, it also had a two phase condition.

The fact that these two totally independent energy balance considerations both required the map "adjustment" by at least 30 or 40%, in order to make any physical sense, must indicate that either the refrigerant mass flow map or the evaporator load estimate were incorrect or changed significantly at some point in the experiments.

These inconsistencies have indicated that there must have been at least one faulty reading in the data used for the parameter estimations. Alternatively, there could have been a calculation error in estimating one or more parameters that affected the energy balance around these components.

Unfortunately, the actual causes of error were extremely difficult to track down. Trying to find out which of the measurements or estimated parameters were incorrect proved to be a an extremely tedious task. The complexity of the issue is related to the fact that every parameter estimation had to be traced back to the original data that it was based on as well as all other parameters that were used in each individual calculation earlier in the sequence of parameter estimations.

F.2 Measurement accuracy

F.2.1 Power transducers

The most basic measurements that had a profound effect on the parameter estimations were the cabinet heater powers. The accuracy of the transducers employed in these power measurements had to be verified.

First, in order to confirm that these transducers have been properly calibrated, they were hooked up in parallel to a highly reliable wattmeter while measuring the power consumption of a light bulb rated at 150 Watts. Both transducer measurements were shown to be within 2% of the wattmeter readings.

A similar transducer accuracy was found while the cabinet heaters were turned on and the actual data were logged for the powers ranging from 0 to about 50 Watts. This was done to prove that the heater control system, which alters the power output by sending the signal intermittently, does not affect the accuracy of the measurement. The wattmeter that was used for calibration was an analog device, similar to those used in residences by utility companies, and therefore effectively did the time averaging of the signal without the possibility of trimming it, like a transducer could have done.

While these transducers appeared to be adequately reliable in the above experiments, it should be noted that under different circumstances they have been known to produce inconsistent values while no power was applied to them. On at least two independent occasions there was a distinctly noticeable "glide" in the calibration value during a 20-minute long experiment. Furthermore, the tare values at 0 Watts power for both heaters obtained from such experiments have varied by up to 16 Watts. This is virtually on same order of magnitude as many typical power measurements, particularly those for the reverse heat leak tests.

When data points with identical temperature settings were compared, it turned out that the power measurements could, in some extreme cases, vary as much as by a factor of three. It is unclear whether the transducers themselves, the controllers or the data acquisition system setup were responsible for such a huge fluctuation. Interestingly enough, the sum of the two powers was a lot more stable, having only a ±20% variation from point to point. This could mean that the split air fraction between the evaporator flows into each compartment could have changed over time, which would affect the effective cooling distribution but not the total load.

While on the subject of power transducers, it should be noted that there were three more of them installed in the system for measuring the total system power as well as condenser and evaporator fan powers. Unlike the heater power transducers, these three never exhibited any "unexpected" behavior. In fact, the fan power measurements varied only ±1 Watt throughout the experiments. The system power data was also very repeatable and fluctuated only ±5% or less.

F.2.2 Temperatures and pressures

Only a handful of the temperatures were measured simultaneously by more than one thermocouple. This was the case with air temperatures inside the refrigerator compartments and the chamber. These temperatures were independently measured by the system controllers and the thermocouples used for data acquisition. These two measurements were always within a fairly reasonable 1-2°F, which was a good indicator that both the controllers and the thermocouples were working properly.

Most of the temperatures and pressures used in the parameter estimations could have been verified using a simple calculation. For example, the pressure at the condenser exit could be calculated as the measured pressure at the condenser inlet less the pressure drop in the condenser. The saturation temperature corresponding to this pressure was on average only 0.6°F different from the measured temperature at this point. Such a good agreement indicated that all three totally independent measurements involved in this simple calculation were more than likely accurate.

Another case where there was an opportunity to get confidence in the accuracy of the readings was the post condenser loop. The pressure drop in it was measured using a differential transducer. When the loop was completely filled with two phase liquid the pressure drop in it was generally about 2 psi. This corresponds to a little less than 2°F in saturation temperature, exactly the kind of difference seen between the temperatures at the inlet and the outlet of the loop.

A lot of the temperatures however had to be examined from a "common sense" perspective. This particularly applies to the air side temperatures. For example, the temperature of the air as it enters through the grille under the refrigerator was in almost all cases within 1°F of the chamber temperature. The temperature of the air as it flows over the condenser fan was, in most cases, 9-10°F higher than ambient.

The fact that there was a consistent flow temperature gradient was an indicator that this thermocouple was functioning properly. Such observations could be further confirmed by noting that the calculated air flow rate over the condenser was in all cases only ±10% of the average. This was actually within the experimental error expected of a calculation based on the difference between two thermocouples with 0.5°F uncertainty each.

All the other temperature and pressure data also seemed to be consistent, repeatable and within a "reasonable range" of values.

F.3 Compressor map considerations

There are three possible reasons why compressor mass flow map could have been unreliable:

1. The actual compressor performance have changed after the map were developed.
2. The conditions under which the map was developed were different from those under which all the later experiments were done.
3. The data used for compressor map development was faulty.

There was a way to illustrate that the compressor performance characteristics have most likely remained fairly stable over the entire duration of testing. The predictions made with the power map, which could be directly verified for each point, appeared to be only about an average of 5 Watts above the actual sensor readings for the later measurements. Therefore, the compressor power data was consistent, unlike the mass flow data. In general, the power required to operate a compressor is nearly linearly dependent on the mass flow it provides. Thus the actual compressor performance characteristics must have remained the same.

The mass flow map had to be extrapolated for use in all the refrigerant side parameter estimations, which inevitably caused an unknown inaccuracy. This map was developed based on data with about 10-20° higher evaporating temperatures than what was typical of the data points used for subsequent parameter estimations. This could be a source of potential problem, but there is a couple of considerations that point out that it is not likely to be a source of any major inconsistencies.

First of all, the mass flow map was developed based on both 2400 and 3600 rpm data over a fairly wide range of data points, which was done to make sure such an extrapolation would be possible. Secondly, if the power map would be developed based only on the same data as the mass flow map, it would still predict the later power consumption data points with a reasonable accuracy. It is not clear why the mass flow map turned out to be less reliable when extrapolated than the power map.

If extrapolation is generally valid, any major inaccuracies must be due to the fact that one or more measurements or parameter estimations that were used in the process of map development were unreliable.

The only parameter estimations that had to be done prior to compressor map development were the cabinet conductances for the freezer and the fresh food

compartments and the post condenser loop conductance. The cabinet conductances were primarily based on the heater powers and a few temperature measurement. All of the temperatures were known to be accurate as discussed above. Thus, the only way there could have been an error in the cabinet conductance estimations was if the power measurements were faulty.

Hypothetically, if the power transducers were measuring higher values for the heater powers than actual by a certain factor then, in the first approximation, the cabinet conductances would have been overestimated by the same factor. In fact, for the purpose of evaporator load calculation, where the heaters and the heat leaks into the compartments were added together, this would have meant that the whole load was overestimated by the same factor. Similar logic could be applied for case of underestimating the heater powers and, consequently, the evaporator load.

The compressor mass flow maps were based on a number of temperature and pressure measurements in addition to heater powers and cabinet conductances. Again, it was not likely that any of the temperature or pressure measurements were incorrect. This leaves the heater powers and the cabinet conductances as the only possible sources of significant error.

The cabinet conductances could not have changed significantly enough to cause this inconsistency. In fact, when Srichai's results were compared to the newly calculated parameter estimates, it was shown that there might have been only about a10% increase in the heat transfer trough the cabinet walls, which is only enough to cause a 3-4% jump in the total evaporator load.

While developing the compressor maps, the heat transfer in the post condenser loop was included in the evaporator load calculation. The system boundaries had to be drawn differently than for other parameters estimations, as explained in Appendix E. While the heat transfer coefficient of the post condenser loop could not have been re-estimated to confirm Srichai's earlier results, the heat transfer in the loop only constitutes 0.5-1.5% of the total evaporator load, and therefore would only have a minimal effect if estimated imprecisely.

Since all three conductances had only minor effects on the map development, the only conceivable explanation that have not been ruled out as a possible cause of inconsistencies were the heater power fluctuations. Even though the accuracy of these transducers have been directly verified at certain conditions, it is apparent that they did not perform consistently during all of the experiments, particularly while developing the compressor map.

It must be pointed out that the cabinet heater power measurements affected both the evaporator load calculation and the compressor map development. On one hand, the fact that the compressor mass flow map calculation had to be "increased" by 40% just to predict a two phase condition at the exit of the condenser could indicate that the map was predicting a mass flow that was that much lower than actual. On the other hand, the evaporator load could have been less than shown by the values calculated based on the heater powers in, which case the map could be correct.

The same argument could be applied when examining the evaporator energy balance. Since it turned out that in order to predict a two phase inlet condition at the evaporator inlet the mass flow map calculation had to be "increased" by about 30%, it is likely that either the map, or the heater power measurements were incorrect.

F.4 Parameter estimation accuracy

As it was pointed out in the previous section, the cabinet conductance estimates were directly affected by any error in the heater power measurement. Their accuracy was almost directly proportional to that of the heaters. However, it should be remembered that in order to obtain these conductances, the air flow over the evaporator coil and the air split fraction must have been known as well. An additional error could have been due to the fact that one or both of these parameters could have been estimated improperly.

The air flow rates over the evaporator and the condenser were, among other things, dependent on the evaporator load calculation which was, in turn, derived from the cabinet heater power measurements. If the heater powers would have been measured consistently higher than actual, these air flows would have to be estimated too large as well. For the air flow over the evaporator, assuming that the air split fraction was correct, the error would be directly proportional to that in the evaporator load, and thus the heater measurement error. The calculation of the air flow over the condenser depended on the sum of the evaporator load and the compressor power consumption. Therefore, it can be shown that the inaccuracy in this calculation would be somewhat less dependent on the error in the evaporator load.

The air split fraction of the air flow over the evaporator was a function of the cabinet conductances, individual heater powers and the air flow rate over the coil. It was extremely hard to find out how well this parameter was estimated, since all five of the above parameters could have been calculated inaccurately.

Basically, both the condenser and the evaporator heat transfer coefficients had to be "guessed" based on some assumption described in the respective sections earlier in this chapter. The overall heat transfer coefficient of the compressor depended on the

mass flow map, and therefore might present an underestimate, since the map is suspected to predict smaller than actual mass flows.

In the nutshell, all the parameter estimates rest fundamentally on the accuracy of the cabinet heater power measurements. An error in these measurements could show up multiple times as the heater measurements were included in a whole set of sequential calculations, somewhat simplified examples of which are presented above.

F.5 General observations and suggestions

None of the major refrigerator components could be tested individually and the fact that both air side and refrigerant side calorimetry was extensively used to obtain the air and refrigerant flow rates could introduce an unknown degree of inaccuracy in every step of the parameter estimation process. In addition to that, there were some other considerations that could make the parameter estimates even less reliable.

First of all, the system was recharged with fresh refrigerant numerous times and, in spite of the fact that vacuum was being pulled on the entire system every time, the purity of refrigerant and the quality of the compressor oil could be dependent on the date a particular experiment was done.

Secondly, the data used in the parameter estimations was taken over a relatively long period of time. It is highly unlikely that the parameters themselves stayed exactly the same while all the data was taken. In this respect, the most suspicious estimate was the evaporator air split fraction.

Thirdly, some parameters could have been easily affected by external factors. For example, the actual cabinet conductances could depend on how well the refrigerator doors were closed on the day of an experiment.

Finally, the air humidity effects were never taken into account, creating yet another source of uncertainty. The evaporator was routinely defrosted every 2 to 3 days and additional experiments have shown that this frequency was sufficient for the purposes of maintaining constant air flow over the evaporator coil, which does not necessarily mean that humidity was constant throughout the experiment.

Under many circumstances, other than the ones described in this Appendix, all the parameter estimations could have been done without giving any indications of a possible error. The only reason a suspicion that there could have been an error in one or more parameter estimations arose was that the thermodynamic state at one particular point was not within a fairly wide bounds of "expected values." If the energy balance calculation resulted in a two phase exit, whether based on accurate results or as a matter of a mere coincidence, this suspicion would not have been triggered in the first place.

Therefore, it must be realized that instrumentation of systems, similar to the one under investigation, should include as many redundant measurements as possible. This must be done in order to make sure that a single false reading, while remaining within "reasonable bounds," would not create a domino effect on all of the parameter estimations. In fact, even when the overall system model, no matter how complex, is used to "check" if the parameter estimations were done correctly, it would only go to predict the same exact measured conditions at each point. Most likely such a model would just replicate the measurements, whether they were correct or incorrect, creating an illusion of a properly described system.

Appendix G

Refrigerator instrumentation

G.1 Previously done instrumentation

The side-by-side Amana refrigerator was originally instrumented by Robert Srichai. The complete details and justification for the thermocouple and transducer placement were presented by Srichai and Bullard (1997).

The original instrumentation included 27 air-side thermocouples located inside the refrigerator cabinets as well as around the condenser and the evaporator ductwork. 37 refrigerant and surface thermocouples were also installed. Five of these were immersion thermocouples with a surface thermocouple installed at each of these locations as well.

Also, at each of the five locations that immersion thermocouples were placed, a pressure transducer was also installed. Absolute pressure was measured at the evaporator exit while gauge pressure was obtained at the compressor exit. Differential transducers were used to measure the pressure drops across the condenser, the liquid line and the suction line. The atmospheric pressure was also logged.

Finally, watt transducers were installed to measure the heater powers, the fan powers and the total system energy consumption.

G.2 New instrumentation

G.2.1 General considerations

Just like for the original thermocouples, 24 AWG type T thermocouple wire was purchased from Omega Engineering. This brought the number of distinct batches of wire that were used in the instrumentation to three. However, in order to minimize the errors that could be caused by using different wire, thermocouples from each batch were connected to different panels, and the panels were calibrated independently.

Furthermore, all the measurements related to the evaporator, the compressor and the captube were done using the wire from the new batch, while the ambient and cabinet temperatures in addition to the condenser and the liquid line related measurements were done using older batches.

G.2.2 Air-side instrumentation

All the air-side thermocouples that were placed throughout the fresh food and freezer compartments were left exactly like they were installed by Srichai. Condenser instrumentation was left intact as well.

Since the experimental study was primarily concentrating on the evaporator modeling, the new evaporator was instrumented more extensively than before. Two thermocouples were put in each duct leading to or from the evaporator. These thermocouples were mounted roughly 1/3 and 2/3 of the way along the horizontal diameter line of each duct about 0.75" away from the duct opening. These thermocouple locations are numbered 1 through 8 in Figure G.1.

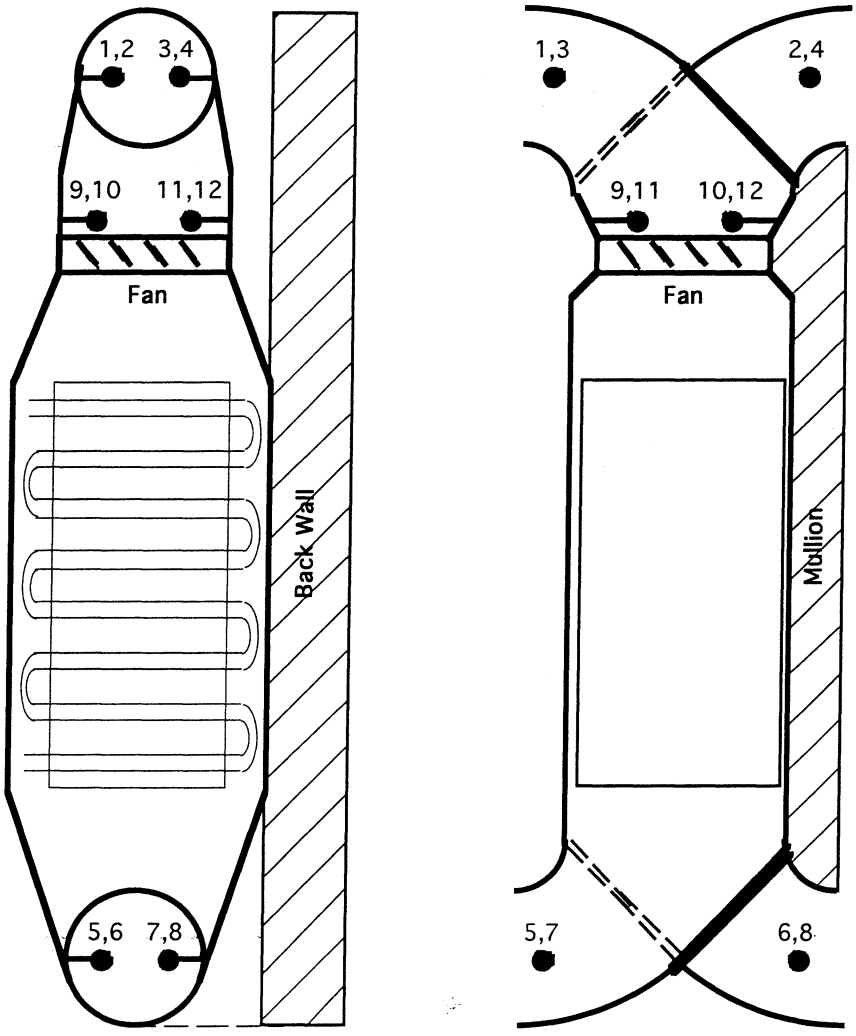

Figure G.1 Air-side evaporator instrumentation

Additionally, four thermocouples were put about 0.5" above the evaporator fan. They were installed in a square pattern as shown in Figure G.1, points 9 through 12. These thermocouples were used to monitor if the air flow temperature was uniform. Also, the average temperature measured by these thermocouples was used to double check the temperature of the air exiting into the compartment that was being cooled, which was also monitored by the thermocouples installed in the air exit ducts (1 and 2 for the freezer or 3 and 4 for the fresh food compartment).

If the temperature of the air inside the duct leading into the compartment *other* than the one being cooled was lower than the average temperature in that compartment, that could indicate that the valve responsible for switching the flow between the compartments might not be directing the entire flow into the compartment that was supposed to be cooled at this stage in the cycle.

G.2.3 Refrigerant-side instrumentation

Most of the refrigerant-side thermocouples were installed at the same exact locations as previously done by Srichai. New thermocouples were installed at the inlets and exits of the evaporator, captube and compressor.

Additional surface thermocouples were attached to the evaporator tube bends at the very bottom of each of the three coils that were joined together to form the new evaporator prototype. The purpose of these measurement was to determine whether the evaporator dry-out effect described in Appendix B for the originally installed coil would be observed in the new evaporator as well.

Just like before, four surface thermocouples were placed around the shell of the new compressor - at the top, bottom, front and back. The average measurement from these thermocouples was used to curve fit the correlation between the compressor shell temperature and the compressor discharge temperature.

The new refrigerant-side instrumentation is shown in Figure G.2.

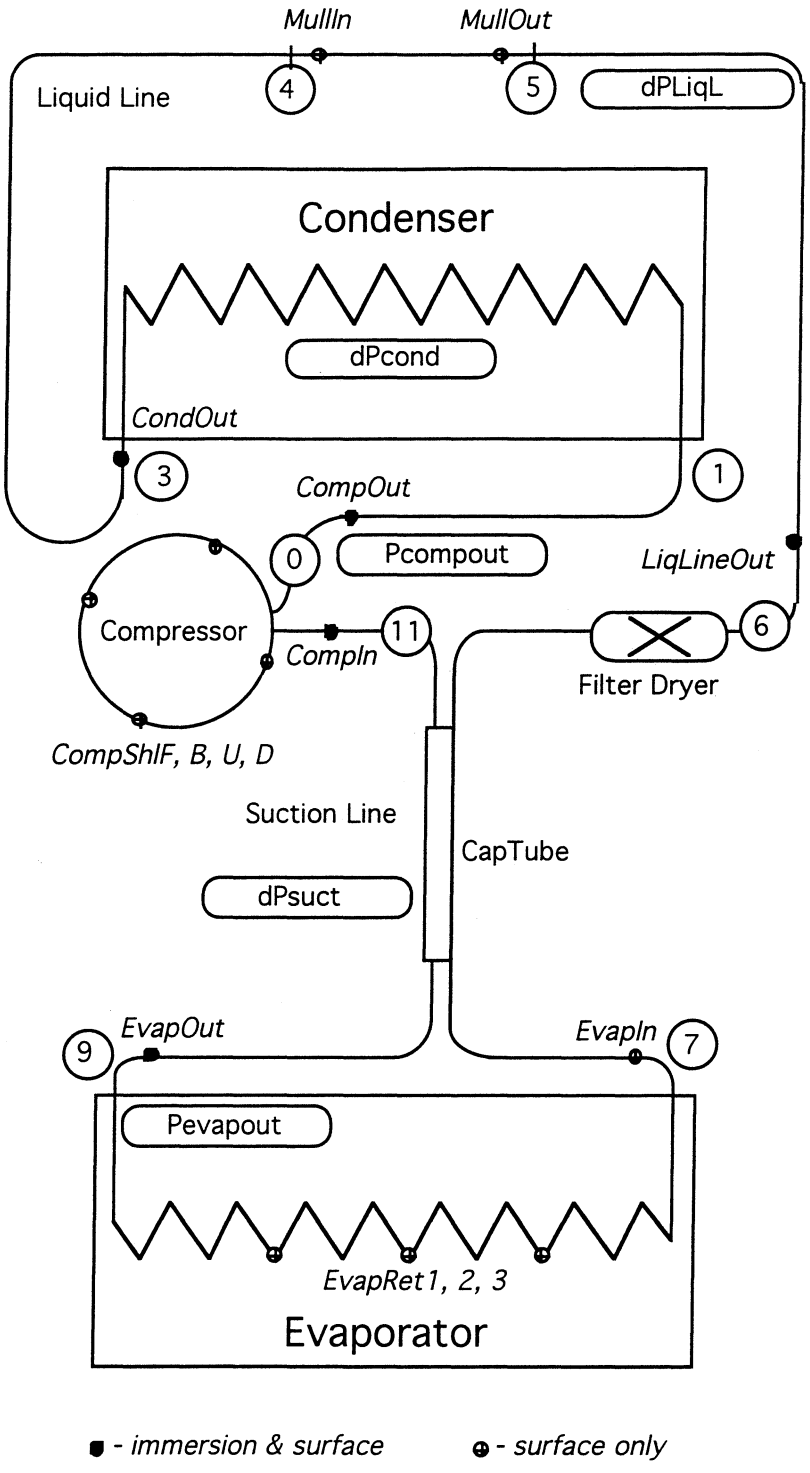

Figure G.2 Refrigerant-side instrumentation